R186

5 R01 OH 2392-02

PB91-188615

FINAL REPORT TO NIOSH

THE IMPACT OF FLOW SEPARATION ON EXPOSURE AND HOOD CAPTURE EFFICIENCY

Michael R. Flynn - Principal Investigator

February 1, 1990

REPRODUCED BY
U.S. DEPARTMENT OF COMMERCE
NATIONAL TECHNICAL
INFORMATION SERVICE
SPRINGFIELD, VA 22161

50272-101

REPORT DOCUMENTATION PAGE	1. REPORT NO.	2.	3 PB91-188615

4. Title and Subtitle The Impact of Flow Separation on Exposure and Hood Capture Efficiency

5. Report Date 1990/02/01

6.

7. Author(s) Flynn, M. R.

8. Performing Organization Rept. No.

9. Performing Organization Name and Address Department of Environmental Sciences and Engineering, University of North Carolina, Chapel Hill, North Carolina

10. Project/Task/Work Unit No.

11. Contract (C) or Grant(G) No.

(C)

(G) R01-OH-02392

12. Sponsoring Organization Name and Address

13. Type of Report & Period Covered

14.

15. Supplementary Notes

16. Abstract (Limit: 200 words) A mathematical model was developed which could predict breathing zone concentration for a worker operating in the vicinity of a local exhaust hood. As part of this effort, a mathematical model was developed to predict breathing zone concentration for a mannequin when a point source of tracer was located downstream. The model was extended to include the situation with a mannequin positioned in front of a flanged circular hood and to include cross drafts and mannequin position with respect to the hood. The results of the study indicated that where workers hold contaminant generating sources and operate in front of or within large booth type hoods, the phenomenon of boundary layer separation was of major importance in determining exposure. Where possible the worker should maintain an orientation such that the line connecting the source and worker is a right angle to, not parallel to, the air stream. Vortex shedding plays the primary role in contaminant transport from the separated recirculation zone. The author concludes that ventilation when used as an engineering control must be used in conjunction with, and not in exclusion to, work practices.

17. Document Analysis **a. Descriptors**

b. Identifiers/Open-Ended Terms NIOSH-Publication, NIOSH-Grant, Grant-Number-R01-OH-02392, End-Date-09-28-1989, Control-technology, Air-quality-control, Control-technology, Air-sampling, Ventilation-systems, Laboratory-workers

c. COSATI Field/Group

18. Availability Statement	19. Security Class (This Report)	21. No. of Pages 155
	22. Security Class (This Page)	22. Price

(See ANSI-Z39.18) *See Instructions on Reverse*

OPTIONAL FORM 272(4-77)
(Formerly NTIS-35)
Department of Commerce

TABLE OF CONTENTS

Final Report for Grant 5 R01 OH02392-02
The Impact of Separation on Exposure and Hood Capture
Principal Investigator: Michael R. Flynn

Summary:

The principal objective of the research was to develop a mathematical model to predict breathing zone concentration for a worker operating in the vicinity of a local exhaust hood. The modeling and experiments were designed specifically to address the importance of boundary layer separation and hood capture efficiency in determining the worker's exposure. All experimental work was designed for and performed with mannequins.

In order to accomplish the main objective three specific aims were delineated in the proposal with experiments to accomplish each --

1) The development of a mathematical model to predict breathing zone concentration (BZC) for a mannequin when a point source of tracer is located downstream;

2) Extension of the above model to include the situation with a mannequin positioned in front of a flanged circular hood, and;

3) Further extension of the results to include cross drafts and mannequin position with respect to the hood.

The significant findings of the work can be summarized as follows:

1) For situations where worker's hold contaminant generating sources and operate in front of or within large booth type hoods the phenomenon of boundary layer separation is of major importance in determining exposure. Where possible the worker should maintain an orientation such that the line connecting the source and worker is a right angles to, not parallel to, the air stream. This minimizes the influence of the separated recirculation zone which forms downstream of objects immersed in fluid flows. (See Manuscript I)

2) Results suggest that it is vortex shedding which plays the primary role in contaminant transport from the separated recirculation zone. This suggests simple but accurate models to estimate concentration in the breathing zone for situations such as booth type hoods. (Manuscripts I and II also Appendix C)

3) The discrete vortex method represents a powerful numerical technique for extending the work to arbitrary worker orientations as well as to examine the effect of

obstacles in the booth, e.g. a spray paint booth. (See Manuscript II; Appendix B contains a listing of the code)

4) The same orientation effect observed with the wind tunnel studies is noted in front of smaller hoods as well, i.e., it is preferable to stand to the side of the hood rather than in the usually recommended position with the source between the worker and the hood. (See Manuscript III)

5) Steady state capture efficiency is by definition 100% and therefore breathing zone concentrations will have no functional dependence upon it. Capture efficiency is a function of time and it is the integral of one minus capture efficiency over time which determines the contaminant hold up in the room. The experiments confirm a strong relationship between this hold-up and measured breathing zone concentrations; while a very weak relationship exists between predicted capture velocity and the breathing zone measurements. (This paper is under preparation see Appendix A)

6) Capture efficiency is a step in the right direction but is only part of the puzzle. The key parameter is concentration in the breathing zone and this depends to a great extent on complex mixing processes generated in many cases as the result of boundary layer separation.

7) An additional paper (Manuscript IV) was prepared on an unexpected topic - exposure variability. Wind-tunnel tracer experiments suggest that contaminant sources external to separated boundary layers result in lower exposure variability than the case of a source within such a mixing zone. This may be a significant finding in identifying factors that are important in determining exposure variability and in answering the question of how many samples are needed to evaluate compliance with exposure standards.

I believe that the most significant conclusion from the work on a practical, applied level is that ventilation as an engineering control must be used in conjunction with, not in exclusion to, work practices. The mind-set that somehow an engineering control such as ventilation can be applied effectively without educating and training the worker on optimal orientation and performance, I believe is faulty. Further research is needed on the nature of the mixing process and in particular air flow around the worker.

MANUSCRIPT I

The Impact of Boundary Layer Separation
on Local Exhaust Design and Worker Exposure

THE IMPACT OF BOUNDARY LAYER SEPARATION ON LOCAL EXHAUST DESIGN AND WORKER EXPOSURE

Dennis K. George, Michael R. Flynn and Randall Goodman

Department of Environmental Science and Engineering

University of North Carolina at Chapel Hill

Chapel Hill, NC 27599

Abstract - The phenomenon of boundary layer separation is an important factor in determining a worker's breathing zone concentration. This paper presents the results of flow visualization and tracer gas studies, conducted in a wind tunnel with a mannequin, designed to examine this phenomenon. A simple conceptual model based on mass transport by vortex shedding, provides a reasonable estimate of the mannequin breathing zone concentration. An empirical model is developed which relates the measured concentration to the distance from the source to the breathing zone, for the situation when the contaminant is released downstream in a uniform flow. Applications of the results are discussed.

INTRODUCTION

One of the more serious threats to employee health is the inhalation of toxic airborne materials produced by various industrial processes. Once inhaled, these contaminants may give rise to a number of deleterious health effects. Occupational health professionals constantly seek ways to reduce these exposures to acceptable levels. Typically, in an industrial environment, it is desirable to remove the contaminant as close to its source as possible, before it has a chance to escape into the general workroom air. This is often accomplished through the use of local exhaust ventilation (LEV).

The size, shape, and configuration of an LEV system are as varied as the industrial

processes they are designed to control. However, all LEV systems have one particular design parameter in common - capture velocity. Capture velocity is defined as the "air velocity at any point in front of the hood, or at the hood opening, necessary to overcome opposing air currents and to captue the contaminated air at that point by causing it to flow into the hood" [1].

Empirically determined equations for calculating the air flow necessary to provide a specific capture velocity have appeared in the literature since Dalla Valle's[2] work in the 1930's. Since that time, several investigators have approached the determination of centerline capture velocity from both the empirical and theoretical standpoint[3-13]. As a basis for the LEV design process, capture velocity has several drawbacks. Deficiencies include: 1) the inability to account for the effect of cross drafts or other air disturbances, 2) the uncertainty involved in shaping the hood and distributing face velocity for the most efficient capture of contaminant[14], 3) the inability to accommodate hot sources or obstructions in the flow, [15] 4) difficulty in application to large contaminant sources, [13] and 5) the inability to predict contaminant concentration in the vicinity of the worker[16].

The most fundamental deficiency in designing an LEV system to provide a specific capture velocity is that it does not tell the designer how effective he or she will be in achieving the overall goal of reducing the concentration of contaminant in the employee's breathing zone. Even when the target capture velocity is achieved, a method does not exist which relates this velocity to the breathing zone concentration. Similarly, a designer who wishes to reduce employee exposure below a specified action level does not have a method for quantitatively determining the ventilation required to do so. One cannot say, for example, that if a particular capture velocity is provided, a certain level of protection is achieved.

Clearly, a method of LEV design that somehow relates design parameters to breathing zone concentration would be most useful in employee protection. However, before such a design method can be developed, it is necessary to understand how the air drawn past

the worker can interact with the contaminant source and give rise to concentrations in the breathing zone.

Analytic models describing flow fields into exhaust hoods[13,16,17] use potential theory as the theoretical basis. In potential flow the air is inviscid, incompressible (constant density) and irrotational (negligible local angular velocity)[18]. These assumptions are valid in the free field where an object is not present to obstruct the flow. While these models have certain applications, instances arise when the worker becomes a significant obstacle in the path of air flowing into the hood.

An object (such as a person) in the flow field calls into question the validity of potential theory in two ways. First, by its very presence, the object is a physical obstruction to the flow of air into the hood. As such it perturbs the boundary conditions for the solution of Laplace's equation. Second, and most important for the discussion here, when fluid flows past a blunt body, a boundary layer is formed on the surface of that body. A portion of the fluid adheres to the surface of the object and thus, near the surface, the motion of a thin layer of the fluid is retarded by frictional forces. Within this layer, fluid velocity increases from zero (at the surface) to the velocity of the free stream (external frictionless flow). This thin layer is called the boundary layer, and is a region in which the viscosity plays a major role, thus violating the inviscid assumption of potential theory.

As fluid approaches a blunt object, e.g. a circular cylinder, a boundary layer forms on the upstream side as depicted in Figure (1). If the flow is frictionless, fluid particles experience increasing acceleration on the upstream side of the cylinder and increasing deceleration on the downstream side. According to Bernoulli's equation this results in decreasing pressure on the upstream side and increasing pressure on the downstream side. Outside the boundary layer the flow is nearly frictionless while inside large frictional forces exist due to the large velocity gradient across the layer.

Consider a fluid particle in the boundary layer moving around the cylinder adjacent to the surface. Because of the high frictional forces inside the layer, the particle uses a

large portion of its kinetic energy circumventing the upstream side of the cylinder. Not enough kinetic energy is left to allow it to continue on its path around the body into the area of increasing pressure on the downstream side. It eventually stops and, because of the increasing pressure in the direction of flow (adverse pressure gradient), it begins moving in the opposite direction (reverse flow). A vortex forms, grows in size, separates from the cylinder surface, and moves downstream.

The point at which separation occurs depends on several factors, one of the most important being the laminar or turbulent nature of the boundary layer. Separation occurs sooner in laminar flow than in turbulent flow. Turbulent flow is more resistant to the adverse pressure gradient and separates farther along the downstream side. This results in a broad wake for laminar flows and a narrower one for turbulent flows[18]. The critical Reynold's number for transition to a turbulent boundary layer on a smooth circular cylinder is on the order of 3×10^5 [19].

The practical importance of this zone of reverse flow is evident when one considers an employee working in a typical position relative to LEV. Employees are normally instructed to position the work between themselves and the source of local exhaust. In this orientation, the worker becomes an obstruction in the flow field and boundary layer separation may occur as the air flows past the worker. Thus, this zone of reverse flow and turbulent mixing develops immediately downstream of the worker. If the source of contaminant is located within this zone, it will be drawn back toward the worker giving rise to significant concentrations of contaminant in the breathing zone. Air entrained into this mixing zone by the vortex formation ultimately determines the concentration of contaminant in it.

The effect of reverse flow on breathing zone concentration was studied by Ljungqvist[20] using a smoke diffuser. The diffuser was placed in a uniform air flow of approximately 0.25 m/s (50 fpm). With no obstruction in the flow, the smoke moved directly toward the LEV source. However, when a test person was placed between the diffuser and the source of air flow, the smoke was clearly directed back toward the person's breathing zone. Ljungqvist

attributes this phenomenon to the stationary wake produced by the person in the air flow. He states that individuals in the flow field create two kinds of vortices; the wake caused by the body itself and those arising from movements of the body. He concludes that either of these two wake structures can completely destroy the intended beneficial effect of an LEV system and that no consideration appears to be given to this problem in standard ventilation design.

In studying push-pull ventilation systems, Hampl and Huges[21] also demonstrate the effect of a person in the flow field of a ventilation system. They observed the collection of smoke by a standard LEV hood with various orientations of air jets used as "pushing" air streams. For each orientation where a test mannequin obstructed the pushing jets, smoke was observed in the area in front of the mannequin. However, when the jet was placed between the smoke and the mannequin, no smoke was observed in the breathing zone and all smoke was captured by the hood. They conclude that the "push jet should be located so that the air impinging on the worker or other obstruction should be minimized".

Van Wagenen[22] studied the effects of positive air flow (blowing rather than exhausting air) on concentrations of various contaminants in a welder's breathing zone. He demonstrates that when directional air flow comes from directly behind the welder, concentrations of fume in the breathing zone are equal to or higher than the breathing zone concentration without any air flow at all. He attributes this to the eddy and convective currents around the welder's body. He also notes that positive air flow at 90^o to the welder's position significantly reduces breathing zone concentration compared to the case without any air flow.

The inability of current design procedure to predict breathing zone concentration is a serious obstacle to optimal LEV design. Understanding the interaction of the reverse flow vortices (formed by the separating boundary layers) with a contaminant source downstream of a worker and how this process transports contaminants into and out of the breathing zone is an important factor in making this prediction. A thorough understanding of this

phenomenon is needed in order to develop models of contaminant concentration within the breathing zone. The purpose of this research is to develop a mathematical relationship to estimate breathing zone concentration as a function of the contaminant flow rate and local exhaust design parameters.

THEORY

The theoretical basis for estimating the concentration of pollutant released in a separated, near-wake zone is extremely complex. The governing equations include the Navier-Stokes, continuity, and species conservation equations. Successful three-dimensional, high-Reynolds number, numerical simulations of near-wake separation bubbles have not been reported, to our knowledge. The most successful approach seems to be a combination of dimensional analysis and wind tunnel experimentation in the area of estimating pollutant concentrations down wind of simple rectangular cubes[23]. This approach has been pursued primarily in regard to tackling the problem of re- entrainment of pollutants discharged from buildings[24]. Research suggests the mechanism of contaminant removal from the recirculation zone may be either turbulent diffusion, or vortex shedding, depending on whether the flow is more nearly two or three-dimensional[25].

A simple conceptual model based on treating the worker as a two-dimensional circular cylinder is presented here with the assumption of vortex shedding as the principal contaminant removal mechanism. A recirculation zone is hypothesized to exist downstream of the cylinder (worker), and a point source of contaminant is releasing tracer gas at a flow (Q_s) within the zone. Contaminant is being removed from the zone by the alternate shedding of vortices. The average steady-state concentration (C_{st}) within the zone is:

$$C_{st} = \frac{Q_s}{Q_v} \tag{1}$$

where Q_s is the contaminant flow into the zone, and Q_v is the air flow out of the mixing

zone.

Recall that vortices form on the downstream side of an object in uniform flow, grow, and separate into the freestream. As vortices move away from the body, a regular, alternating pattern of shedding is noted. The frequency with which these vortices are shed is described by a dimensionless quantity called the Strouhal number (S):

$$S = \frac{fD}{U} \tag{2}$$

where f is the frequency of vortex shedding, D is the diameter of object, and U is the velocity of fluid stream. The Strouhal number remains constant at about 0.21 for Reynolds numbers from 400 to about 200,000[26]. In an industrial setting, Reynolds numbers around workers will almost always fall below 200,000.

Solving equation (2) for f and substituting 0.21 for S gives the frequency with which these vortices are shed downstream:

$$f = \frac{0.21U}{D} \tag{3}$$

The frequency is from one side of the cylinder only and the vortices are formed alternately first on one side of the cylinder then on the other. The total frequency at which a vortex is shed from either side of the cylinder is twice the frequency from a single side, or $2f$. The air entrained into the near-wake region is proportional to this total frequency and the volume of the eddies shed.

If the dimensions (volume) of these vortices were known, an estimate of the rate at which contaminant is removed from the zone (via vortex shedding) could be obtained. A first order approximation for the volume of such a vortex is based on the concept of the formation region. The formation region is the zone immediately downstream of the cylinder and extends until fluid from outside the wake crosses the wake axis[27]. Studies[28,29]

suggest that the formation region is approximately a cylinder diameter wide in the range of Reynold's numbers studied here. If one assumes the height of the formation region is as tall as the cylinder (H) and one half the volume is cleared with each vortex shed[25], then the vortex volume (V) is:

$$V = \frac{\pi}{8} D^2 H \tag{4}$$

Since:

$$Q_v = 2fV \tag{5}$$

a simple approximation for the average steady state concentration is:

$$C_{st} = \frac{19 Q_s}{\pi U H D} \tag{6}$$

The principal assumption of this approach is that vortex shedding is the predominant mechanism in contaminant removal from the breathing zone of a worker. In contrast to this convective-air-movement approach is the idea of contaminant removal by turbulent diffusion. Many researchers studying the transport of contaminant in the wake downstream of a bluff body consider turbulent diffusion to be the most important consideration[30-32].

MATERIALS AND METHODS

In an attempt to obtain an empirical estimate of the size and nature of this reverse flow zone, a visualization study was conducted. A continuous source of smoke was achieved by blowing room air through a suction flask containing titanium tetrachloride. A dense smoke was forced out of the flask, through several feet of tygon tubing, and out of a 0.64 cm (0.25 in.) diameter glass tube mounted on a ring stand. Thus, a cloud of white smoke

could be continuously generated. Figure (2) illustrates this smoke source in a uniform air velocity of approximately 0.5 m/s (100 fpm).

An anthropometric mannequin was also placed in the flow in two different orientations (A and B). In orientation A, the air flow comes from behind the mannequin (typical orientation of worker with respect to LEV). The effect of the mannequin on the smoke source in this orientation is depicted in figure (3). In orientation B, the smoke source is still in front of the mannequin, but the uniform air flow comes from the side of the mannequin rather than from behind. Figure (4) illustrates the behavior of the smoke with the mannequin in orientation B.

To study quantitatively the impact of this turbulent mixing zone on worker exposure, a separate experiment was designed to examine the breathing zone concentration of a tracer gas contaminant. As with the smoke, the mannequin was positioned in orientations A and B. In each orientation the source of contaminant was placed in front of the mannequin. In orientation A, the source of contaminant was between the mannequin and the LEV source. Thus, the opportunity existed for the separated boundary layer to interact with the source and pull contaminant back toward the mannequin. In orientation B, with flow at 90^o, the turbulent zone was formed to the side of the mannequin with less of a chance for interaction with the source.

Exposure comparisons between the two orientations were made by placing a contaminant source at specified distances from the mannequin in each orientation and monitoring the breathing zone concentration. Curves were obtained by plotting breathing zone concentration as a function of the distance (Z) from the source to the mannequin's chest along a line parallel to the wind tunnel floor. To determine any effects due to velocity, these concentration versus distance curves were obtained at three different wind tunnel velocities.

The experiments were carried out in a wind tunnel 1.52 m high X 1.52 m wide X 2.44 m deep (5 ft. X 5 ft. X 8 ft.). The tunnel was equipped with an airfoil and honey-

comb at the entrance to reduce turbulence. The rear wall of the tunnel consisted of peg board with 0.64 cm (0.24 in.) holes. This board served to create a perforated plenum for better air distribution across the tunnel. The average air velocity in the wind tunnel was determined by obtaining a velocity profile at three different tunnel depths. Each profile consisted of twenty equally spaced points at a tunnel cross section for a total of sixty measurements. The arithmetic mean of all velocity values was taken as the average tunnel velocity. Measurements were obtained with a calibrated "hot wire" anemometer. A blast gate was installed in the duct leading to the tunnel to regulate air flow.

Data were taken at wind tunnel velocities of; 0.25 m/s (49 fpm), 0.77 m/s (152 fpm), and 1.35 m/s (265 fpm). [Note: Since the tunnel was calibrated without the mannequin in place, these velocities have been adjusted in proportion to the amount of tunnel cross section blocked by the mannequin, approximately 6%]. These velocities were selected to give Reynolds numbers in the same range as those for air flowing around a worker in a uniform flow such as a spray booth. The Reynolds numbers associated with these velocities are 3368, 10,443, and 18,343 respectively. The diameter used to calculate the Reynolds numbers is the breadth of the mannequin chest as measured just under the armpits (20.3 cm (8 in.)).

The anthropometric mannequin used was a commercial mannequin 1.04 m (3.42 ft.) tall and 20.3 cm (8 in.) wide at the chest. One end of a 0.64 cm (0.25 in.) rubber hose was inserted into the back of the mannequin's head and mounted in the mouth about 10.2 cm (4 in.) from the top of the head. The other end of the hose was connected to a Mobile Infrared Analyzer (MIRAN) located outside of the tunnel. In this manner the MIRAN samples from the "breathing zone" of the mannequin.

Sulfur hexafluoride (SF_6) was the tracer gas selected for this experiment. The gas was metered from a certified-standard, gas cylinder of 10% SF_6 through a 0.64 cm (0.25 in.) diameter ceramic sphere. The sphere was mounted on a ring stand approximately 0.69 m (2.25 ft.) from the floor of the wind tunnel. Pores in the sphere allow the gas to diffuse in

all directions. The flow of pure SF_6 was 2.36 X 10^{-7} m^3/s (0.0005 cfm) in all experiments.

The mannequin was placed on the centerline of the wind tunnel about 0.6 m (2 ft.) from the tunnel face in the typical orientation with respect to exhaust (i.e. facing the rear of the tunnel). The SF_6 diffuser was also placed on the centerline of the tunnel at a distance of 1.27 cm (0.5 in.) downstream of the mannequin. Thus the source of contaminant was between the mannequin and the source of exhaust.

The tunnel velocity was set at 1.35 m/s (265 fpm) (corrected velocity) and the SF_6 flow at 2.36 X 10^{-7} m^3/s (0.0005 cfm). The system was allowed to equilibrate for 10 minutes, then the breathing zone concentration, as measured by the MIRAN, was logged and integrated over a 10 minute period with a data logger. In this manner, a time weighted average concentration was obtained for that 10 minute period at the given distance. After the logging period, the SF_6 source was turned off and the tunnel was allowed to purge for 10 minutes. After the purging period the SF_6 diffuser was moved 2.54 cm (1 in.) downstream and the process was repeated. Thus, concentrations were obtained at distances ranging from 1.27 cm to 45.72 cm (0.5 in. to 18.0 in.). The experiments were repeated at 0.77 m/s (152 fpm) and then 0.25 m/s (49 fpm).

A repeat of the entire procedure was conducted with the mannequin in orientation B, i.e., with air flowing from the side. The contaminant source was again moved incrementally outward, away from the mannequin's body, and the breathing zone concentration measured for each distance.

RESULTS

The results of the smoke experiment are shown in Figures (3) and (4). When the smoke source was within about 0.31 m (12 in.) of the mannequin in orientation A, the majority of the smoke was drawn back toward the mannequin and swirled within the breathing zone. As the distance between the smoke source and the mannequin increased beyond 0.31 m

(12 in.), the amount of smoke drawn back toward the mannequin decreased. However, the effect of the turbulent zone on the smoke source could still be observed out to distances of about 0.46 m (18 in.). In orientation B, with flow coming from the side, virtually none of the smoke was drawn back into the mannequin's breathing zone (Figure (4)). The smoke moved downstream in basically the same pattern as that from the unobstructed source.

Results for the quantitative experiments are given in Figures (5), (6), and (7) which plot breathing zone concentration as a function of the distance from the source to the mannequin. The upper curve represents flow coming from behind the mannequin (typical worker orientation A) and the lower curve plots each of the same points with flow coming from the side (orientation B). Note from these plots the significant difference in breathing zone concentration between the two orientations. At each velocity, the breathing zone concentration was much greater with the mannequin oriented in the typical position with respect to LEV than when orientated with flow coming from the side. As with the smoke, this effect was particularly pronounced out to distances of at least 0.31 m (12 in.).

Figure (8) illustrates the data (orientation A) plotted in dimensionless terms. The horizontal axis is a dimensionless distance term, R/D where R is the straight line distance from the mannequin's mouth to the SF_6 source and D is the width of the mannequin at the chest. The vertical axis is the natural logarithm of another dimensionless term, C_{bz}/C_{wm}, where C_{bz} is the measured breathing zone concentration and C_{wm} refers to the overall "well mixed" concentration within the tunnel (source flow/tunnel flow).

Plotting the data in this manner effectively collapses the concentrations observed at all three velocities on to a single line. A least-squares regression analysis of this data gives the following empirical formula:

$$C_{bz} = 695 C_{wm} (0.135)^{R/D} \tag{7}$$

with an $r^2 = 0.94$. Thus, for this data set, most of the variability in breathing zone

concentration can be explained by the factors considered in this study. Knowing the distance from the mannequin to the source, the mannequin width, the source flow and the tunnel flow, the breathing zone concentration can be predicted with reasonable accuracy.

The theoretical predictions of the steady state concentration (C_{st}) in the mixing zone given by eq.(6) are compared with the average measured breathing zone concentration (C_{bz}) within one body distance (i.e. 8 inches) in Table I. This average measured value is calculated as the arithmetic mean of the readings taken out to 8 inches from the mannequin's body, at a given velocity. As the data shows, agreement is quite good with the error ranging from +11% to a -17% and correlated with Reynolds number.

DISCUSSION

With the mannequin in orientation A, i.e., uniform air flow from behind, the effect of the separated boundary layer is noted at distances of at least 0.31 m (12 in.) in both the smoke and the SF_6 experiments. Assuming that a linear extrapolation to a person 0.5 m (20 in.) at the chest is appropriate, this would indicate that a significant amount of contaminant could be drawn back toward a worker from a contaminant source as far away from the body as 0.75 m (30 in.). Thus, boundary layer separation is likely to be important in virtually any operation in which the source of contaminant is handled, and a nearly uniform air flow is present e.g. spray painting.

On the other hand, when the mannequin is positioned with flow coming from the side, the turbulent zone formed by the separated boundary layer has less opportunity for interaction with the source. This is reflected by the fact that virtually no smoke and very little SF_6 is detected in the breathing zone of the mannequin in this orientation.

At each velocity, the peak concentration occurs at a source distance of about two inches. At this distance the source is essentially in the hands of the mannequin. The peak is most probably due to the effect of additional turbulent air motion around the hands and

arms of the mannequin.

The reasonable agreement between the theoretical prediction of eq.(6) and the average of the measured breathing zone concentration within one body width is encouraging. The results suggest the importance of vortex shedding. The fact that eq.(6) overestimates at low velocity (Reynolds number) and underestimates at high velocity may reflect the growing importance of turbulent diffusion and enhanced transport. Further research is underway to evaluate and model the mechanisms of transport into and out of the mixing zone.

CONCLUSIONS

The mannequin experiments suggest that boundary layer separation plays a significant part in determining the concentration of contaminant in the breathing zone. The interaction of the separated boundary layer with a contaminant source downstream of a person in uniform flow can pull contaminant back into the breathing zone of the person. This is indicated by the higher concentration measured when the mannequin is in the typical worker position with the air flow coming from behind and the contaminant source downstream. The amount of contaminant observed in the breathing zone is much less when the mannequin is positioned such that the air could flow from the side. The turbulent mixing zone is formed more to the side of the mannequin and thus has less opportunity to interact with the contaminant source.

These results suggest that in situations such as paint booths where a worker is immersed in a uniform flow, a higher level of control may be achieved by standing to the side the workpiece rather than with the back to the flow. One should be cautious when extrapolating to real life situations, however. A stationary mannequin and a passive source were studied in this experiment. In industrial situations, workers are seldom stationary and contaminant sources are not typically passive, i.e., contaminant usually issues from

the source with some momentum and direction. In addition, the influence of other obstructions, i.e. workpieces and machinery, and the boundary layers associated with them must also be considered. Although these restrictions may limit the applicability of the results; it appears that improvement in contaminant control is possible by considering worker orientation with respect to air flow.

The ability to draw one line through all the data with such a high correlation indicates that some consistent mechanism(s) such as vortex shedding and/or turbulent diffusion are at work removing contaminant from the reverse flow zone. While the simple model presented in eq.(6) and the approximate agreement with data does not in itself confirm vortex shedding as the mechanism, it does provide a reasonably accurate conceptual model. If vortex shedding is, in fact, the significant mechanism, the model previously discussed must be expanded to consider the three-dimensional nature of the problem. Recent visualization studies using the test smoke indicate that air flowing down over the mannequin's head into the mixing zone plays an important part in determining the dimensions of, and concentrations in, the mixing zone.

A theoretically complex problem relating to the effect of the separated boundary layer on breathing zone concentration is introduced when the freestream velocity is no longer uniform but accelerating. This is the case in the majority of industrial situations involving hoods for such operations as welding, manual powder transfer, etc. In front of a hood it would be expected that the additional acceleration given to the air as it moves around the object would alter the characteristics of the turbulent zone. It is possible that this additional acceleration may act to decrease the size and influence of this downstream vortical mixing zone. Additionally, air flows into a hood from all directions, causing velocity vectors in three dimensions as opposed to the two dimensional uniform flow situation studied here. Further research into this phenomenon is presently underway.

ACKNOWLEDGEMENTS

Support for this research was provided by the National Institute for Occupational Safety and Health, grant 5 R01 OH02392-01 and the Shell Oil Company Foundation.

REFERENCES

1. **American Conference of Governmental Industrial Hygienists**: *Industrial Ventilation - A Manual of Recommended Practice*, 19th ed. Lancing Michigan, American Conference of Governmental Industrial Hygienists, (1986).

2. **Dalla Valle, J.M.**: "Studies in the Design of Local Exhaust Hoods." Doctoral Dissertation, Harvard University, Boston, MA, 1930.

3. **Silverman, L.**: Centerline Velocity Characteristics of Round Openings Under Suction. *J. Ind. Hyg. Tox.* 24(9):257-266 (1942).

4. **Silverman, L.**: Centerline Velocity Characteristics of Narrow Exhaust Slots. *J. Ind. Hyg. Tox.* 24(9):267- 276 (1942).

5. **Fletcher, B.**: Centerline Velocity Characteristics of Rectangular Unflanged Hoods and Slots Under Suction. *Ann. Occup. Hyg.* 20:141-146 (1977).

6. **Fletcher, B.**: Effects of Flanges on the Velocity in Front of Exhaust Ventilation Hoods. *Ann. Occup. Hyg.* 20:265-269 (1978).

7. **Fletcher, B.; Johnson, A.E.**: Velocity Profiles Around Hoods and Slots and the Effects of an Adjacent Plane. *Ann. Occup. Hyg.* 25:365-372 (1982).

8. **Garrison, R.**: Centerline Velocity Gradients for Plain and Flanged Local Exhaust Inlets. *Am. Ind. Hyg. Assoc. J.* 42(10):739-746 (1981).

9. **Garrison, R.**: Velocity Calculation for Local Exhaust Inlets - Empirical Design Equations. *Am. Ind. Hyg. Assoc. J.* 44(12):937-940 (1983).

10. **Garrison, R.**: Velocity Calculation for Local Exhaust Inlets - Graphical Design Concepts. *Am. Ind. Hyg. Assoc. J.* 44(12):941-947 (1983).

11. **Tyaglo, I.G.; Shepelev, I.A**: Dvizhenie vozdushnogo potpha k vytyazhnomu otverstiyv [Air Flow near an Exhaust Opening]. *Vodosnabzhenie i Sanitarnaya Tekhnika.* 5:24- 25 (1970) [in Russian].

12. **Drkal, F.**: Stromungsverhaltnisse bei runden Saugoffnungen mit Flansch [Flow Conditions near Flanged Round Openings under Suction]. *Heiz. Luft. Haustech.* 21:271-273 (1970) [in German].

13. **Flynn, M.R.; Ellenbecker, M.J.**: The Potential Flow Solution for Air Flow into a Flanged Circular Hood. *Am. Ind. Hyg. Assoc. J.* 46(6):318-322 (1985).

14. **Ellenbecker, M.J.; Gempel, R.F. ; Burgess, W.A.**: Capture Efficiency of Local Exhaust Ventilation Systems. *Am. Ind. Hyg. Assoc. J.* 44(10):752-755 (1983).

15. **Esmen, N.A.; Weyel, D.A.; McGuigan, F.P.**: Aerodynamic Properties of Exhaust Hoods. *Am. Ind. Hyg. Assoc. J.* 47(8):448-453 (1986).

16. **Heinson, R.J.; Choi, M.S.**: Advanced Design Methods in Industrial Ventilation. in *Ventilation '85 - Proceedings of the 1st International Symposium on Ventilation for Contaminant Control.* Elsevier Science New York (1985).

17. **Flynn, M.R.; Ellenbecker, M.J.**: Capture Efficiency of Flanged Circular Local Exhaust Hoods. *Ann. Occup. Hyg.* 30(4):497-513 (1986).

18. **White, F.M.**: *Fluid Mechanics.* 2nd ed. McGraw - Hill Book Company. New York (1986).

19. **Schlichting, H.**: *Boundary-Layer Theory.* 7th ed. McGraw-Hill Book Company, New York (1979).

20. **Ljungqvist, B.**: "Some Observations on the Interaction Between Air Movements

and the Dispersion of Pollution." Document D8, Swedish Council for Building Research. Stockholm, Sweden (1979).

21. **Hampl, V.; Hughes, R.T.**: Improved Local Exhaust Control by Directed Push-Pull Ventilation Systems. *Am. Ind. Hyg. Assoc. J.* 47(1):59-65 (1986).

22. **Van Wagenen, H.D.**: "Assessment of Selected Control Technology Techniques for Welding Fumes." Research Report, National Institute for Occupational Safety and Health Cincinnati, OH (1979).

23. **Vincent, J.H.**: Scalar Transport in the Near Aerodynamic Wakes of Surface-Mounted Cubes. *Atmos. Environ.* 12:1319-1322 (1978).

24. **Fackrell, J.E.**: Parameters Characterising Dispersion in the Near Wake of Buildings. *Journal of Wind Engineering and Industrial Aerodynamics.* 16:97-118 (1984).

25. **MacLennan, A.S.M.; Vincent J.H.**: Transport in the near Aerodynamic Wakes of Flat Plates. *J. Fluid Mech.* 120:185-197 (1982).

26. **Roshko, A.**: "On the Development of Turbulent Wakes from Vortex Streets". NACA Rep. 1191 (1954).

27. **Gerrard, J.H.**: The Mechanics of the Formation Region of Vortices Behind Bluff Bodies. *J. Fluid Mech.* 25:401-413 (1966).

28. **Norberg, C.**: Interaction Between Freestream Turbulence and Vortex Shedding for a Single Tube in Cross- Flow. *Journal of Wind Engineering and Industrial Aerodynamics.* 23:501-514 (1986).

29. **Bloor, M.S.**: The Transition to Turbulence in the Wake of a Circular Cylinder,. *J. Fluid Mech.* 19(2):290-304 (1964).

30. **Humphries, W.; Vincent, J.H.**: An Experimental Investigation of the Detention of Airborne Smoke in the Wake Bubble Behind a Disk. *J. Fluid Mech.* 73(3):453- 464 (1976).

31. **Humphries, W.; Vincent, J.H.**: Experiments to Investigate Transport Processes in the Near Wakes of Disks In Turbulent Air Flow. *J. Fluid Mech.* 75(4):737- 749 (1976).

32. **Humphries, W.; Vincent, J.H.**: Near Wake Properties of Axisymmetric Bluff Body Flows. *Appl. Sci. Res.* 32:649-669 (1976).

Table I. Comparison between Theoretical and Measured Average Concentrations in the Separated Boundary Layer

WIND TUNNEL VELOCITY (fpm)	THEORETICAL CONCENTRATION FROM EQ. #6 (ppm)	MEASURED CONCENTRATION (AVERAGE VALUE) (ppm)	ERROR
49	27.2	24.5	+11%
152	8.8	8.3	+1%
265	5.0	6.0	-17%

FIGURE CAPTIONS

Figure 1 - Boundary layer separation around a circular cylinder in uniform flow. Adapted from reference 18.

Figure 2 - Smoke source in an unobstructed uniform velocity of 100 fpm.

Figure 3 - Smoke source placed downstream of mannequin in orientation A (uniform velocity of 100 fpm). Arrow indicates direction of air flow.

Figure 4 - Smoke source placed downstream of mannequin in orientation B (uniform velocity of 100 fpm).

Figure 5 - Plot of SF6 concentration as a function of source distance for the typical position (orientation A) and the situation when air flow is from the side at 90^{o} (orientation B) in a uniform velocity of 49 fpm.

Figure 6 - Plot of SF6 concentration as a function of source distance for the typical position (orientation A) and the situation when air flow is from the side at 90^{o} (orientation B) in a uniform velocity of 152 fpm.

Figure 7 - Plot of SF6 concentration as a function of source distance for the typical position (orientation A) and the situation when air flow is from the side at 90^{o} (orientation B) in a uniform velocity of 265 fpm.

Figure 8 - Semi-Log plot of dimensionless concentration as a function of dimensionless source distance (orientation A) for different wind-tunnel flows (Q_h).

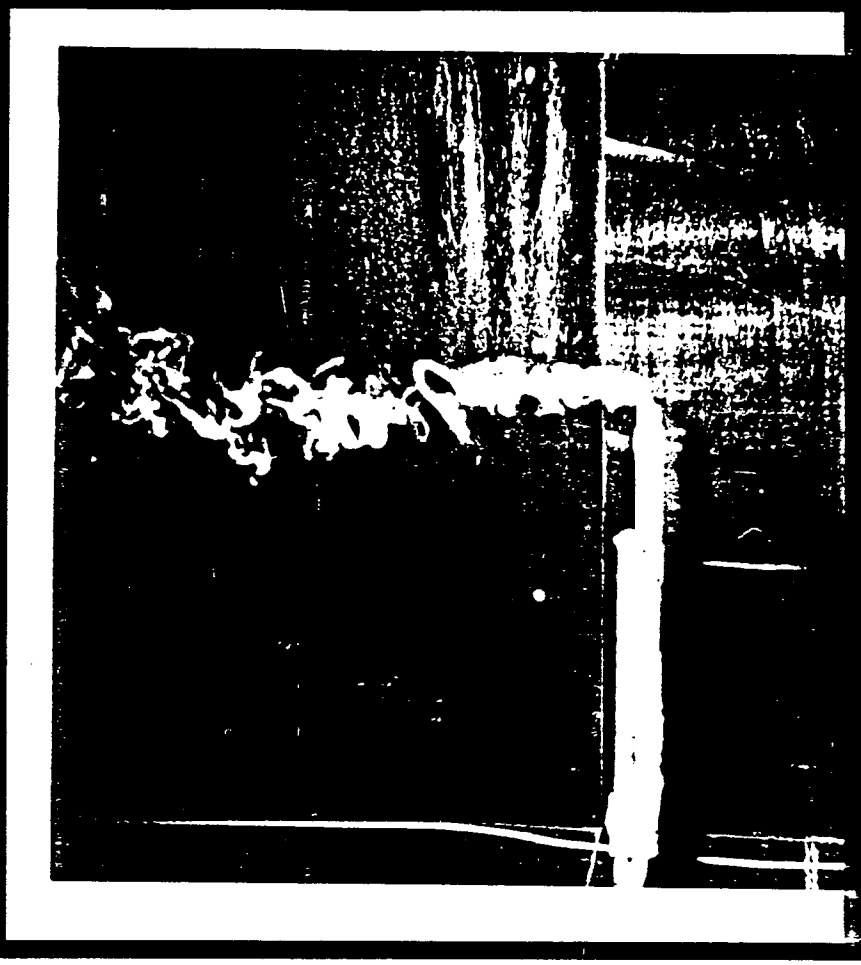

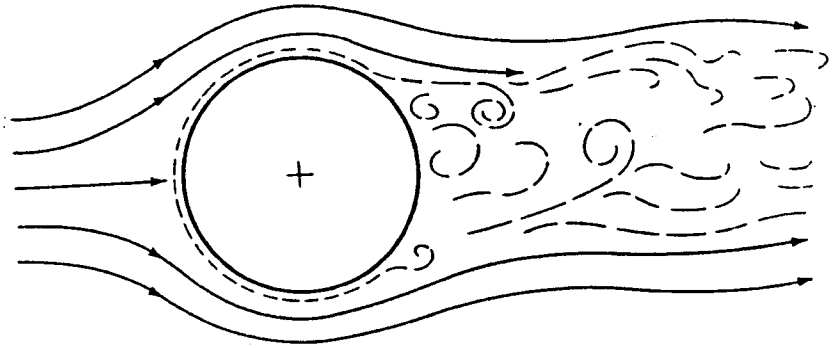

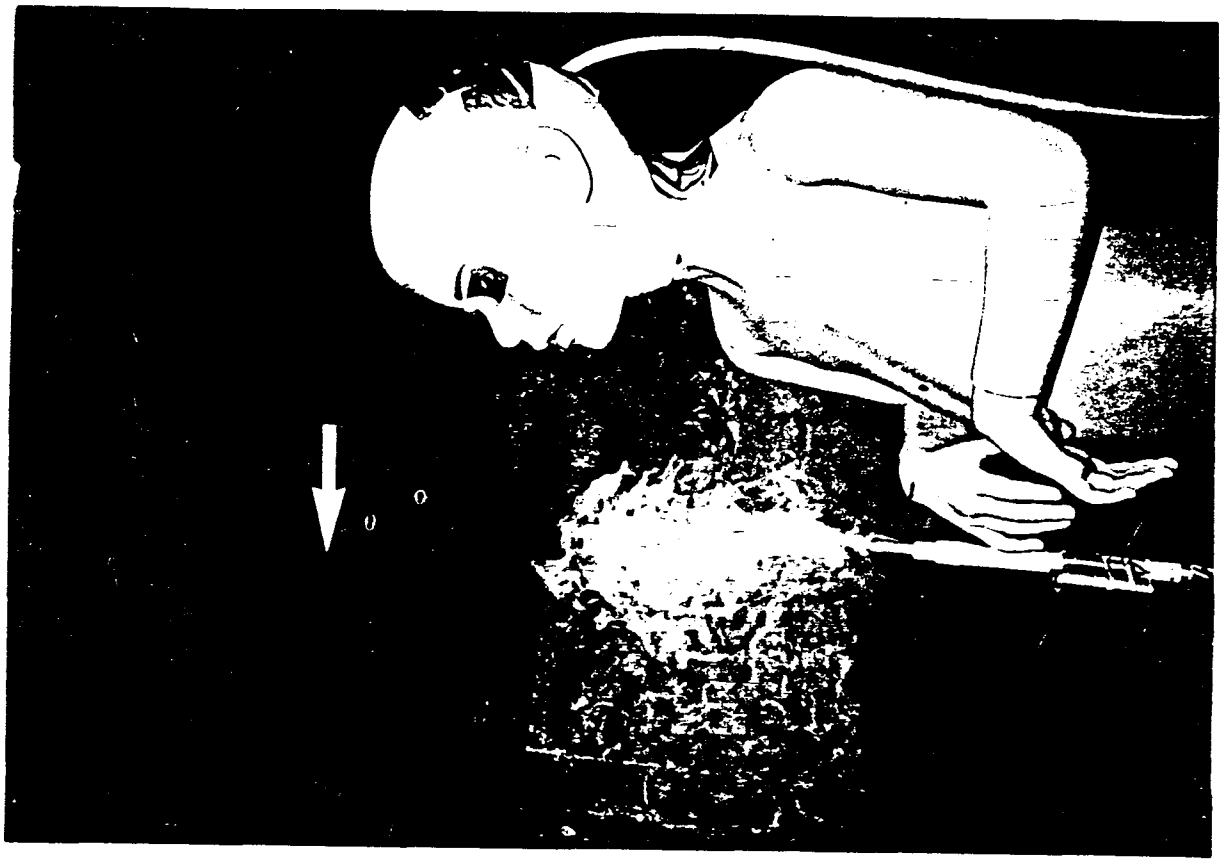

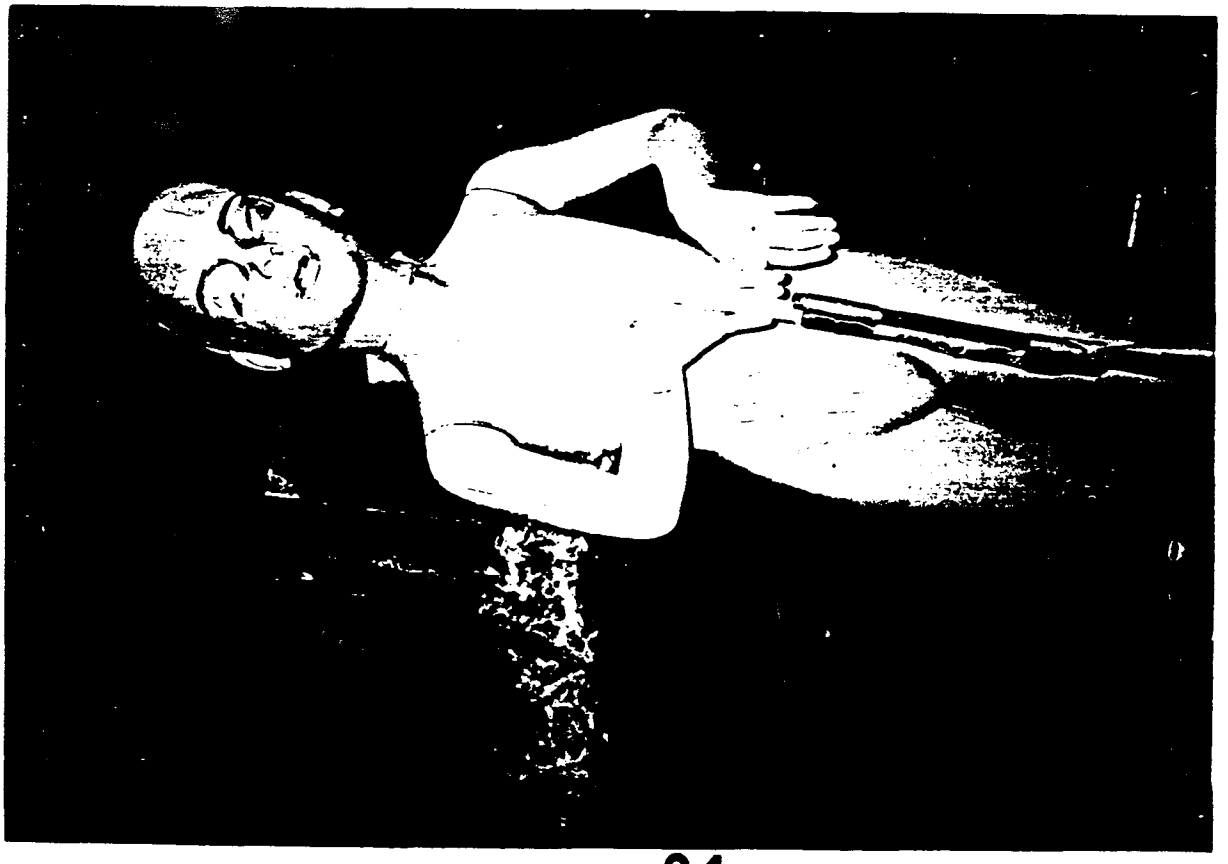

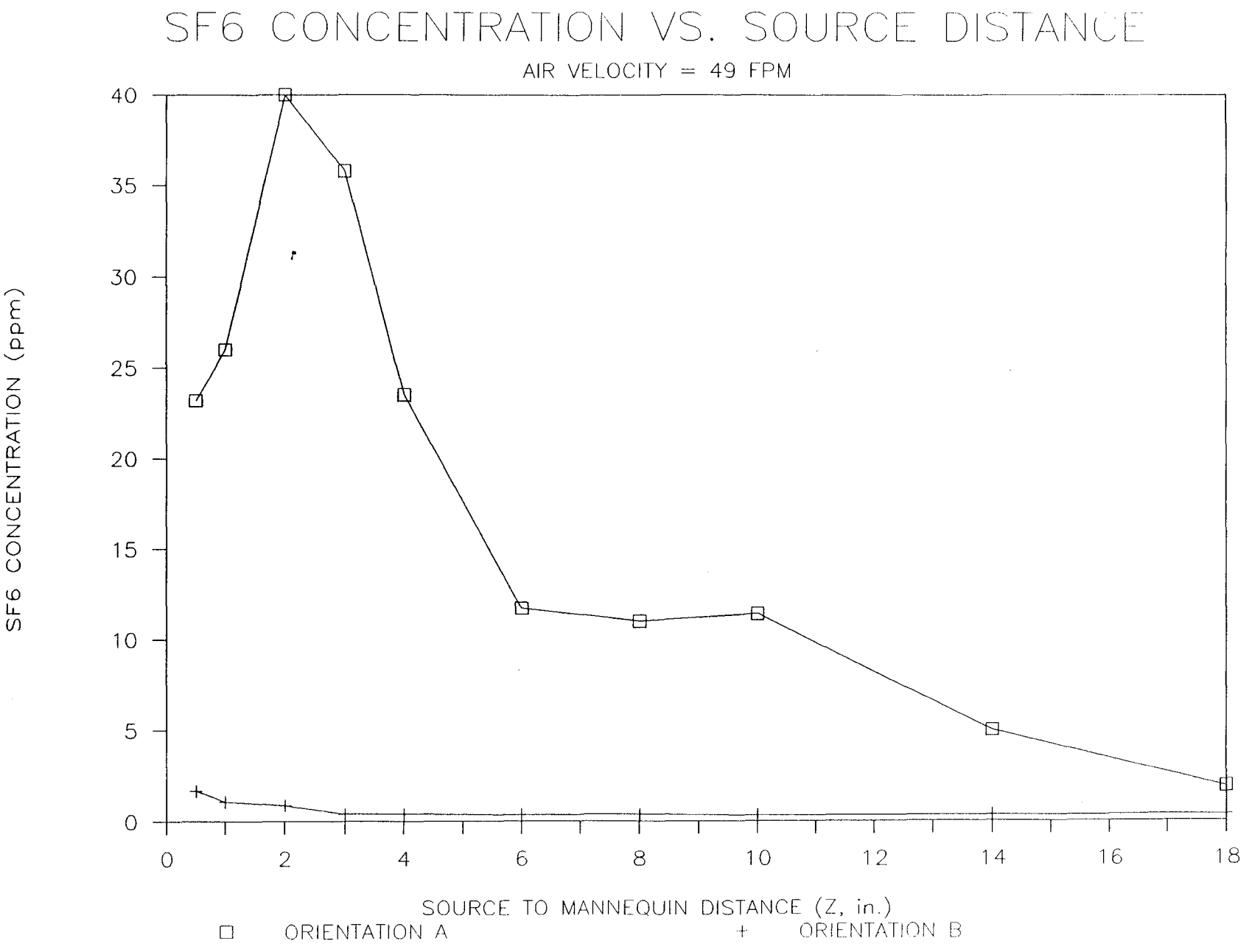
SF6 CONCENTRATION VS. SOURCE DISTANCE
AIR VELOCITY = 49 FPM
SF6 CONCENTRATION (ppm)
0
5
10
15
20
25
30
35
40
0
2
4
6
8
10
12
14
16
18
SOURCE TO MANNEQUIN DISTANCE (Z, in.)
ORIENTATION A
ORIENTATION B

SF6 CONCENTRATION VS. SOURCE DISTANCE

AIR VELOCITY = 152 FPM

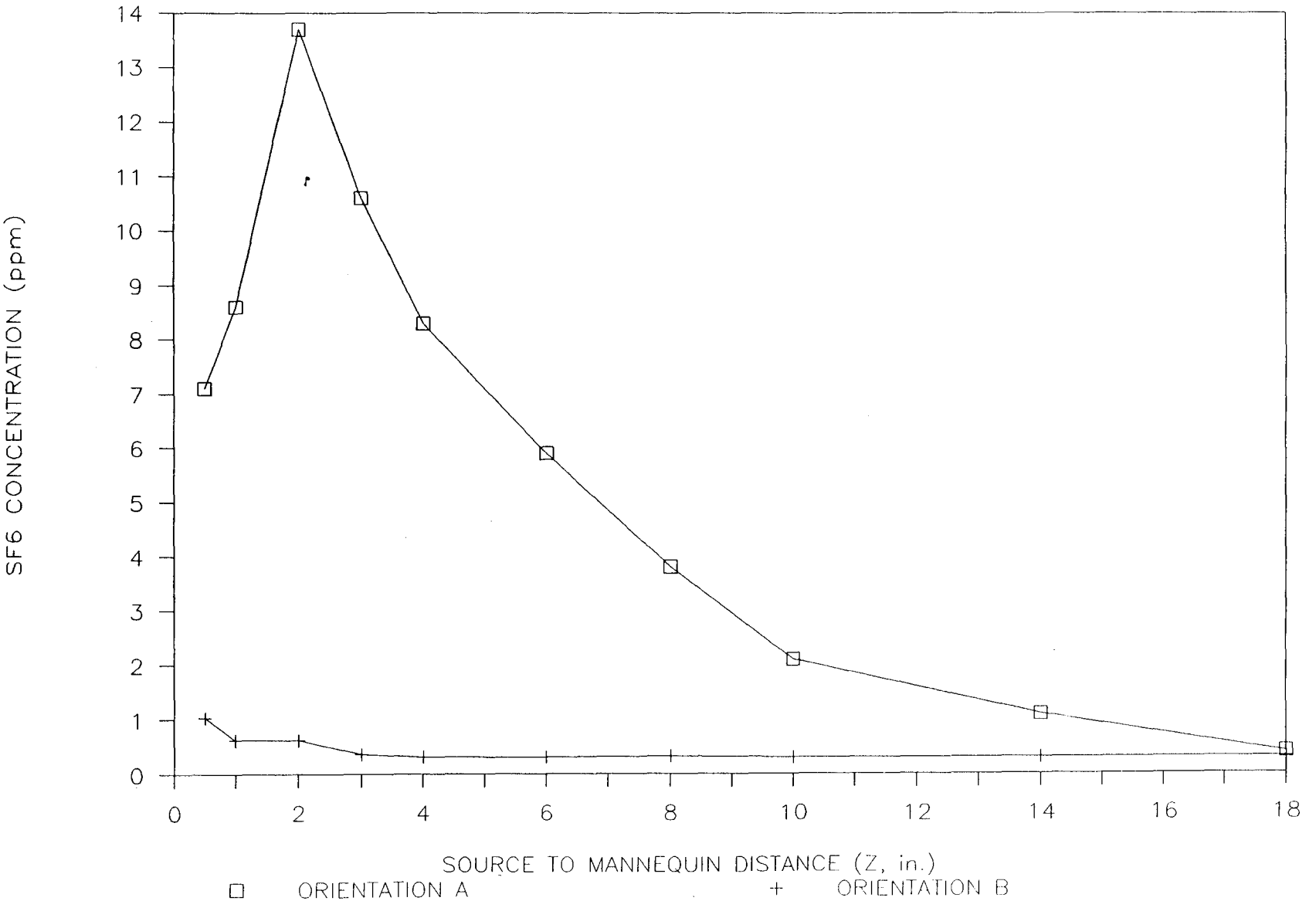

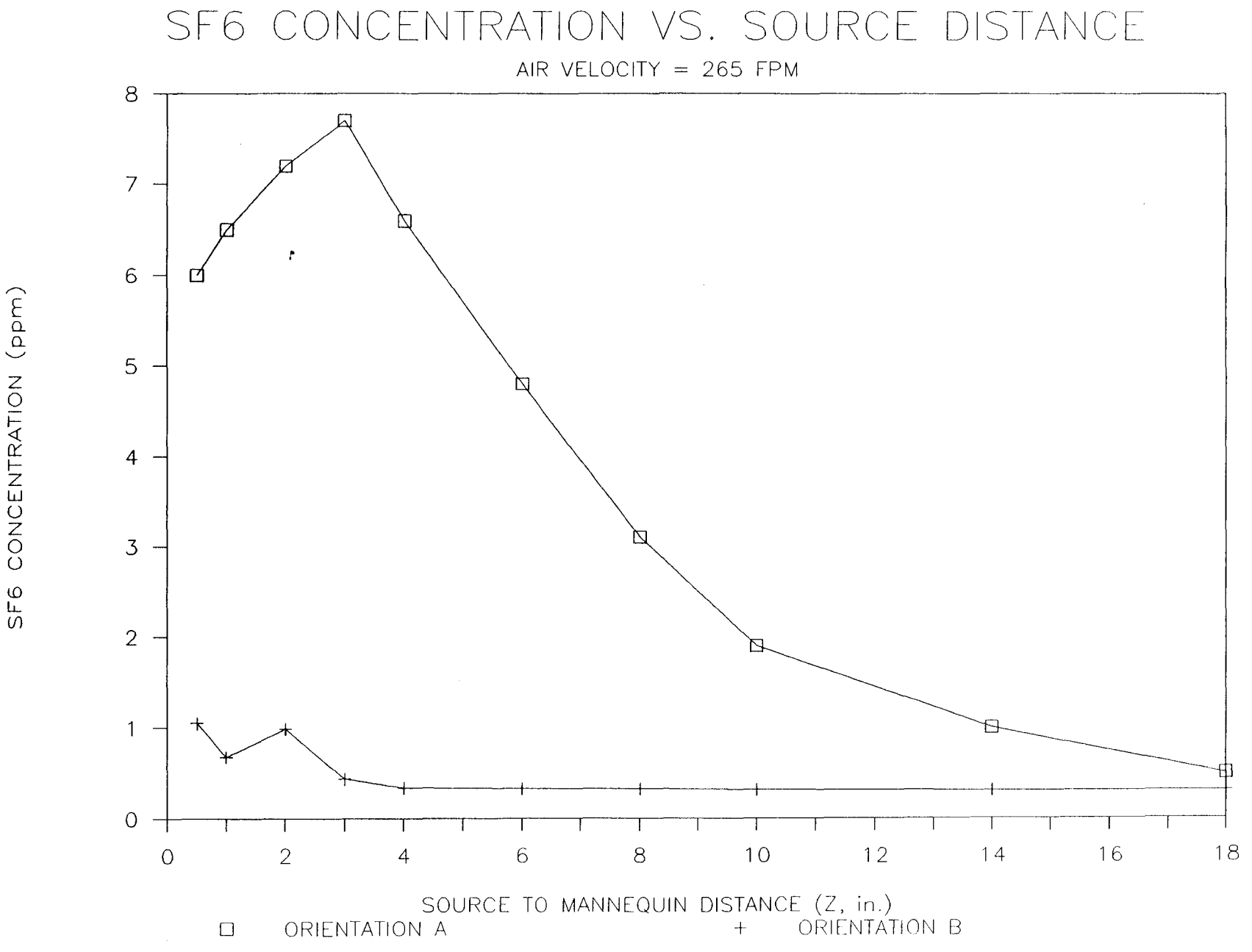
SF6 CONCENTRATION VS. SOURCE DISTANCE
AIR VELOCITY = 265 FPM
SF6 CONCENTRATION (ppm)
0
1
2
3
4
5
6
7
8
0
2
4
6
8
10
12
14
16
18
SOURCE TO MANNEQUIN DISTANCE (Z, in.)
ORIENTATION A
ORIENTATION B

MANNEQUIN BREATHING ZONE CONCENTRATIONS

Qs = 0.005 CFM OF 10% SF6

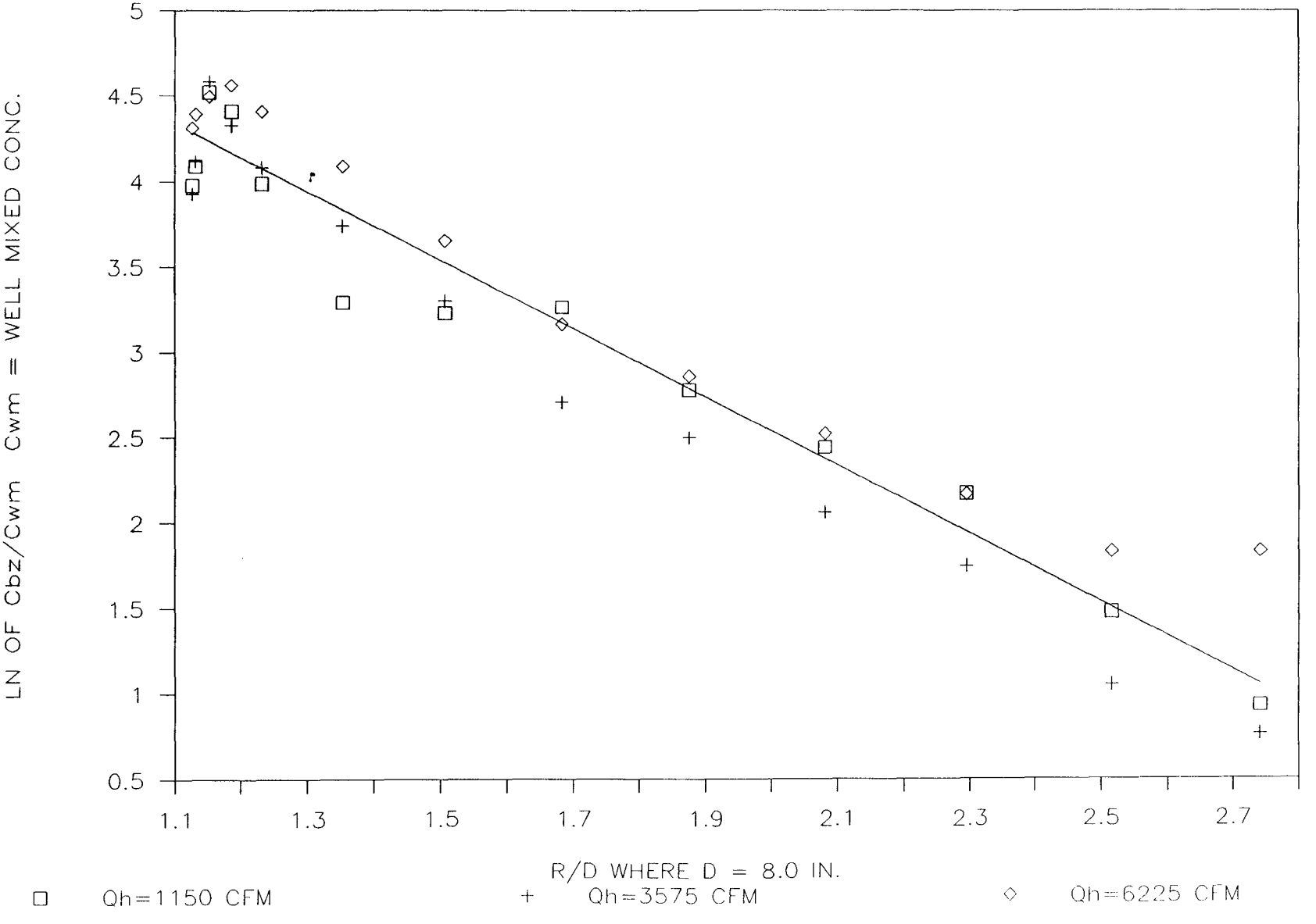

MANUSCRIPT II

Factors Affecting the Design of Local Exhaust Ventilation for the Control of Contaminants Hand-Held Sources

Factors Affecting the Design of Local Exhaust Ventilation for the Control of Contaminants from Hand-Held Sources

Michael R. Flynn, and William K. Shelton

Department of Environmental Sciences and Engineering,
University of North Carolina at Chapel Hill, Chapel Hill, NC 27599

Abstract – Tracer gas concentrations generated from a hand-held source are measured in the breathing-zone of a mannequin positioned in front of flanged circular exhaust hoods in various configurations. Statistical analyses suggest that, other things being equal, it is preferable to position the mannequin (worker) to the side of the hood rather than in the conventional orientation with source between the body and the hood. The experiments show an unexpected increase in exposure as the source-to-hood distance decreases for small hoods. The importance of work- practices used in conjunction with engineering controls is indicated.

Introduction

Local Exhaust Ventilation (LEV) is an engineering control designed to reduce the concentration of airborne pollutants to acceptable levels by removing the contaminant at its source. The ability to accomplish this depends upon the hood exerting a velocity field of sufficient strength to overcome the momentum of the source and induce capture before mixing into the breathing zone can occur.

The importance of the velocity field into the hood is reflected by current practice [1-2], and in LEV research.[3-6] The concept of capture velocity plays a central role in design; and formulas abound[7] for determining centerline velocity into hoods of various shapes and sizes. Studies[8-9] emphasize the importance of not only the velocity but the velocity gradient into the hood as well. Despite the emphasis on the velocity field and centerline

velocity in particular, there appears to be little work, experimental or otherwise, that relates the parameter of interest, i.e. breathing-zone concentration, to the basic design variables.

Many of the models for estimating hood velocity fields, both empirical and theoretical, are based on unobstructed flow into the inlet. In reality these hoods are often employed in situations where the worker holds some type of contaminant generating device, e.g. a welding electrode, in close proximity to the hood. The situation is now complicated by viscous flow around the worker which results not only from air moving around the body to enter the hood; but also from any body motions involved in performance of the task, and any air currents induced by the source itself.

The important questions from a control perspective are: (1) what are the critical factors (and their functional relationship) that determine whether the hood can capture the contaminant prior to its being mixed into the breathing zone; and (2) do velocity fields into unobstructed hoods provide the most reasonable predictor of the hood's ability to do this? This paper examines some of the factors important in answering question 1 while a companion paper[10] examines question 2.

Factors determining an individual's exposure who works with a hand-held source ventilated by an exterior hood include: (1) the mass flow of pollutant, (2) the source configuration and momentum, (3) the hood air flow, (4) the hood size and shape, (5) the distance of the worker from the hood, and (6) the position of the worker and source with respect to the hood. Other important factors include the activity level of the worker and workplace, the air supply configuration, and thermal factors. A complete characterization of the problem is complex, but the factors listed above can be manipulated carefully in an experiment to examine how the mixing region around a worker competes with the hood flow to affect exposure.

The experimental work presented here examines tracer gas concentration in the breathing zone of a mannequin from a small hand held point source as a function of the basic

design parameters mentioned above. The results suggest that the orientation of the worker with respect to the hood and the source, is an important variable in determining the concentration in the breathing zone. An unexpected interaction between hood size and source-to-hood distance is also observed.

Theory

The prediction of gas or vapor concentration in ventilated spaces is governed by a mass balance which states that the rate of accumulation is equal to the rate of generation minus the rate of removal:

$$V dC = Q_s dt - \frac{Q_h}{K} dt \tag{1}$$

where: dC is the differential concentration, dt the differential time, V the room volume, Q_s the contaminant flow, Q_h the ventilation exhaust air flow, and the K factor is used to account for non-uniform mixing. At steady state the average concentration in the room is:

$$C_{avg} = \frac{KQ_s}{Q_h} \tag{2}$$

If a source begins generating contaminant at time $t = 0$ in a one-inlet one-outlet (hood) room; and the hood captures a fraction, (η_e) of the source where η_e is a function of time; then the average concentration in the room at any time T is:

$$C(T) = \frac{Q_s}{V} \int_0^T (1 - \eta_e) dt \tag{3}$$

At steady state $\eta_e = 1.0$ and the concentration is given by equation (2). Thus, η_e which is the capture efficiency, must approach 1.0 in any real steady state situation. It is the integral of capture efficiency with respect to time which determines the volume of contaminant held up in the room at any particular moment. Exposure is related to this

"hold up" which is a function of the room mixing pattern, but more importantly in LEV applications, the mixing that develops in the vicinity of the worker, source, and hood.

As air moves around the worker toward the hood, boundary layer separation will occur and result in the formation of reverse flow eddies and turbulence capable of transporting contaminant back toward the breathing zone. The size and characteristics of the mixing zone formed in this fashion have been studied both experimentally[11] and from a theoretical perspective[12] for the case of a mannequin (worker) in a uniform onset flow. While these results might reasonably be extended to large booth-type hoods, the mixing zone formed between a worker and a smaller hood is not well characterized.

In addition to the boundary layer separation phenomenon, the body will act as an obstruction forcing more air to come from the sides (increased radial flow). This reduces the control velocity the hood can generate (reduced axial flow) and further vertical penetration of the contaminant into the breathing zone is possible. This altered flow pattern is likely to be exacerbated close to small hoods where, in the extreme case, the presence of the body begins to approach an infinite wall.

Both mechanisms described above are likely to be important in determining the effectiveness of local exhaust hoods. Research[11] shows the importance of the air flow direction in controlling exposure in uniform flow. In that instance it was preferable to keep the air flow at right angles to the line connecting a hand-held source and the breathing-zone. This orientation minimizes the size and "reach" of the mixing-zone.

The primary hypothesis of this work is that the same orientation is preferable in front of local exhaust hoods. The size and impact of the mixing-zone should be minimized in the 90° position and this position should also improve capture velocities. The purpose of this research is to test this hypothesis and determine which of the design variables are most important in reducing exposure.

Methods and Materials

A department store mannequin 41 inches in height was modified such that a continuous air sample could be withdrawn through the mouth. A 0.25 inch diameter diffusing stone was placed in the hands of the mannequin through which 10% sulfur hexafluoride tracer gas was metered at a flow of 0.78 lpm (0.027 cfm). The mannequin was positioned in front of flanged circular hoods in either one of two positions. In position 1 the source is on the centerline but the mannequin stands to the side such that a line connecting the source and mannequin is at right angles to the hood centerline. In position 2 the source is on the hood centerline as is the mannekin itself. This represents the standard configuration where the source is located between the hood and the worker. Figure 1 presents a plan view of the orientations.

Flanged circular hoods of 4, 9, and 12 inches in diameter were operated at flows of 100, 300, and 535 cfm. The mannequin-source configurations described above were positioned such that the source was located at either 6 or 9 inches from the hood face. An infrared spectrophotometer was used to measure sulfur hexafluoride concentration in the mannequin breathing zone over a period of 20 minutes. A data logger sampling at 1 Hz, stored half-minute averages for the 20 minute logging time. The time-weighted average concentrations for the last four minutes of the logging period were used as the variates in the statistical study.

The initial experimental design included four factors: (1) hood flow (Q), (2) hood diameter (D), (3) source-to-hood centerline distance (Z), and (4) mannequin position, 1 or 2, (POS). There are 36 combinations of experimental conditions; each was replicated twice resulting in 72 values of breathing zone concentration.

Results and Analysis

The raw data are presented in Table I. Table II displays results from an initial five-way ANOVA performed to evaluate the individual significance of each factor. The analysis confirms the absence of any bias in the repititions (the RUN variable) and illustrates the importance of position. A paired t-test confirms that concentration was significantly lower ($p < 0.01$) when the mannekin was oriented 90^o to the centerline (POS=1) than in the 180^o position (POS=2).

Originally a full four-way ANOVA was planned with all interaction terms however, despite control efforts, a certain background level of sulfur hexafluoride resulting from leakage on the positive pressure side of the fan persisted. The level was inversely correlated with flow through the hood, and was assessed in a worst case scenario for each of the three flows. The worst case contribution from leakage for the last four minutes of the logging period for the 100, and 300 cfm flow rates are respectively: 0.016 ppm, and 0.010 ppm. The leakage was negligible at the highest flow of 535 cfm. The inverse correlation of flow and leakage made the use of interaction terms across the flow variable questionable, therefore all analyses were performed either within a flow or by lumping all flows together.

A three-way fixed factor Model I ANOVA was run with mannequin position (POS), hood diameter (D), and source-to- hood distance (Z) as the fixed factors. All interactions were examined. The three-way Model I ANOVA is:

$$Y_{ijkl} = \mu + \alpha_i + \beta_j + \gamma_k + \alpha_i \times \beta_j + \alpha_i \times \gamma_k + \beta_j \times \gamma_k + \alpha_i \times \beta_j \times \gamma_k + \epsilon_{ijkl} \quad (5)$$

where Y_{ijkl} is a concentration measurement taken at the ith position, the jth hood diameter, the kth distance, and the lth replication. μ is the grand mean and ϵ is the error term, assumed to be normally distributed. The terms α, β, and γ are offsets from μ due to the effects of position (POS), hood diameter (D), and source-to-hood distance (Z) respectively.

The results of this ANOVA are presented in Table III. Position is significant, $p < 0.025$; as is the interaction between diameter and distance (Z×D) $p < 0.004$. The mean value of the measured concentration for position #1 is 0.018 ppm and for position #2, 0.021 ppm. Figure 2 presents a graph of the mean values of the measured concentration as a function of hood diameter at both the 6 and 9 inch distances. The curves appear almost inverted images; suggesting higher exposure at closer distances from the small hood.

Separate ANOVA's for each hood flow were also performed using the model in equation (5). These results are presented in Tables IV-VI in order of increasing flow. For a flow of 100 cfm the third order interaction of position, diameter, and distance is significant $p < 0.025$. At 300 cfm no term shows significance although diameter and distance are suggestive. At 535 cfm the conclusions of the overall ANOVA are replicated, i.e. significance of position and the interaction term of diameter and distance.

Discussion

The question of scaling to realistic flows and dimensions is important. In order to maintain geometric similarity experimental dimensions would have to be multiplied by a factor of from about 1.5 to 2. To maintain dynamic similarity i.e., Reynolds number equality, velocities would need to go down by the same factor. This translates into hood flows 1.5 to 2 times the experimental values. The Industrial Ventilation Manual[1] recommends capture velocities of 50-100 fpm for sources with negligible momentum, as is the case here. Based on the equations in the manual all centerline locations that were examined experimentally at the 535 cfm flow, will have at least a 50 fpm predicted capture velocity when scaled to actual conditions by the factors mentioned above.

In view of the leakage problem and the scaling issues, the emphasis is on results obtained at the 535 cfm flow. However, the ANOVA in Table II suggests that hood flow (Q), by itself is, a relatively unimportant variable in determining breathing zone concentration for the cases examined here. If, in fact, higher flows result in lower concentrations then

the leakage effect would accentuate this relationship, not obscure it. It is evident that the leakage does not cause a systematic bias by flow, and higher flow does not insure lower concentration, as might seem intuitive. Figure 3 presents mean concentration by flow for both positions. The plot indicates the consistent superiority of position #1 but also shows that the highest flow has both the maximum and minimum average exposure depending on position.

The most credible and important results are obtained at the 535 cfm flow. Here leakage is not a factor; the distance- diameter (Z-D) interaction and the position effect (POS) are reported with confidence. The results show that position #1 offers superior protection to the standard orientation other factors being equal. In addition, counter to what is expected, for the small hood the closer position results in greater exposure. Figure 4 shows the relationship between concentration and diameter for both Z locations at the 535 cfm flow when the worker is in position #2 (180°). At the Z=6 inch location, the concentration reaches a minimum with the 9 inch diameter hood while at the 9 inch position it reaches a maximum there. A similarly shaped curve is shown in Figure 5 for position #1 but without the dramatic differences.

The position effect has been cited[11,13-14] in other studies as a significant factor in determining exposure and it is confirmed here. If boundary layer separation is responsible then as the hood diameter grows large in relation to the worker a stronger effect would be noted. This is supported here by observing that the maximum concentration (0.041 ppm) occurred in position 2 with the large hood, at 535 cfm, and a source-to-hood distance of 6 inches. As the hood size approaches the mannequin width (about 8-12 inches) it is hypothesized that the tendency for air to flow around the mannequin rather than from the side increases, resulting in separation eddies and increased backflow. The observed increase in concentration as source- hood distance is reduced with the smaller hood may result from the body acting primarily as an obstruction; forcing increased radial flow from the sides and reducing control velocities. Boundary layer separation is also likely to be a

factor.

The results presented here were conducted in a room with essentially no crossdrafts or activity. Every effort was made to minimize disturbances which could not be accurately quantified. These laboratory conditions do not represent real world industrial operations. In many situations the hood will have to overcome air currents generated by the worker and/or surrounding equipment. Further research is needed to examine these factors and how their importance compares to the effects noted above. Extension of these results to actual operations must be done with caution. The source used here was a gas of very low velocity (about 20 fpm at the source). In situations where high velocities of generation are involved the importance of overcoming the source momentum must be considered as well.

Conclusions

Local exhaust hoods are designed to protect worker health by reducing the concentration of toxic airborne contaminants in the breathing-zone. This form of ventilation is one of the main engineering controls selected by industrial hygienists when more economical and effective methods are unsuitable for the operation in question. Local exhaust ventilation, (LEV) like all engineering controls, receives preference in the hierarchy of control options because it removes the responsibility for achieving control from the worker. The reasoning is that if the sysytem is well designed and maintatined, control is obtained without the worker needing to actively intervene. This in contrast to the personal protective equipment option where control requires the worker to not only wear the device properly but take responsibility for determining breakthrough etc.

The results presented here suggest that when a worker is involved with a low momentum, hand held source of pollution; positioning the body 90° to the centerline (POS=1) offers superior protection than the standard 180° orientation (POS=2). This orientation effect was the single most significant factor in controlling exposure observed in this study. The results argue for active training in work practices in conjunction with well-designed

engineering controls. The observation that exposure increases with proximity to the small hood at a fixed flow suggests more complicated aerodynamics are at work than can be addressed with the standard capture velocity approach.

Acknowledgements

Support for this research was provided by the National Institute for Occupational Safety and Health, grant 5 R01 OH02392-01.

REFERENCES

1. American Conference of Governmental Industrial Hygienists: *Industrial Ventilation - A Manual of Recommended Practice*, 20th ed. ACGIH, Cincinnati, OH (1988).

2. Burgess, W.A.; Ellenbecker, M.J.; Treitman, R.D.: *Ventilation for Control of the Work Environment*, John Wiley & Sons Inc., New York, (1989).

3. Flynn, M.R.; Miller C.T.: The Boundary Integral Equation Method (BIEM) for Modeling Local Exhaust Hood Flow Fields. Am. Ind. Hyg.Assoc. J. 50(5):281 (1989).

4. Conroy, L.M.; Ellenbecker, M.J.; Flynn, M.R.: The Prediction and Measurement of Velocity into Flanged Slot Hoods. Am. Ind. Hyg. Assoc. J. 49(5):226 (1988).

5. Esmen, N.A.; Weyel, D.A.; McGuigan, F.P.: Aerodynamic Properties of Exhaust Hoods. Am. Ind. Hyg. Assoc. J. 47(8):448 (1986).

6. Garrison R.P.; Park, C.: Evaluation of Models for Local Exhaust Velocity Characteristics – Part Two: Velocity Gradients for an Inlet near a Boundary Surface. Am. Ind. Hyg. Assoc. J. 50(4):204 (1989).

7. Braconnier, R.: Bibliographic Review of Velocity Fields in the Vicinity of Local Exhaust Hood Openings. Am. Ind. Hyg. Assoc. J. 49(4):185 (1988).

8. Drinker, P.; Hatch, T.: *Industrial Dust.* McGraw Hill, New York. (1936)

9. Brandt, A.D.: *Industrial Health Engineering.* John Wiley & Sons. New York (1947).

10. Shelton, W.K.; Flynn, M.R.: The Relationship between Capture Efficiency and Breathing-Zone Concentration. Under preparation.

11. George, D.K.; Flynn, M.R.: The Impact of Boundary Layer Separation on Local Exhaust Design and Worker Exposure. In Press. Appl. Ind. Hyg.

12. Flynn, M.R.; Miller, C.T.: Discrete Vortex Methods for the Simulation of Boundary Layer Separation Effects on Woker Exposure. Submitted to Am. Ind. Hyg. Assoc. J.

13. Tum Suden, K.D.; Flynn, M.R.; Goodman, R.: Computer Simulation in the Design of Local Exhaust Hoods for Shielded Metal Arc Welding. In Press Am. Ind. Hyg. Assoc. J.

14. American Welding Society: Fumes and Gases in the Welding Environment. (1979)

Table I -- Raw data: CBZ is the time weighted average concentration of sulfur hexafluoride measured in the mannequin's breathing zone.

RUN	POS	D (IN)	Q (CFM)	Z (IN)	CBZ (PPM)
1	1	4	100	6	0.02
1	1	4	100	9	0.014
1	1	4	300	6	0.02
1	1	4	300	9	0.007
1	1	4	535	6	0.016
1	1	4	535	9	0.009
1	1	9	100	6	0.016
1	1	9	100	9	0.019
1	1	9	300	6	0.033
1	1	9	300	9	0.031
1	1	9	535	6	0.014
1	1	9	535	9	0.015
1	1	12	100	6	0.013
1	1	12	100	9	0.026
1	1	12	300	6	0.025
1	1	12	300	9	0.02
1	1	12	535	6	0.024
1	1	12	535	9	0.005
1	2	4	100	6	0.024
1	2	4	100	9	0.024
1	2	4	300	6	0.021
1	2	4	300	9	0.009
1	2	4	535	6	0.028
1	2	4	535	9	0.014
1	2	9	100	6	0.016
1	2	9	100	9	0.02
1	2	9	300	6	0.033
1	2	9	300	9	0.028
1	2	9	535	6	0.013
1	2	9	535	9	0.025
1	2	12	100	6	0.017
1	2	12	100	9	0.018
1	2	12	300	6	0.025
1	2	12	300	9	0.023
1	2	12	535	6	0.041
1	2	12	535	9	0.023
2	1	4	100	6	0.026
2	1	4	100	9	0.016
2	1	4	300	6	0.025
2	1	4	300	9	0.01
2	1	4	535	6	0.016
2	1	4	535	9	0.014

Table I -- Continued

2	1	9	100	6	0.017
2	1	9	100	9	0.018
2	1	9	300	6	0.021
2	1	9	300	9	0.021
2	1	9	535	6	0.015
2	1	9	535	9	0.016
2	1	12	100	6	0.008
2	1	12	100	9	0.025
2	1	12	300	6	0.005
2	1	12	300	9	0.014
2	1	12	535	6	0.014
2	1	12	535	9	0.024
2	2	4	100	6	0.027
2	2	4	100	9	0.014
2	2	4	300	6	0.024
2	2	4	300	9	0.016
2	2	4	535	6	0.029
2	2	4	535	9	0.016
2	2	9	100	6	0.016
2	2	9	100	9	0.016
2	2	9	300	6	0.016
2	2	9	300	9	0.021
2	2	9	535	6	0.015
2	2	9	535	9	0.029
2	2	12	100	6	0.018
2	2	12	100	9	0.016
2	2	12	300	6	0.024
2	2	12	300	9	0.014
2	2	12	535	6	0.021
2	2	12	535	9	0.019

Table II -- Five Factor ANOVA for all data

Source	Sum of Squares	df	Mean square	F-ratio	P
RUN	0.000074	1	0.000074	1.669	0.20
POS	0.000203	1	0.000203	5.584	0.04
Q	0.000040	2	0.000020	0.446	0.64
D	0.000042	2	0.000021	0.476	0.62
Z	0.000105	1	0.000105	2.370	0.13
ERROR	0.002839	64	0.000044		

Table III -- FOUR WAY ANALYSIS OF VARIANCE FOR ALL DATA

DEP VAR: BZCREV N: 72 MULTIPLE R: .564

SOURCE	SUM-OF-SQUARES	DF	MEAN-SQUARE	F-RATIO	P
POS	0.000203	1	0.000203	5.41	0.02
D	0.000042	2	0.000021	0.56	0.57
Z	0.000105	1	0.000105	2.80	0.10
POS*D	0.000050	2	0.000025	0.67	0.52
POS*Z	0.000021	1	0.000021	0.56	0.46
D*Z	0.000478	2	0.000239	6.36	0.00
POS*D*Z	0.000149	2	0.000075	1.99	0.15
ERROR	0.002254	60	0.000038		

TABLE IV -- ANALYSIS OF VARIANCE FOR 100 CFM DATA

DEP VAR: BZCREV N: 24 MULTIPLE R: .899

SOURCE	SUM-OF-SQUARES	DF	MEAN-SQUARE	F-RATIO	P
POS	0.000003	1	0.000003	0.32	0.58
D	0.000055	2	0.000027	3.32	0.07
Z	0.000003	1	0.000003	0.32	0.58
POS*D	0.000020	2	0.000010	1.22	0.33
POS*Z	0.000033	1	0.000033	3.96	0.07
D*Z	0.000216	2	0.000108	13.07	0.00
POS*D*Z	0.000089	2	0.000044	5.37	0.02
ERROR	0.000099	12	0.000008		

TABLE V -- ANALYSIS OF VARIANCE FOR 300 CFM DATA

DEP VAR: BZCREV N: 24 MULTIPLE R: .750

SOURCE	SUM-OF-SQUARES	DF	MEAN-SQUARE	F-RATIO	P
POS	0.000020	1	0.000020	0.41	0.54
D	0.000351	2	0.000176	3.53	0.06
Z	0.000140	1	0.000140	2.82	0.12
POS*D	0.000056	2	0.000028	0.57	0.58
POS*Z	0.000002	1	0.000002	0.03	0.86
D*Z	0.000156	2	0.000078	1.57	0.25
POS*D*Z	0.000039	2	0.000020	0.39	0.68
ERROR	0.000596	12	0.000050		

TABLE VI -- ANALYSIS OF VARIANCE FOR 535 CFM DATA

DEP VAR: BZCREV N: 24 MULTIPLE R: .816

SOURCE	SUM-OF-SQUARES	DF	MEAN-SQUARE	F-RATIO	P
POS	0.000345	1	0.000345	8.91	0.01
D	0.000070	2	0.000035	0.91	0.43
Z	0.000057	1	0.000057	1.47	0.25
POS*D	0.000015	2	0.000007	0.19	0.83
POS*Z	0.000001	1	0.000001	0.027	0.87
D*Z	0.000308	2	0.000154	3.98	0.05
POS*D*Z	0.000127	2	0.000063	1.64	0.24
ERROR	0.000465	12	0.000039		

FIGURE CAPTIONS

Figure 1 -- Plan View of the mannequin-hood positions. POS=1 is the preferred orientation 90^{o} to the hood centerline. POS=2 is the standard 180^{o} position.

Figure 2 -- Plot of concentration vs. hood diameter for all flows by source-to-hood distance (Z).

Figure 3 -- Plot of concentration vs. hood flow by position.

Figure 4 -- Plot of concentration vs. hood diameter by source-to-hood distance (Z), for the 535 cfm flow and mannequin position #2.

Figure 5 -- Plot of concentration vs. hood diameter by source-to-hood distance (Z), for the 535 cfm flow and mannequin position #1.

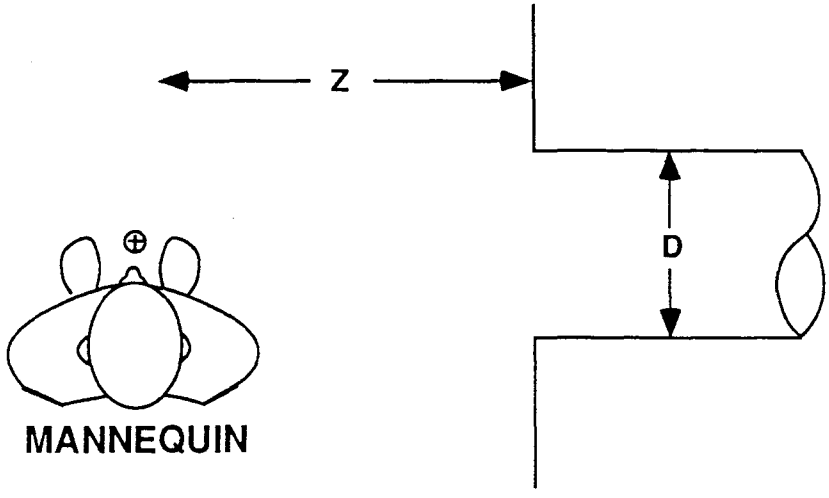

POS = 1

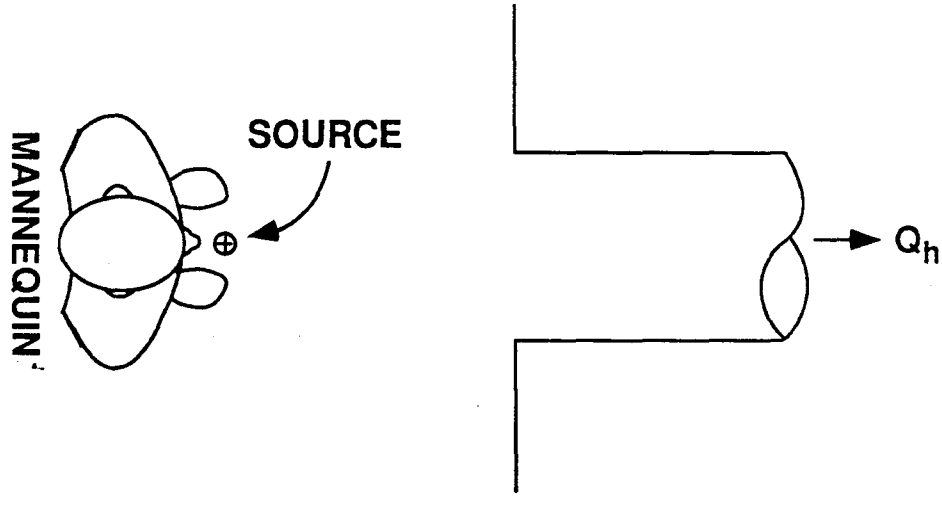

POS = 2

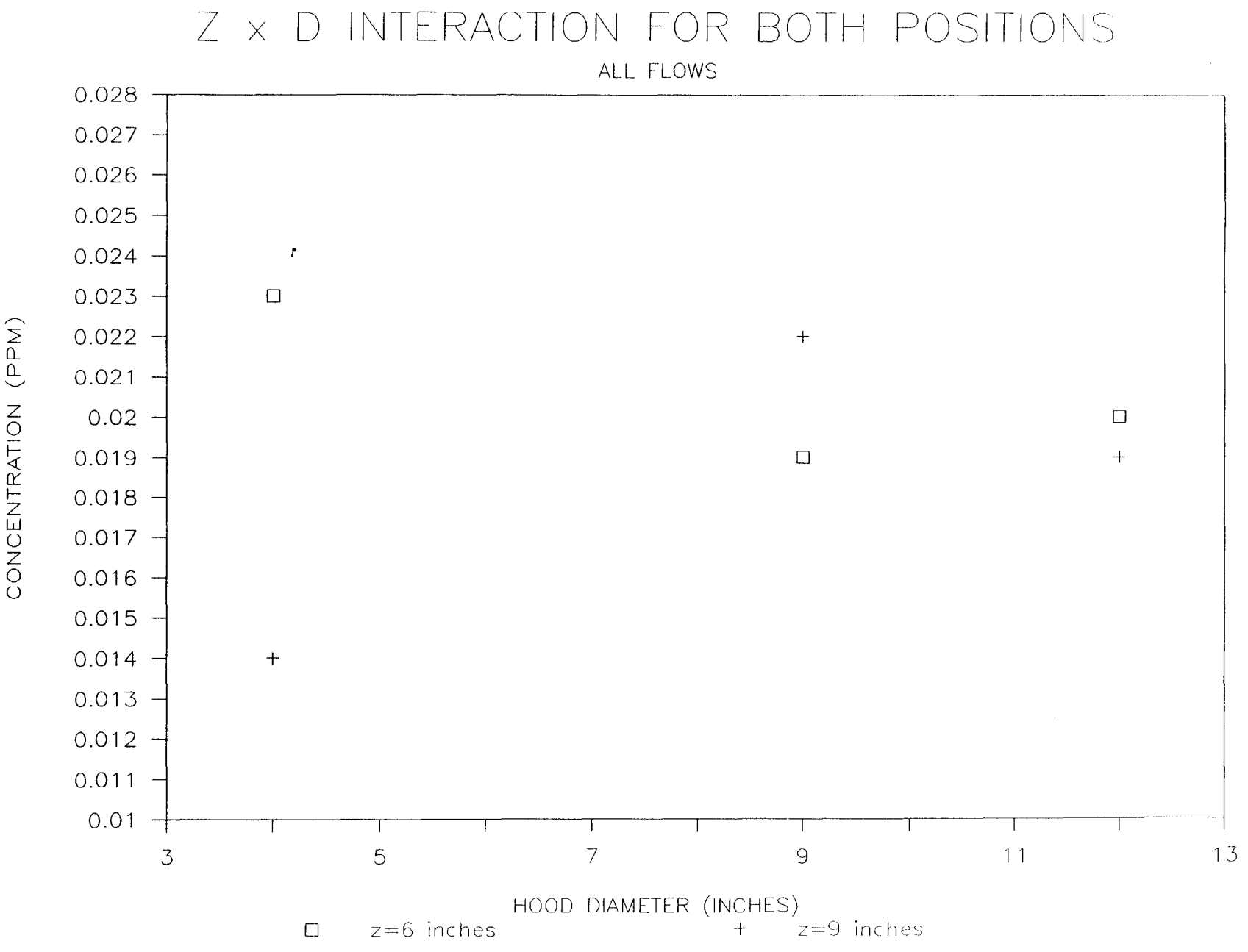
Z x D INTERACTION FOR BOTH POSITIONS
ALL FLOWS
CONCENTRATION (PPM)
0.028
0.027
0.026
0.025
0.024
0.023
0.022
0.021
0.02
0.019
0.018
0.017
0.016
0.015
0.014
0.013
0.012
0.011
0.01
3
5
7
9
11
13
HOOD DIAMETER (INCHES)
z=6 inches
z=9 inches

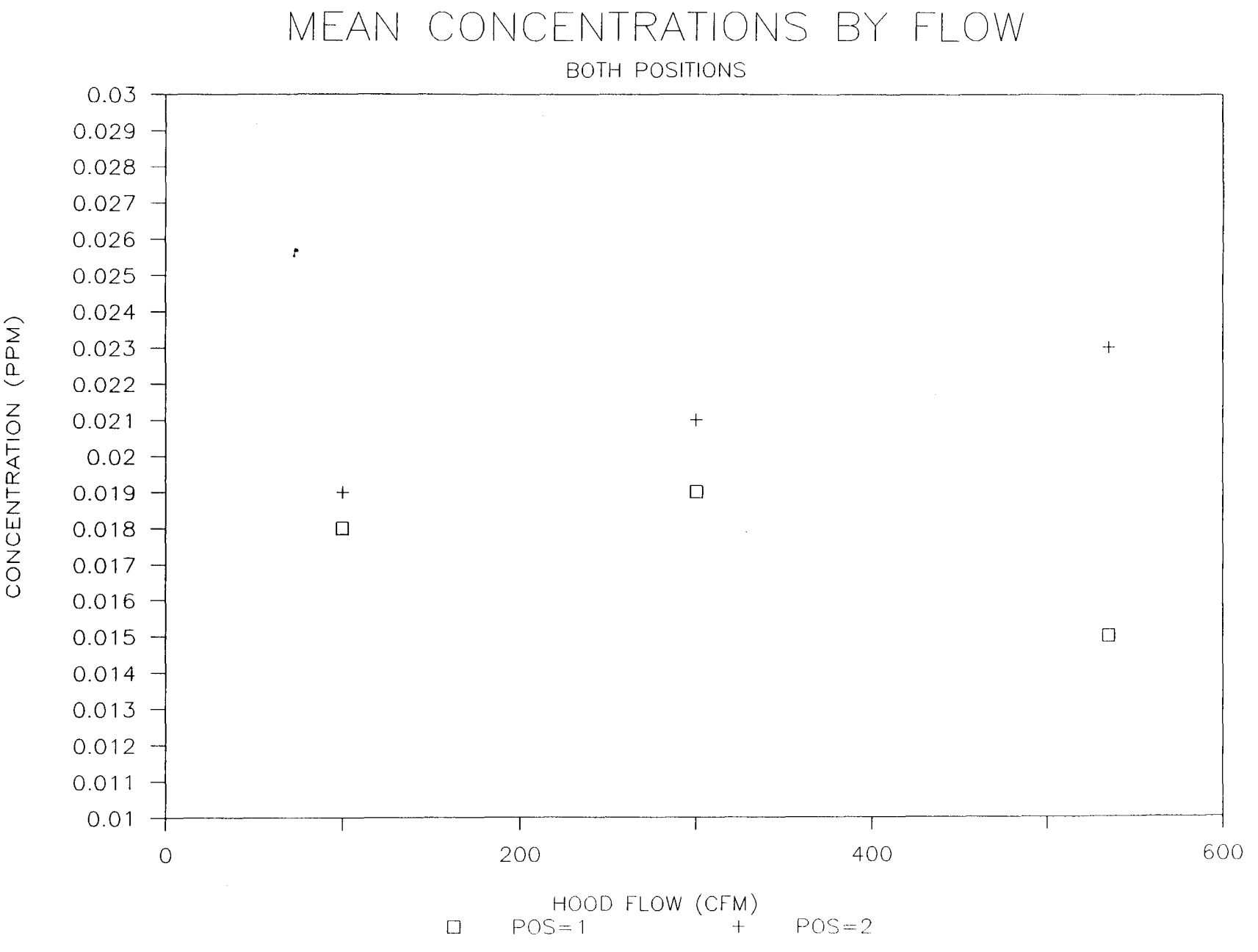
MEAN CONCENTRATIONS BY FLOW
BOTH POSITIONS
CONCENTRATION (PPM)
0.03
0.029
0.028
0.027
0.026
0.025
0.024
0.023
0.022
0.021
0.02
0.019
0.018
0.017
0.016
0.015
0.014
0.013
0.012
0.011
0.01
0
200
400
600
HOOD FLOW (CFM)
POS=1
POS=2

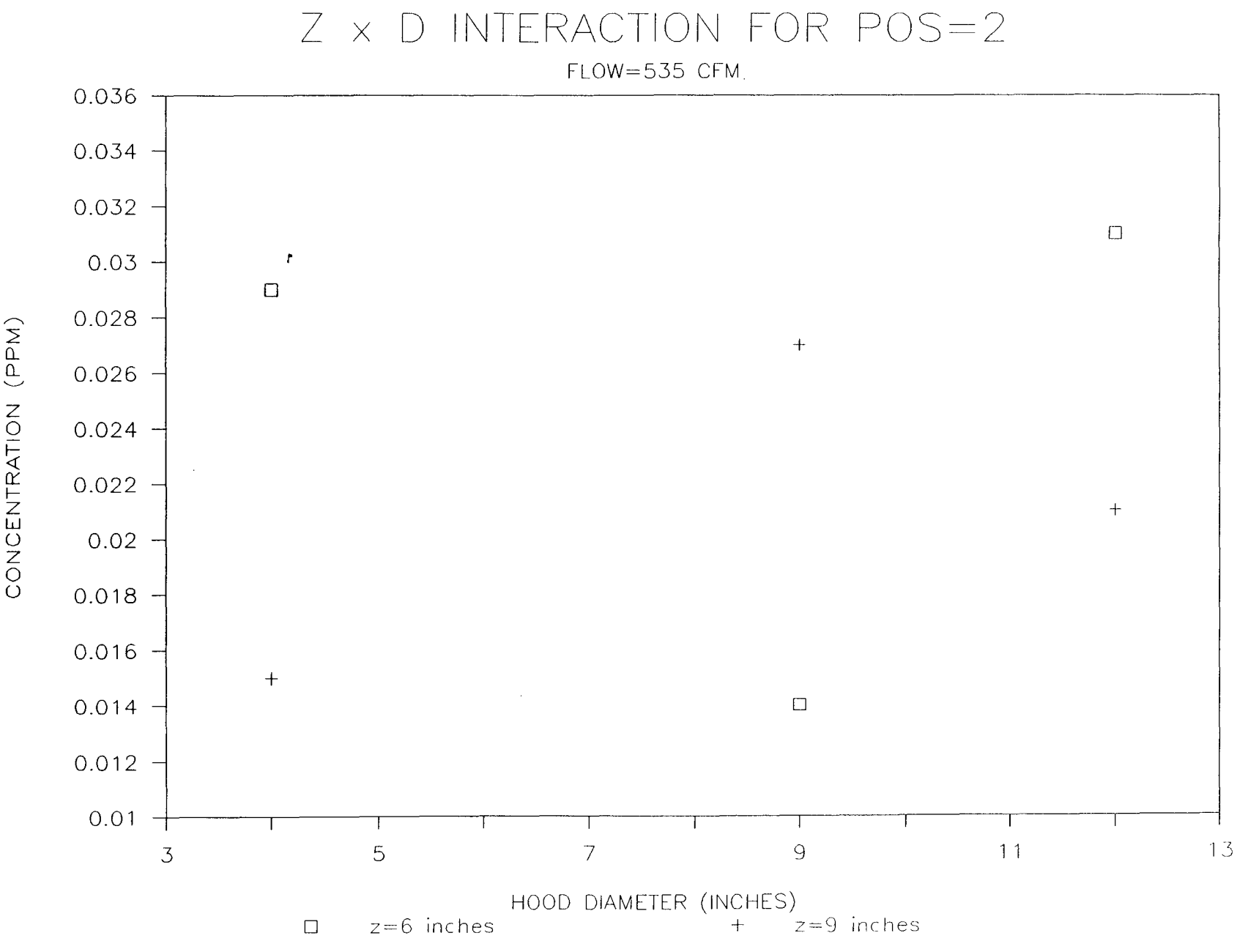
Z x D INTERACTION FOR POS=2
FLOW=535 CFM.
CONCENTRATION (PPM)
0.036
0.034
0.032
0.03
0.028
0.026
0.024
0.022
0.02
0.018
0.016
0.014
0.012
0.01
3
5
7
9
11
13
HOOD DIAMETER (INCHES)
z=6 inches
z=9 inches

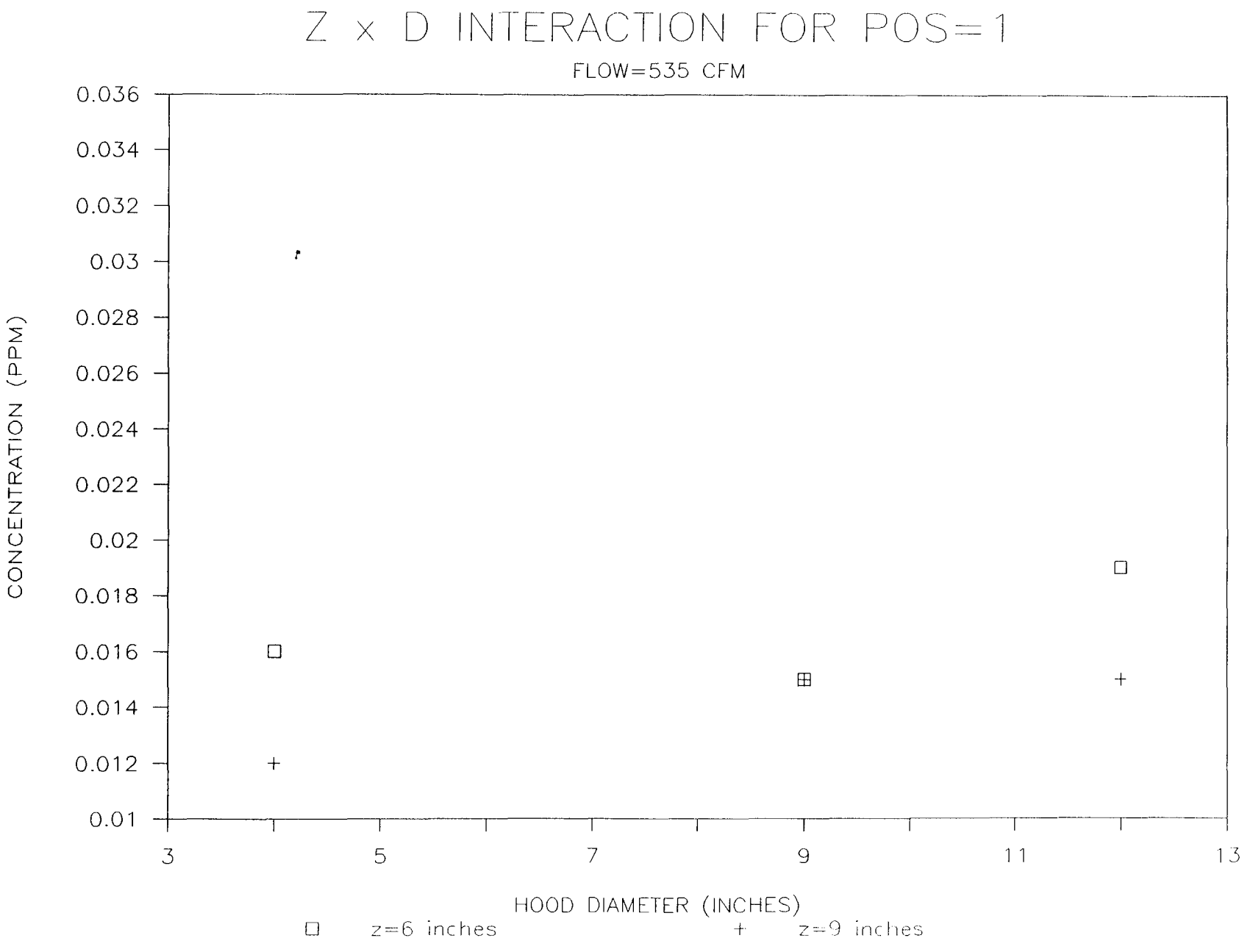
Z x D INTERACTION FOR POS=1
FLOW=535 CFM
CONCENTRATION (PPM)
0.036
0.034
0.032
0.03
0.028
0.026
0.024
0.022
0.02
0.018
0.016
0.014
0.012
0.01
3
5
7
9
11
13
HOOD DIAMETER (INCHES)
z=6 inches
z=9 inches

MANUSCRIPT III

Discrete Vortex methods for the Simulation of

Boundary Layer Separation Effects on

Worker Exposure

Discrete Vortex Methods for the Simulation of Boundary Layer Separation Effects on Worker Exposure

Michael R. Flynn and Cass T. Miller

Department of Environmental Sciences and Engineering
University of North Carolina at Chapel Hill
Chapel Hill, NC 27599-7400

Abstract - The discrete vortex method is a numerical technique for the solution of the two-dimensional Navier-Stokes equations in vorticity-transport form. The technique is employed here, with appropriate modifications, to simulate boundary layer separation around a worker and to assess the implications for exposure. Approximations include: 1) representation of the worker as a two-dimensional elliptic cylinder, and 2) contaminant transport by vortex shedding exclusively. The model results in estimates of breathing-zone concentration that are in reasonable agreement with laboratory wind tunnel experiments.

INTRODUCTION

Studies[1-4] show that an important variable in the control of worker exposure to toxic airborne pollutants is the position of the worker with respect to the air flow direction. Research[1-4] suggests that in some instances the standard exhaust configuration; i.e., source of contaminant between the worker and the exhaust, is not the most effective orientation. Laboratory experiments[3,5] and field studies[6] demonstrate a beneficial reduction in breathing zone concentration when the worker is positioned such that the air flows from the side, rather than around the back. In this orientation the turbulent wake entrains less contaminant into the breathing zone than it does in the standard configuration, see e.g. Ljungqvist[1].

The phenomenon of interest is known as boundary layer separation, and it occurs as any fluid flows around a bluff body, e.g., air around a person. It results in the formation of counter-rotating eddies on the downstream side of the body, which in the case of a ventilation application may lead to contaminant transport into the breathing zone. The key parameters, in terms of contaminant control, are the position of the polluting source and the size and position of the worker's breathing zone with respect to the separated, near-wake region. If the near-wake encompasses both the source and the breathing-zone, then higher exposures are expected than if it does not.

Recent wind tunnel studies[5] with anthropometric mannequins demonstrate the profound impact of worker position with respect to air flow on the breathing-zone concentration. A simple model was developed to estimate breathing-zone concentration, based upon a two-dimensional vortex shedding mechanism. The agreement of that model[5] with experiment suggests that the vortex shedding phenomenon is a useful conceptual tool for modeling worker exposure.

The objective of this research is to develop a computer model to solve the governing equations of fluid mechanics for the time-dependent air flow around a worker immersed in a uniform free stream. The essential feature of this model is the ability to capture the formation and evolution of the near-wake, reverse-flow zone, and thus permit the industrial hygiene engineer to examine the influence of changing air direction, worker position, and air speed on the position and size of this near-wake zone.

THEORY

The transport of a gaseous pollutant released in the recirculating wake formed as air flows around a worker is a complex problem. The governing equations include: 1) the turbulent, three-dimensional, unsteady Navier-Stokes equations and an associated turbulence model (e.g. the $k-\epsilon$ model[7]); 2) the continuity equation; 3) a species conservation

equation to account for convective and diffusive transport; and 4) the conservation of energy equation. Appropriate boundary conditions must be specified for the solution of these coupled, and highly nonlinear partial differential equations.

Experimental work[5] suggests that for the purpose of estimating exposure, a two-dimensional approach may provide a reasonable approximation to the physics of the problem. By modeling the worker as a circular cylinder, estimates of breathing zone concentration were derived using dimensional analysis.[5] The two-dimensional approach, while lacking some rigor, puts the problem within the realm of practical solution and provides a basis upon which to proceed to more complex and realistic simulations. In the computer code developed here, the worker is modeled as an elliptic cylinder of aspect ratio 0.5. This reflects the fact that people tend to be wider (shoulder to shoulder) than deep (front to back).

Turbulence is neglected here by assuming: 1) that coherent vortex structures in turbulent flow are similar to those found in laminar flow and 2) contaminant transport is dominated by vortex shedding, not turbulent diffusion. The first assumption appears reasonable in view of recent research[8-9] indicating that in turbulent wakes behind bluff bodies "the general topological features present in the phase-averaged motions bear a strong resemblance to those in the forced periodic motions in laminar flow."[9] The second assumption is supported by the experimental work referenced above[5] and also by other studies.[10] It is clear, however, that a complete model will ultimately have to consider contaminant transport by turbulent diffusion as well as vortex shedding.

If one characterizes a worker by the shoulder to shoulder dimension, perhaps 2-3 ft, and air velocities are on the order of 10 - 500 fpm; then Reynolds numbers (Re) are on the order of 2000 - 150,000. This is in the subcritical and transition range indicating that turbulent boundary layers probably do not exist until after separation. These approximations reduce the dimensionality and complexity of the problem, but also limit the accuracy of the model.

The resulting equations that govern the incompressible laminar flow of air around a

worker are the continuity (conservation of mass) equation:

$$\nabla \cdot \vec{V} = 0 \tag{1}$$

and the Navier-Stokes equations (conservation of linear momentum):

$$\frac{\partial \vec{V}}{\partial t} + (\vec{V} \cdot \nabla)\vec{V} = \nu \nabla^2 \vec{V} - \nabla P \tag{2}$$

where ν is the kinematic viscosity, and P the dynamic pressure. $\vec{V}$ is the two-dimensional velocity field:

$$\vec{V} = u\hat{\imath} + v\hat{\jmath} \tag{3}$$

In two-dimensional, incompressible flow the presence of only one vorticity component permits simplification of the Navier-Stokes equations to the vorticity-transport equation.

$$\frac{\partial \xi}{\partial t} + (\vec{V} \cdot \nabla)\xi = \nu \nabla^2 \xi \tag{4}$$

where the vorticity (ξ) is

$$\xi = \frac{\partial v}{\partial x} - \frac{\partial u}{\partial y} \tag{5}$$

Through the use of the stream function Ψ, the continuity equation becomes Poisson's equation:

$$\nabla^2 \Psi = -\xi \tag{6}$$

and the x and y velocity components are respectively:

$$u = \frac{\partial \Psi}{\partial y} \tag{7}$$

$$v = -\frac{\partial \Psi}{\partial x} \tag{8}$$

The boundary conditions which must be satisfied for flow around an obstacle with a boundary Ω are

$$\vec{V} \cdot \hat{n} = 0 \tag{9}$$

$$\vec{V} \cdot \hat{\tau} = 0 \tag{10}$$

where $\hat{n}$ is the outward unit normal, and $\hat{\tau}$ the counterclockwise unit tangential to the boundary Ω. Boundary conditions at infinity are

$$\vec{V}(\infty, y, t) = \vec{V_0} \tag{11}$$

$$\vec{V}(x, \infty, t) = \vec{V_0} \tag{12}$$

where $\vec{V_0}$ is the freestream velocity.

An analytic solution does not exist for the problem of two-dimensional incompressible flow around an elliptic cylinder with boundary layer separation. A numerical technique is required to approximate the solution. Possibilities include the finite-element, finite-difference, and discrete-vortex methods. Finite-difference solutions for flow around circular cylinders are reported by several authors[11-12] and low-Reynolds number vortex shedding

around a circular cylinder has been achieved using finite-element methods[13]. However, these Eulerian approaches suffer from truncation error and numerical viscosity as the Reynold's number of the flow increases.[14]

In order to circumvent the problem and obtain reasonable high-Reynold's number simulations an algorithm was developed by Chorin[14-15] called the discrete vortex method. This technique has been investigated and applied by several author's successfully for flow around circular cylinders[16-19]. The discrete-vortex-method (DVM) is a Lagrangian approach, and does not employ a grid; it thus avoids the numerical viscosity problem and is more efficient at the Reynold's numbers of interest in ventilation problems, about 5,000-100,000.

The method employed here is adapted from several sources,[14-20] with an elliptical-coordinate interpolation scheme within the boundary layer added to customize the algorithm for the elliptic cylinder. The details of the method, its derivation, and convergence properties may be found in the aforementioned works and the references therein. Only a brief outline of the method is given here.

The discrete vortex method relies upon the fact that vorticity is a material property of the fluid that is convected and diffused. It is possible to use the method of fractional steps[20] and split the vorticity-transport equation into Euler's equation and the diffusion equation, each being respectively:

$$\frac{\partial \xi}{\partial t} + (\vec{V} \cdot \nabla)\xi = 0 \tag{13}$$

and

$$\frac{\partial \xi}{\partial t} = \nu \nabla^2 \xi \tag{14}$$

The solution[20] for the diffusion equation, with an impulse initial condition, is a Gaussian distribution of zero mean and variance (σ^2):

$$\sigma^2 = 2\nu\Delta t \tag{15}$$

where Δt is a finite interval of time. The solution for Euler's equation depends upon a theorem[21] that guarantees, for incompressible flow, that a given velocity field may be decomposed into the sum of a potential flow and a rotational flow. The potential flow is generated here by means of a submerged panel technique[19,22] and the rotational flow is generated by discretizing the vorticity into "blobs"[14] or modified line vortices. As the vortices enter the flow they induce their own velocity fields, which are added to the potential velocity components.

Vorticity is generated as air flows around the worker's body by the action of viscosity in the boundary layer adjacent to the workers clothes and skin. In order to mimic the physical problem, Chorin[15] developed the concept of a numerical boundary layer governed by the Prandtl boundary layer equations. Within the boundary layer vortex sheets are formed to cancel the tangential velocity at selected generation points on the surface of the body. The equations which govern the flow in the numerical boundary layer are:

$$\frac{\partial \xi}{\partial t} + (\vec{V} \cdot \nabla)\xi = \nu \frac{\partial^2 \xi}{\partial y^2} \tag{16}$$

where

$$\xi = -\frac{\partial u}{\partial y} \tag{17}$$

When used in connection with the boundary layer, x and y refer to the tangential and normal directions to the boundary respectively. Similarly, within the boundary layer, the u, v notation refers to the tangential and normal velocity components respectively. In developing the code for flow around an elliptic cylinder appropriate co-ordinate transformations are necessary.

The boundary layer equation is also subject to the method of fractional steps. Euler's equation, Equation (4), is again obtained, along with a simplified diffusion equation:

$$\frac{\partial \xi}{\partial t} = \nu \frac{\partial^2 \xi}{\partial y^2} \tag{18}$$

The solution for this diffusion equation is identical to the solution for Equation (14) except that the displacement occurs within the boundary layer in the y-direction only, i.e., normal to the boundary.

The problem of airflow around a two-dimensional elliptic cylinder is thus broken down into two sub-problems. The first is a numerical boundary layer within which vorticity is generated and convected according to Equation (4) and diffused according to Equation (18). The boundary conditions are given by Equations (9), (10), and (12). The vorticity within the numerical boundary layer exists in the form of discrete vortex sheets. These are transformed into blobs (modified line vortices) once they move outside of the numerical boundary layer. The second sub-problem deals with the convection, Equation (13), and diffusion, Equation (14), of the blobs outside the numerical boundary layer. Equations (9)–(12) define the boundary conditions in this region.

NUMERICAL METHODS

The airflow around an elliptic cylinder is a time dependent problem. It is the entrainment of air into the near-wake region that results in the periodic shedding of vortices. It is assumed here that this ultimately determines the concentration to which the worker is exposed. The solution of the governing equations presented above is accomplished by discretizing the problem in time and marching forward. At time $t = 0$ there is no motion; at the very next instant an impulse acceleration to the free stream velocity is assumed. The ellipse is defined by a major axis (2A) and a minor axis ($2B$).

The surface of the elliptic cylinder is generated by the use of submerged panel tech-

niques.[19,22] In this method the cylinder is created by placing 20 panels, or source elements of finite length, within the perimeter of the ellipse. They are arranged in the pattern of a smaller concentric ellipse (see Fig 1). The strengths of each of the panels are calculated such that they produce a zero normal velocity at 20 control points spaced at equal arc lengths around the perimeter of the ellipse. Thus the surface of the cylinder is, in fact, a streamline in the combination flow resulting from the panels and the cross flow.

At the first time step, there is not yet any vorticity in the flow, therfore the flow around the ellipse is potential flow only. The panel solution for the potential-flow velocity field around an elliptic cylinder immersed in a uniform free stream was validated against the analytic solution presented in Lamb[23]. In subsequent time steps the panel strengths are calculated to maintain a zero normal velocity at the control points, for conditions that include vorticity and a uniform cross draft. The repeated adjustment to the source strengths requires the simultaneous solution of 20 equations at each time step, one for each control point. Fortunately the coefficient matrix is constant, allowing for the use of an efficient lower-upper-decomposition solver.

The vorticity is introduced within the numerical boundary layer at each time step by generating vortex sheets at each of the control points of sufficient strength (γ) to cancel the tangential velocity present at that control point. The strength of a single sheet needed to do this is $2V_t$ where V_t is the tangential velocity at the control point. At the first time step the tangential velocity is due to the panels and the uniform flow (i.e. the potential flow) only, subsequently however, the rotational components from blobs and sheets in the flow also contribute to the tangential velocity. In the algorithm developed here multiple sheets are generated at each of the control points such that no sheet has a strength greater, in absolute value, than 10% of the freestream velocity, i.e. $\gamma \leq 0.1V_0$. This improves the convergence properties of the algorithm.[15] The numerical boundary layer thickness (δ) is $2A\sqrt{Re}$.

Vortex sheets are characterized by their strength, which is essentially a velocity, and

also by their length, (h). In this simulation the sheet length is equal to the perimeter of the elliptic cylinder divided by the number of control points (20) or $h = 0.242211$ ft. As the sheets are convected and diffused, some will move outside of the numerical boundary layer, these sheets undergo a metamorphosis and become blobs with a circulation, (k), where $k = h\gamma$. Sheets that diffuse into the cylinder on their first displacement are removed from the calculation domain, while sheets or blobs that cross the surface subsequently are reflected and/or changed depending on various rules, see e.g. Bui and Oppenheim[20].

The ith vortex blob moves according to the following equations:

$$x_i^{n+1} = x_i^n + \Delta t u_i^n + \eta_i^1 \tag{19}$$

$$y_i^{n+1} = y_i^n + \Delta t v_i^n + \eta_i^2 \tag{20}$$

where u is the x velocity component, v is the y velocity component, and the superscript n refers to the time step. The variables η^1 and η^2 are independent random variables drawn from a Gaussian distribution of zero mean, and variance given in Equation (15). The velocity components for the ith vortex located at (x_i^n, y_i^n), at time step n are

$$u_i^n = -(2\pi)^{-1} \left(\sum_{r_{ij}>l} k_j \frac{y_i^n - y_j^n}{r_{ij}^2} + \sum_{r_{ij}\leq l} k_j \frac{y_i^n - y_j^n}{l r_{ij}} \right) \tag{21}$$

$$v_i^n = (2\pi)^{-1} \left(\sum_{r_{ij}>l} k_j \frac{x_i^n - x_j^n}{r_{ij}^2} + \sum_{r_{ij}\leq l} k_j \frac{x_i^n - x_j^n}{l r_{ij}} \right) \tag{22}$$

where

$$r_{ij} = \sqrt{(x_i^n - x_j^n)^2 + (y_i^n - y_j^n)^2} \tag{23}$$

l is a cut-off value[14,16-17] that permits a smooth transition from sheets to blobs; its value here is 0.0771 ft. Vortex sheets do not contribute to blob displacement.

Vortex sheets move according to:

$$x_i^{n+1} = x_i^n + \Delta t u_i^n \tag{24}$$

$$y_i^{n+1} = y_i^n + \Delta t v_i^n + \eta_i^1 \tag{25}$$

where the tangential and normal velocities of the ith sheet are

$$u_i^n = U_\delta(x_i^n) - \frac{1}{2}\gamma_i - \sum_j \gamma_j d_j \tag{26}$$

$$v_i^n = \frac{-(I_1 - I_2)}{h} \tag{27}$$

and

$$d_j = 1 - |x_i^n - x_j^n|/h \tag{28}$$

$$I_1 = U_\delta(x_i^n + h/2)y_i^n - \sum_j \gamma_j d_j^+ y_j^{*n} \tag{29}$$

$$I_2 = U_\delta(x_i^n - h/2)y_i^n - \sum_j \gamma_j d_j^- y_j^{*n} \tag{30}$$

$$d_j^+ = 1 - \left(|x_i^n + h/2 - x_j^n|/h\right) \tag{31}$$

$$d_j^- = 1 - \left(|x_i^n - h/2 - x_j^n|/h\right) \tag{32}$$

The summation in Equation (26) is over all j vortex sheets such that $y_j^n > y_i^n$; the summation in Equation (29) is over all j vortex sheets such that $0 \leq d_j^+ \leq 1$; and the summation in Equation (30) is over all j sheets such that $0 \leq d_j^- \leq 1$. y_j^{*n} is the smaller of y_i^n, y_j^n; h is the sheet length, and Δt is the time step. Notice that diffusion occurs here only in the direction normal to the surface. The $U_\delta(x)$ notation indicates the velocity at the edge of the numerical boundary layer at the specified tangential coordinate x.

The algorithm splits the movement into a diffusion step with one half the variance, a convective step and finally another diffusion step, again with half the variance. This improves the accuracy of the fractional step method[19-20]. Table 1 presents a brief summary of the algorithm.

RESULTS

The simulations conducted here represent the flow of air around a worker by modeling him/her as a two-dimensional elliptic cylinder. The cylinder is 2.0 ft wide, (A = 1.0 ft) and 1.0 ft deep (B = 0.5 ft). These dimensions are a reasonable representation of a human. The free stream velocity was set to 50 fpm, with the direction of air flow perpendicular to the major axis, thus giving a Reynolds number of 10,417. Graphic representations of the velocity field at several different times are given in Figures 2–5.

A time increment of 0.002 minutes was selected for the runs displayed here. Figure 2 shows the development of the flow at 50 time steps or a total elapsed time of 0.1 minute. A clockwise spinning eddy (negative vorticity) can be observed approximately 3.0 ft in the downstream, (y), direction. The velocity vectors are scaled proportionally to the speed and indicate the direction of the air flow at the particular moment in time. Figure 3 shows the flow at 100 time steps (0.2 min.). The eddy from Figure 2 has now weakened and moved to

a downstream location of approximately $(x, y) = (-0.5, 6.0)$. A weak counterclockwise eddy is about 3.0 ft downstream and the formation of the near-wake eddy (negative vorticity here) adjacent to the downstream side of the worker is evident. As the flow begins to develop Figures 4 and 5 illustrate the periodic shedding and growth of eddies, and their motion downstream. With a total of 200 time steps Figure 5 gives a picture of the flow at an elapsed time of 0.2 minutes. Several eddies of various sizes are arranged with alternating signs of vorticity in the downstream direction.

The maximum source strength allowed was 10% of the free stream velocity i.e. 5 fpm. The simulations displayed here were run on a Convex C220 mid-range supercomputer and took a total of about 13–14 hours of CPU time. At the end of 200 time steps there were approximately 7000 computational elements in the domain. There was no attempt, at this stage of the work, to introduce Vortex-in-cell algorithms[19] or predictor-corrector convectors[19] to improve the speed of the program. Simulations of the initial stages of the flow are possible on desktop machines, but at longer run times more computational elements are introduced, and speed and memory requirements dictate the use of more powerful machines.

Convergence of the algorithm was investigated heuristically by halving the time step. No significant differences were found in the estimates of vortex size or shedding frequency (which are reported below). Point comparisons of velocities at the different time steps are not an appropriate convergence criterion due to the sensitivity of the algorithm to small perturbations, see Sethian and Ghoniem.[24]

DISCUSSION

The velocity fields displayed in Figures (2)–(5) indicate the important effect of the near-wake region. The reverse flow eddies that form, and subsequently shed downstream, are important in governing the transport of contaminant in this region. A source of pollu-

tion positioned in this near wake region will be subject to the recirculating flow and hence to transport into the breathing zone. This is the case when a worker handles a contaminant generating process and has his/her back to the flow direction.

A simple model[5] to predict the average dimensionless concentration (C_{avg}), of a passive tracer released in the near-wake zone is:

$$C_{avg} = \frac{Q_s}{Q_v} \tag{33}$$

where Q_s is the flow of tracer gas and Q_v is the effective purging flow of pure air into the zone i.e. air entrained into the near-wake from outside of the separated boundary layers, adjusted for mixing. An estimate[5] of Q_v is

$$Q_v = 2\frac{fV_v}{K} \tag{34}$$

where f is the frequency of vortex shedding from one side of the cylinder, V_v is the vortex volume and K is a mixing factor. V_v and f are estimated from the computer graphics displayed in the developed flows shown in Figures 4 and 5.

In the sequence of simulations shown, the velocity field is displayed every 50 time steps, or every 0.1 minute. By examining the motion of one vortex center from one sequence to the next it appears that the vortex centers average about 2.5 feet in the downstream (y) direction in 0.1 minute indicating a vortex street speed of 25 fpm. The spacing between vortex centers is about 2 feet in the y direction or 4 feet between centers of the same spin giving a frequency of shedding (f) from one side of 6.25 per minute, and a Strouhal number (S) of 0.25. This value is in good agreement with that commonly accepted for circular cylinders of 0.21[25] at this Reynolds number.

$$S = \frac{fD}{U} \tag{35}$$

A visual examination of vortices in the near wake region indicates that they are approximately ellipses 1.5 ft long and 0.8 ft wide; thus having an area of about 0.94 ft^2. The vortex volume for use in Equation (34) is obtained by multiplying the vortex area by the height of the cylinder (person). Equation (33) can then be employed to obtain the average concentration in the near-wake region. By the laws of similarity[25] the results may be scaled to any size provided the Reynolds numbers are equivalent. For the anthropometric mannequin experiments[5] referenced earlier, experiments at 150 fpm correspond to the Reynolds number simulated here. The mannequins corresponding cross body dimension, (D), was 0.667 ft giving a frequency, f=56.25 per minute. Scaling the vortex area according to the ratio of the cross body dimensions gives a vortex area for the mannequin of 0.133 ft^2; and with a mannequin height of 3.42 ft, a vortex volume, V_v, of 0.456 ft^3.

With a source flow of 0.0005 cfm of pure SF_6 our estimate of the average concentration in the near-wake, using $K = 1$ in Equation (34), is 9.75 ppm. The average measured breathing zone value when the source was within 8 inches of the mannequin was 8.8 ppm.[5] These two concentrations would not be expected to be equivalent since the theoretical prediction is an average value over a somewhat ill-defined volume, and the measured breathing-zone concentration is a small subset of the near-wake region. However the agreement is encouraging given the limitations of the approach.

The definition of the near-wake region is important in evaluating the volume over which Equation (33) is expected to apply. Clearly, the flow Q_v must be pure air. The region must be relatively close to the cylinder where clean air from outside the wake is entrained. For the circular cylinder the so-called "formation region" would appear to be the area of concern. Gerrard[26] defines the end of the formation region as the point "where fluid from outside the wake first crosses the axis." Measurements[27-28] show for a circular cylinder this point to be on the order of 1-2 diameters downstream of the end of the cylinder. Studies are presently underway to examine the vortex shedding approach and to define a meaningful near-wake zone.

CONCLUSIONS

The direction of air flow with respect to the worker and the contaminant source is an important factor in determining the concentration of pollutant in the breathing zone. The phenomenon of boundary layer separation is responsible for the formation of rotating eddies on the downstream side of the worker. These eddies can transport contaminant into the breathing zone and reduce the effectiveness of the intended ventilation.

The discrete vortex method can simulate effectively the time dependent flow phenomenon of vortex shedding past an elliptic cylinder. This simulation is a valuable tool in understanding how the recirculation zone forms and changes periodically in time. This two-dimesional approach yields estimates of concentration that are in reasonable agreement with measured values, although further validation and study are needed to refine and improve the model. The discrete vortex method has an important advantage over finite difference and finite element approaches in that it avoids the problem of numerical viscosity associated with small grid sizes.

The model requires substantial computer resources to examine the vortex shedding phenomenon; modifications to improve speed and accuracy are under study. Simulations employing three-dimensional vortex methods are also possible and may provide more reasonable, although expensive, estimates of worker exposure.

ACKNOWLEDGEMENTS

This research was supported, in part, by NIOSH grant 1 R01 OH02392-01, and a grant from the Shell Oil Company Foundation.

REFERENCES

1. Ljungqvist B.: Some observations on the interaction between air movements and the dispersion of pollution., Swedish Council for Building Research, 1979.

2. Van Wagenen, H.D.: Assessment of Selected Control Technology Techniques for Welding Fumes, DHEW (NIOSH) Publication No. 79-125, January 1979.

3. Tum Suden, K.D., M.R. Flynn, and R. Goodman: Computer Simulation in the Design of Local Exhaust Hoods for Shielded Metal Arc Welding, In Press Am. Ind. Hyg. Assoc. J.

4. Herriot, N.R. and J. Wilkinson: Laminar Flow Booths for the Control of Dust, Filt. and Sep. March-April pp 159-164, 1979.

5. George D.K. and M.R. Flynn: The Impact of Boundary Layer Separation on Worker Exposure, submitted to Appl. Ind. Hyg.

6. Piney, M., F. Gill, C. Gray, D. Jones, and J. Worwood: Air contaminant control: the Case History approach - Learning from the past and looking to the future, Ventilation '88 Proceedings of the Second International Symposium on Ventilation for Contaminant Control, J.H. Vincent ed., 1989.

7. Launder, B.E. and D.B. Spalding: The Numerical Computation of Turbulent Flows, Comp. Mthds. Appl. Mech. and Engng. (3):269-289, 1974.

8. Cantwell, B., and D. Coles: An experimental study of entrainment and transport in the turbulent near wake of a circular cylinder. J. Fluid. Mech. (136):321-374, 1983.

9. Perry, A.E., and T.R. Steiner: Large-scale vortex structures in turbulent wakes behind bluff bodies. Part 1. Vortex formation processes. J. Fluid Mech. (174):233-270. 1987.

10. MacLennan, A.S.M., and J.H. Vincent: Transport in the near aerodynamic wakes of flat plates. J. Fluid. Mech. (120):185-197. 1982.

11. Fornberg, B.: Steady viscous flow past a circular cylinder up to Reynolds number 600. J. Comp. Phys. (61):297-320. 1985.

12. Ta Phouc, L. and R. Bouard: Numerical solution of the early stage of the unsteady viscous flow around a circular cylinder: a comparison with experimental visualization and measurements. J. Fluid. Mech. (160):93-117. 1985.

13. Brooks, A.N. and T.J.R. Hughes: Streamline Upwind/Petrov Galerkin Formulations for Convection Dominated Flows with Particular Emphasis on the Incompressible Navier-Stokes Equations. Comp. Mthds. Appl. Mech. and Engng. (32):199-259, 1982.

14. Chorin, A.J.: Numerical study of slightly viscous flow, J. Fluid Mech. 57(4):785-796. 1973.

15. Chorin, A.J.: Vortex Sheet Approximation of Boundary Layers, J. Comput. Physics. 27:428-442. 1978.

16. Cheer, A.Y.: Numerical Study of Incompressible Slightly Viscous Flow Past Blunt Bodies and Airfoils, SIAM J. Sci. and Stat. Comput., 4(4):685-705, 1983.

17. Cheer, A.Y.: Unsteady separated wake behind an impulsively started cylinder in slightly viscous fluid, J. Fluid Mech., 201:485-505, 1989.

18. Stansby, P.K. and A.G. Dixon: Simulation of flows around cylinders by a Lagrangian vortex scheme. Appl. Ocean Res. (5):167-178, 1983.

19. Tiemroth, E.C.: The simulation of viscous flow around a cylinder by the random vortex method. Doctoral Dissertation, University of California, Berkeley. 1986.

20. Bui, T.D., and A.K. Oppenheim: Evaluation of Wind Effects on Model Buildings by the Random Vortex Method, Appl. Numer. Math., 3:195-207, 1987.

21. Batchelor, G.K.: An introduction to fluid dynamics. Cambridge University Press. Cambridge, U.K. 1967.

22. Anderson, D.A., J.C. Tannehill, and R.H. Pletcher: Computational Fluid Mechanics and Heat Transfer, Hemisphere, New York, 1984.

23. Lamb, H.: Hydrodynamics, Dover, New York, 1945.

24. Sethian, J.A., and A.H. Ghoniem: Validation Study of Vortex Methods. J. of Comput. Physics. (74):283-317. 1988.

25. White, F.: Fluid Mechanics, McGraw-Hill, New York, 1986.

26. Gerrard, J.H.: The mechanics of the formation region of vortices behind bluff bodies. J. Fluid. Mech. (25):401-413. 1966.

27. Norberg, C.: Interaction between freestream turbulence and vortex shedding for a single tube in cross-flow. J. Wind Eng. Ind. Aerodyn. (23):501-514. 1986.

28. Bloor, S.: The transition to turbulence in the wake of a circular cylinder. J. Fluid. Mech. (19):290-304. 1964.

TABLE I

Summary of discrete vortex algorithm

Within each time step:

1. Calculate panel strengths to maintain a 0 normal velocity at the control points on the ellipse.

2. Calculate the tangential velocity at the control points as the vector sum of the rotational and potential components.

3. Calculate the vortex sheet strengths at the control points.

4. Diffuse all computational elements, both sheets and blobs.

5. Metamorphosis i.e. change and/or remove computational elements from domain as needed.

6. Convect all computational elements

7. Metamorphosis

8. Diffuse all elements

9. Metamorphosis

FIGURE CAPTIONS

Figure 1 – Submerged panels used to generate the surface of the elliptical cylinder. The flow into or out of the panels is adjusted during each time step to assure a zero velocity normal to the cylinder at each of the control points indicated. The control points also represent the initial location of the vortex sheets.

Figure 2 – Velocity field around an elliptic cylinder (worker) after 0.1 minute. Free stream velocity is 50 fpm. A single clockwise-spinning eddy is located at (-.25, 2.9), units in feet.

Figure 3 – Velocity field around an elliptic cylinder (worker) after 0.2 minute. Free stream velocity is 50 fpm. An elliptical eddy with clockwise spin is forming immediately downstream of the worker.

Figure 4 – Velocity field around an elliptic cylinder (worker) after 0.3 minute. Free stream velocity is 50 fpm. Vortices of opposite spin follow one another downstream, transporting any contaminant generated near the body.

Figure 5 – Velocity field around an elliptic cylinder (worker) after 0.4 minute. Free stream velocity is 50 fpm.

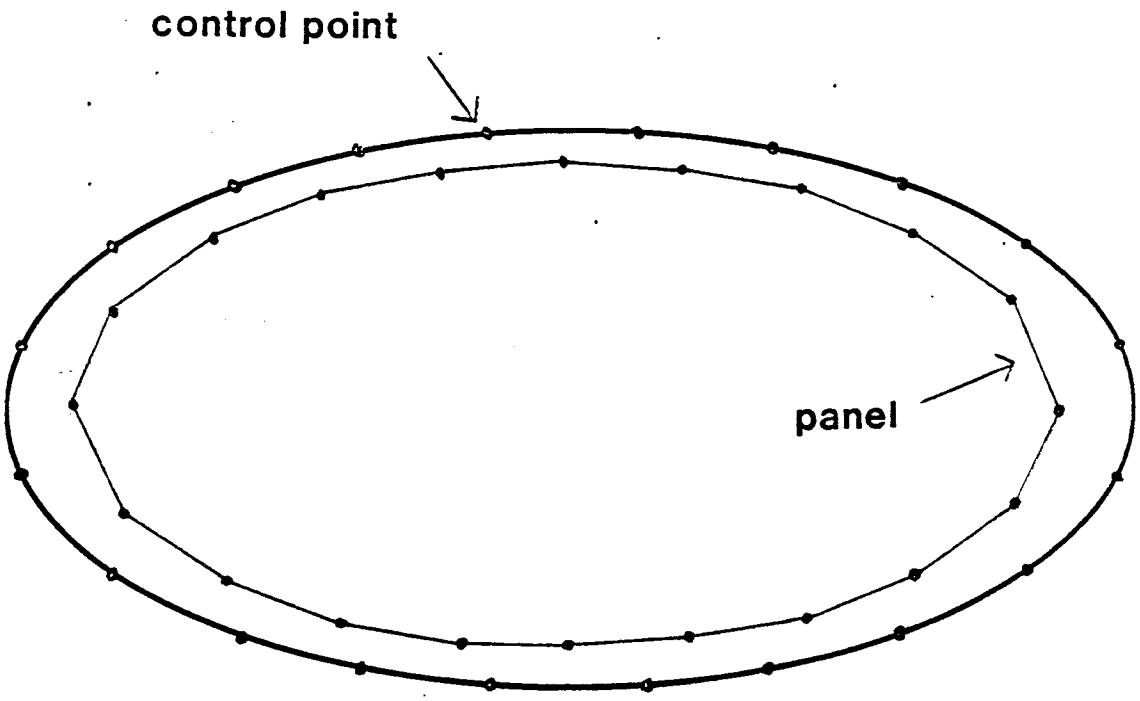
control point
panel

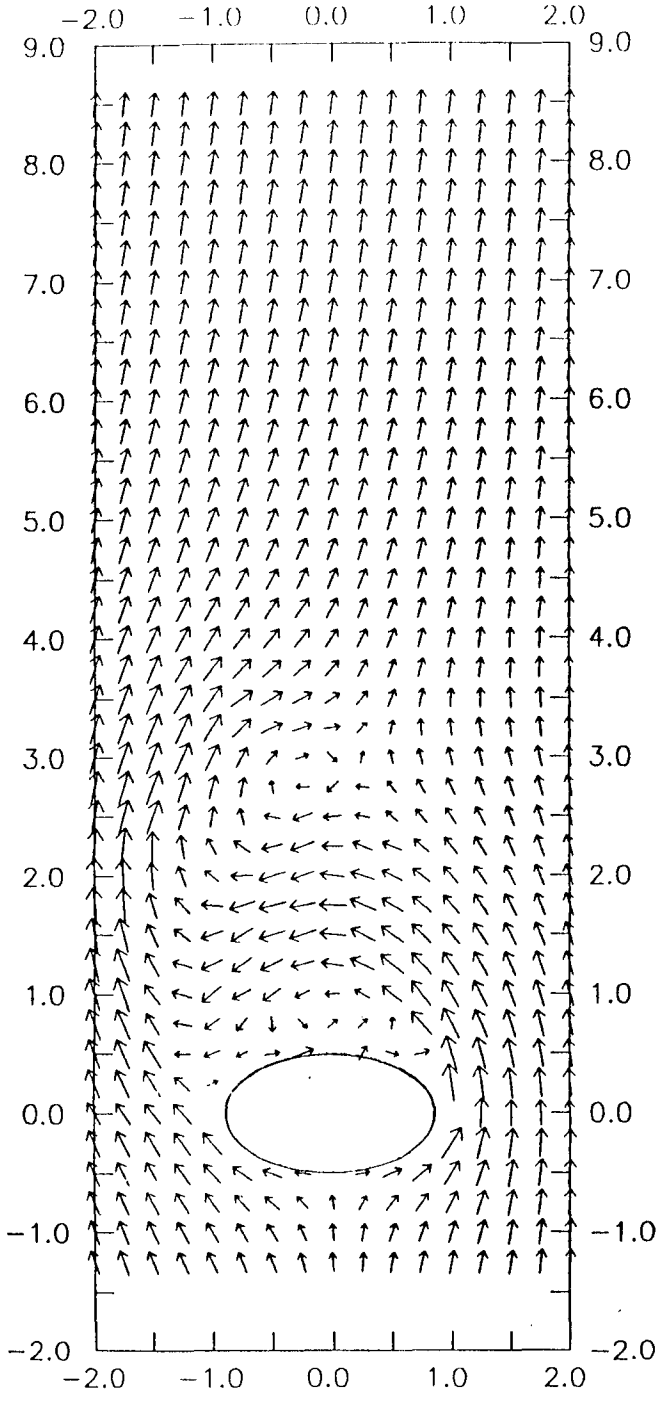
−2.0
−1.0
0.0
1.0
2.0
9.0
8.0
7.0
6.0
5.0
4.0
3.0
2.0
1.0
0.0
−1.0
−2.0

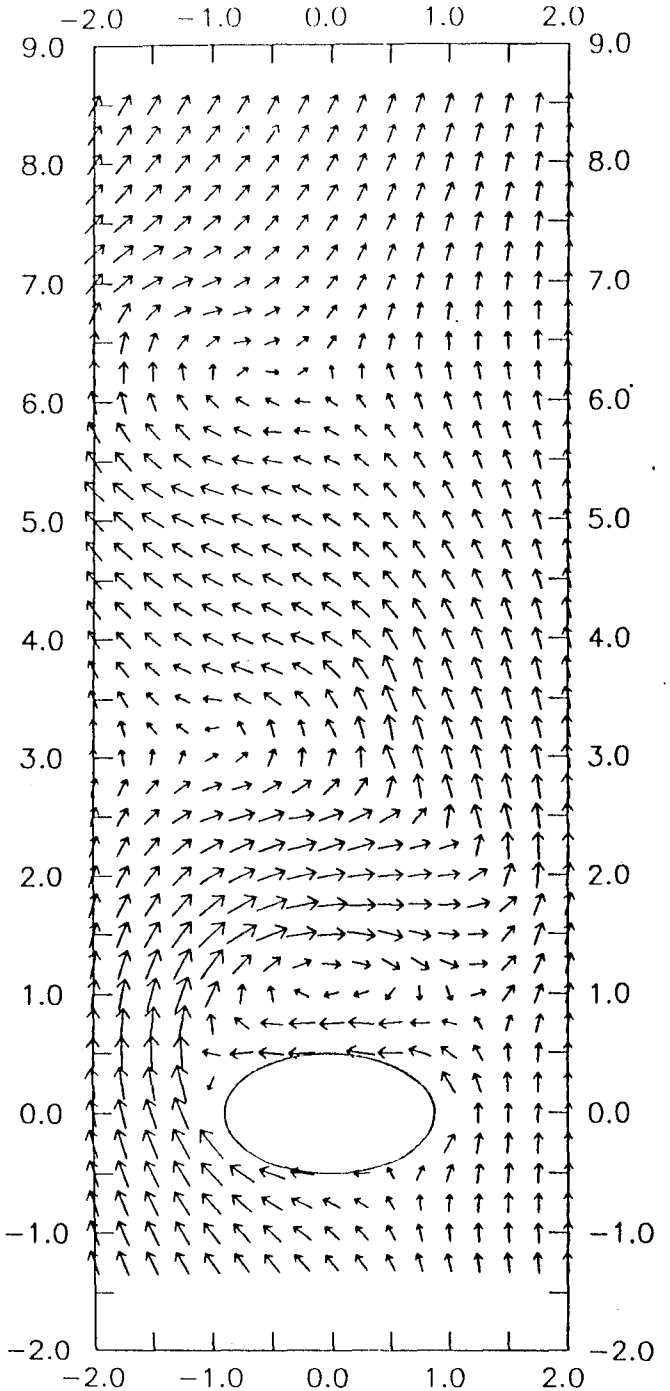
−2.0
−1.0
0.0
1.0
2.0
9.0
8.0
7.0
6.0
5.0
4.0
3.0
2.0
1.0
0.0
−1.0
−2.0

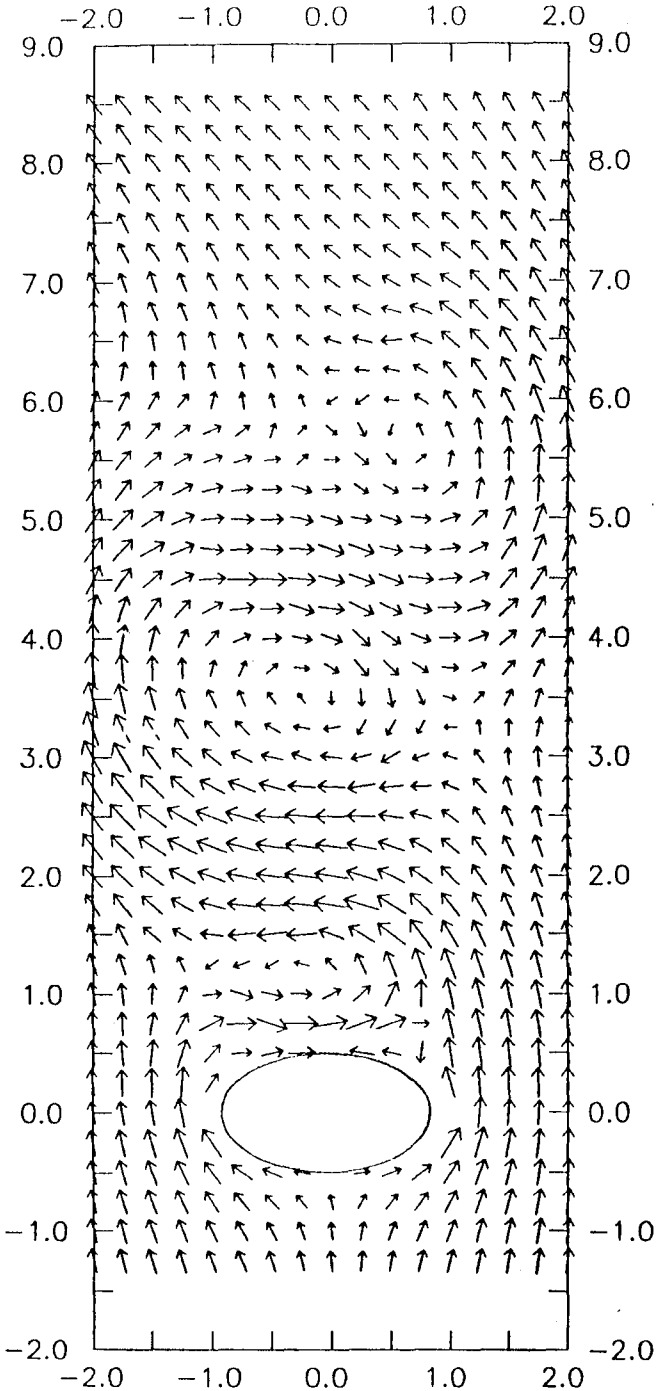
−2.0
−1.0
0.0
1.0
2.0
9.0
8.0
7.0
6.0
5.0
4.0
3.0
2.0
1.0
0.0
−1.0
−2.0

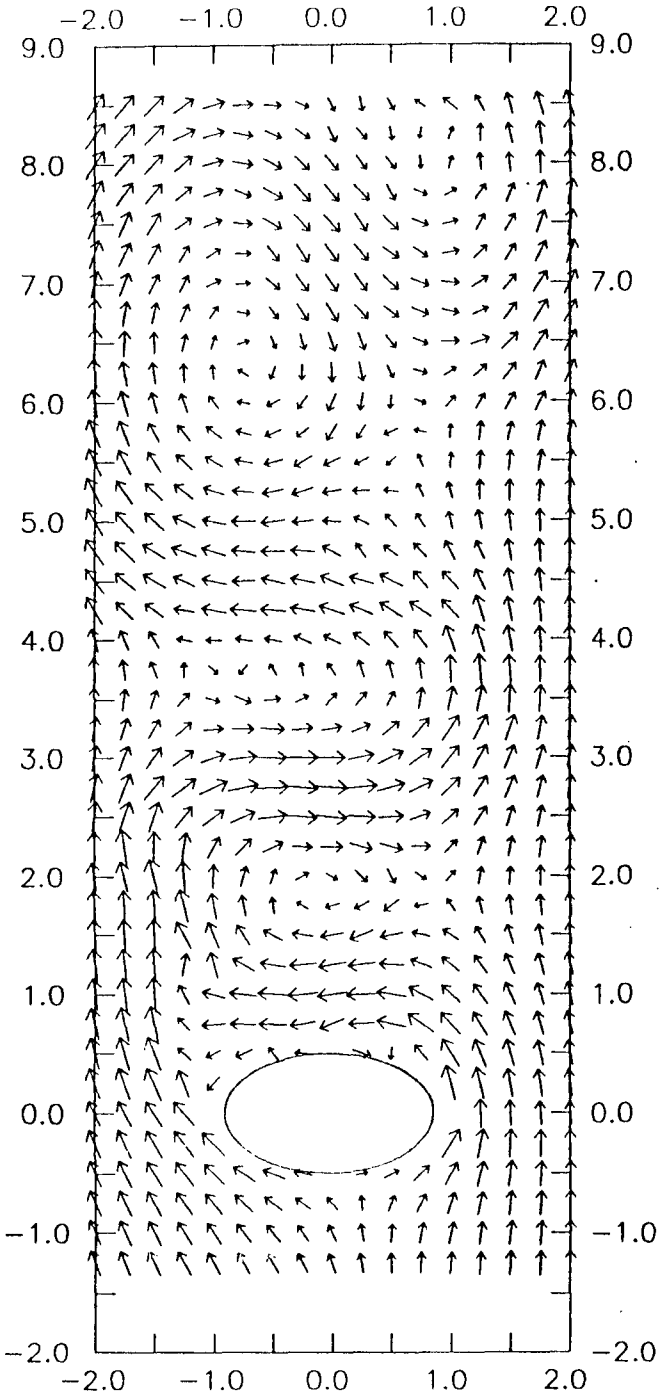
−2.0
−1.0
0.0
1.0
2.0
9.0
8.0
7.0
6.0
5.0
4.0
3.0
2.0
1.0
0.0
−1.0
−2.0

MANUSCRIPT IV

Aerodynamics and Exposure Variability

Aerodynamics and Exposure Variability

Michael R. Flynn and Dennis K. George

Department of Environmental Sciences and Engineering

University of North Carolina at Chapel Hill

Chapel Hill, NC 27599-7400

Abstract - Laboratory measurements of exposure using a mannequin and a point source of tracer gas suggest that locating a contaminant source within a separated boundary layer, results in greater exposure variability than when the source is outside such a region. The results provide information for estimating the relative exposure variability between processes under different aerodynamic conditions.

Introduction

The integral of breathing zone concentration, C, with respect to time defines an individual's exposure over a finite period, T. Exposure is typically expressed as an equivalent time-weighted average C_{twa} by dividing by the interval.

$$C_{twa} = \frac{1}{T}\int_0^T C dt \tag{1}$$

Although the time-weighted average forms the basis of industrial hygiene standards and field evaluations, the large variation in measured exposure makes it difficult to interpret the significance of a single, or even multiple, measurements for specific job.

Ideally the hygienist would like an accurate estimate of the percent of time an employee is above or below some criteria level. Depending on the pharmacology and toxicity of the contaminant this information may be interpreted quite differently. The amount of sampling needed to conclude that an employee exceeds a given exposure standard, a fixed percent

of the time, at an arbitrary confidence level depends upon knowing the variability of that exposure. In general this information is unavailable and, depending upon its magnitude, can be quite expensive to evaluate; more samples being required to estimate a greater level of variation.

Models to predict exposure variability for a given job would assist in estimating the number of samples needed to characterize exposure and evaluate compliance. While such a model would be quite complex, it appears worthwhile to examine some of the factors affecting exposure variance.

Theory

Variation in exposure corresponds to spatial and temporal variation in the concentration field and the worker's location within it. Work at a fixed location and essentially steady-state conditions will result in low exposure variability compared to a job with rapid changes in location through steep concentration gradients (which may also change as a function of time).

The factors affecting exposure variability include changes in: (1) the contaminant generation rate, (2) the air velocity field, (3) the relative location of the source and worker, and (4) the worker activity level. This research focuses on items (2) and (3) above for a fixed rate of contaminant generation, and examines how the aerodynamics of the flow field influence exposure variability.

When a worker is positioned in a current of air or moves relative to stationary air, the phenomenon of boundary layer separation produces a recirculating wake on the downstream side of the body. This recirculating flow can entrain contaminant into the breathing zone and represents an important determinant in the level of exposure. Experimental[1] and field studies[2-3] demonstrate that the mean exposure is reduced when the source of pollutant is external to this recirculating flow.

An important factor in minimizing the effect of this phenomenon is the orientation of the worker with respect to the air flow direction. If the worker holds the source downstream with the airflow from his or her back (position #2) then the recirculating region is large enough to encompass the source in almost any hand-held position. This results in high exposure compared to the case with airflow directed from the side where the source is outside such a recirculating region (position #1), see Figure 1. Although the effect on mean levels of exposure has been demonstrated,[1-3] the assessment on exposure variability has not been addressed. The principal hypothesis of this work is that location of a contaminant source within the near-wake formed by a separated boundary layer will result in higher exposure variability than when the same source is external to such a region.

This hypothesis results from literature review in the related area of contaminant transport in building wakes. Research suggests that "For point sources within the wake the distribution of concentration will be very dependent on the position of the source, and concentration will necessarily be higher than average in the vicinity of the source."[4] While "For sources...with material entrained into the near wake, the concentration tends to be fairly uniform throughout the near wake.."[4] In addition, measurements (to be reported elsewhere) of the concentration distribution, for sources within the near wake of mannequins in uniform wind tunnel flows indicates substantial concentration gradients within the recirculation zone. It is postulated that the concentration gradients established as the result of the source position within the separated boundary layer result in increased variability of exposure compared to the situation where sources are external to such regions.

The extent of recirculating regions downstream of workers in uniform flow was assessed in wind tunnel experiments using mannequins.[1] Flows were such that Reynold's number similarity was maintained for actual workers in air streams with velocities of 25-130 fpm. Smoke generators were used to estimate the length of recirculation which was determined by observation to be approximately one body-width (10-12 inches for the mannequin) downstream for orientation #2. In position #1 smoke visualization results were difficult

to quantify, but the entrainment into the breathing zone appeared minimal at distances greater than 1-3 inches. In position 1 the arms appeared to be primarily responsible for generation of wakes that influenced the source.

In view of the hypothesis, the variability of exposure for position #2 should be greater than position #1 based on the location of the source with respect to the mixing zone. This work is designed to examine this hypothesis.

Methods and Materials

Wind-tunnel studies were conducted with a mannequin and sulfur hexafluoride tracer gas to examine exposure levels and how orientation of the mannequin with respect to air flow direction affected mean exposure.[1] The experiments also provide information on factors affecting the variability of exposure, which is presented here.

Concentrations of sulfur hexafluoride were measured in the breathing zone of a department store mannequin 41 inches in height. The tracer source was a 0.25 inch diameter porous ceramic sphere which was positioned at various distances (Z) from the mannequin along a line perpendicular to the torso at chest height, about 2.25 ft from the wind-tunnel floor. At each distance the breathing-zone concentration was measured with an infrared spectrophotometer and recorded with a data logger to generate a 10 minute time-weighted average exposure.

The mannequin was oriented in either position #1 or position #2 within a 5 ft square wind tunnel. Air velocities of 49, 152 and 265 fpm were generated past the mannequin-source arrangement for each combination of position and Z location. Details of the experiments are reported elsewhere.[1]

Results and Discussion

Our hypothesis suggests that the variability of position #2 measurements should

exceed the variability of position #1 values ($\sigma_2^2 > \sigma_1^2$) based on the effect of the separated boundary layer. In order to maintain comparability, data points from 3 to 10 inches inclusive were selected from each position at all three flows for analysis. All of these points are within a recirculating zone in position #2 but outside such a wake in position #1.

In order to conduct a valid statistical comparison of the variation, appropriate indices must be defined and distributional assumptions examined. While the variance of a given set of measurements is straightforward to calculate; it is common in assessing exposures to assume a lognormal distribution of concentration and to characterize variability with the geometric standard deviation (GSD). This transformation removes the positive correlation between the mean and variance, common in occupational exposure measurements.

The data selected for analysis here (Table I.) fit a lognormal distribution better than a normal one based on a visual examination of rankit plots. A Kolmogorov-Smirnov goodness-of-fit test with Lilliefors option[5,6] suggests that maximum deviations from the fitted lognormal distributions are significant and the fit is not a particularly good one.

The objective in characterizing the distribution is to select appropriate statistical tests to reach conclusions regarding the significance of differences between the position #1 and position #2 variances. The usual F-test is sensitive to departures from normality as is Bartlett's test[6]. A method less sensitive to sample departures from normality, the log-Anova test,[6] is used here on the natural logarithms of the measured concentrations.

The log-ANOVA or Scheffe-Box test was performed to evaluate the hypothesis that $\sigma_1^2 = \sigma_2^2$; where σ_i^2 is the variance of the natural logarithms of the 10 minute time-weighted average concentrations measured in the ith position ($\sigma_1^2 = 0.0119$ while $\sigma_1^2 = 0.6708$). In the Scheffe-Box test employed here the two samples (position 1 and position 2) are each broken down into 4 random sub-groups. A modfied analysis of variance is used to compare sample-to-sample variation to within-sample variation as calculated from the sub-groups. The appropriate test statistic is an F value which, for the data here, contained 1 degree of freedom for the samples (2-1) and 6 degrees of freedom (8-2) for the sub-groups. The

calculated $F_{(1,6)}$ was 41.32 indicating a significant difference, $p < 0.001$.

The results clearly support the conclusion that $\sigma_2^2 > \sigma_1^2$. The question remaining is - can this difference be ascribed to the boundary-layer separation phenomenon or is it an effect primarily of flow and/or distance. For example, it is possible that at one flow or one location position #2 is so much more variable than position #1 that the difference observed overall is due to this location or flow. In order to examine this possibility two additional tests were conducted one by flow and the other by location.

In the first case the data are grouped by flow for each position. This results in 3 samples of 5 for each position. The variance of the logarithms of exposure is presented in Table II. The data show that within either position the variance is relatively homogeneous regardless of flow. This is supported by Hartley's maximum F-test[6] which evaluates the ratio of the highest to lowest variance within a given position. For position #1 this ratio is 3.22 and for position #2 it is 1.45; both are well below the 5% critical value of 20.6. In addition, regardless of the flow level the position #2 variance is always greater than the variance in position #1.

In the second case the data are grouped by source-to- mannequin distance (Z), this results in 5 samples of three for each position. The variance of the logarithms of the exposure are displayed in Table III. Hartley's maximum F- test again supports the relative homogeneity of variance regardless of location for a given position. Maximum F's for positions #1 and #2 are respectively 4.67 and 5.99 with a critical value at the 5% confidence level of 39.0. The position #2 variance is always greater than position #1 variance regardless of Z.

These additional tests suggest that the increased variability of exposure that occurs in position #2 is due to the location of the source within a separated boundary layer and that the actual velocity and/or source-to breathing zone distances are less important in determining the observed differences.

Conclusions

Exposure variance for a given job is an important variable for interpreting field evaluations of occupational health standards. The experimental work here suggests that when the source of pollutant is within a mixing zone formed by boundary layer separation then the variance of the exposure will be greater than if the source is external to such a region. While the results here focus on worker position as the generator of such a separted region; such examples will occur in any instance where there is relative motion between the air and a bluff body.

Work occuring in large recirculating eddies formed by air movement around machines, or internal walls and boundaries will likely result in greater exposure variability when the pollutant source is within such a zone. The number of measurements needed to evaluate exposure is likely to be greater for such situations. This should serve as a crude guide to help industrial hygienists identify situations of high exposure variability on a relative basis.

Acknowledgements

This work was supported by National Institute for Occupational Safety and Health grant # 5 R01 OH02392-01 and the Shell Oil Company Foundation.

References

1) George, D.K.; Flynn, M.R.; Goodman, R.G.: The Impact of Boundary Layer Separation on Local Exhaust Design and Worker Exposure. In Press Applied Occupational and Environmental Hygiene.

2) Tum Suden, K.D.; Flynn, M.R.; Goodman. R.G.: Computer Simulation in the Design of Local Exhaust Hoods for Shielded Metal Arc Welding. In Press Am. Ind. Hyg. Assoc. J.

3) Speight, F.Y.; Campbell, H.C.: *Fumes and Gases in the Welding Environment* Miami, American Welding Institute. (1979).

4) Fackrell, J.E.: Parameters characterising dispersion in the near wake of buildings. Journal of Wind Engineering and Industrial Aerodynamics, 16:97-118 (1984).

5) Wilkinson, L.: *SYSTAT: The System for Statistics.* Evanston, IL. SYSTAT, Inc. (1986).

6) Sokal, R.R.; Rohlf, J.F.: *Biometry* 2nd ed. W.H. Freeman and Co. San Francisco, CA (1981).

Table I. Raw Data: Position, Air Velocity, Source Location (Z) and Natural Log of the 10 minute TWA exposure of mannequin to Sulfur Hexafluoride.

Position	Z (inches)	Air Velocity (fpm)	Ln of Exposure
1	3.0	49	-0.89159
1	4.0	49	-0.91629
1	6.0	49	-0.99425
1	8.0	49	-0.96758
1	10.0	49	-1.0788
1	3.0	152	-0.99425
1	4.0	152	-1.13943
1	6.0	152	-1.1711
1	8.0	152	-1.10866
1	10.0	152	-1.17118
1	3.0	265	-0.82098
1	4.0	265	-1.0788
1	6.0	265	-1.10866
1	8.0	265	-1.10866
1	10.0	265	-1.13943
2	3.0	265	2.04122
2	4.0	265	1.887069
2	6.0	265	1.568615
2	8.0	265	1.131402
2	10.0	265	0.641853
2	3.0	49	3.577947
2	4.0	49	3.157
2	6.0	49	2.459588
2	8.0	49	2.397895
2	10.0	49	2.433613
2	3.0	152	2.360854
2	4.0	152	2.116255
2	6.0	152	1.774952
2	8.0	152	1.335001
2	10.0	152	0.741937

Table II. The Variance of the logarithms of exposure by position and freestream air velocity

Position	Air Velocity (fpm)	Variance
1	49	0.005329
1	152	0.005329
1	265	0.017161
2	49	0.286225
2	152	0.414736
2	265	0.327184

Table III. The Variance of the logarithms of exposure by position and source-to-mannequin distance (Z).

Position	Source-Mannequin-Distance (inches)	Variance
1	3.0	0.007569
1	4.0	0.013225
1	6.0	0.0081
1	8.0	0.006561
1	10.0	0.002209
2	3.0	0.657721
2	4.0	0.458329
2	6.0	0.217156
2	8.0	0.4624
2	10.0	1.014049

Figure 1. Mannequin-source configuration

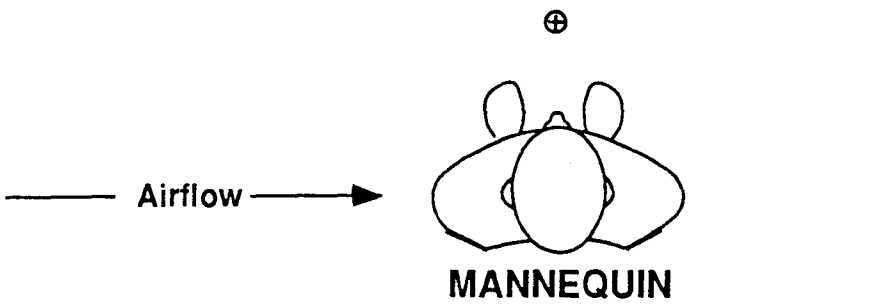

POSITION # 1

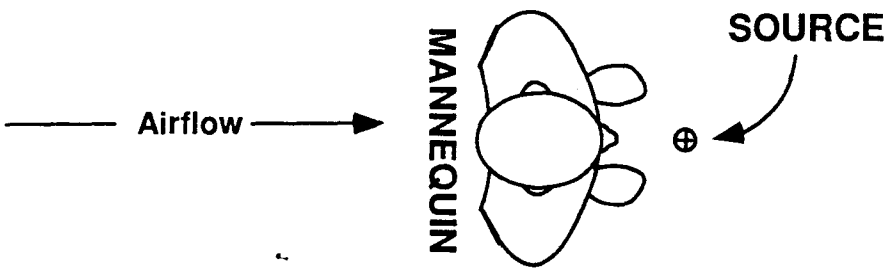

POSITION # 2

APPENDIX A

The Relationship Between Breathing Zone Concentration and Capture Efficiency

Appendix A. The Relationship between Breathing Zone Concentration and Capture Efficiency

Introduction

An important premise of this research is that there exists a functional relationship between the capture efficiency (η_e) of a local exhaust hood and the worker's breathing zone concentration (C_{bz}). It was postulated in the proposal that breathing zone concentration was proportional to the fraction of contaminant escaping the hood i.e., $1 - \eta_e$. Implicit in this analysis was that capture efficiency is a readily determined steady state value; in fact capture efficiency is a time dependent phenomenon which complicates the analysis. The proper theoretical development is presented below.

Theory

The prediction of gas or vapor concentration in ventilated spaces is governed by a mass balance which states that the rate of accumulation is equal to the rate of generation minus the rate of removal:

$$VdC = Q_s dt - \frac{Q_h}{K} dt \tag{1}$$

where: dC is the differential concentration, dt the differential time, V the room volume, Q_s the contaminant flow, Q_h the ventilation exhaust air flow, and the K factor is used to account for non-uniform mixing. At steady state the average concentration in the room is:

$$C_{avg} = \frac{KQ_s}{Q_h} \tag{2}$$

If a source begins generating contaminant at time $t = 0$ in a one-inlet one-outlet (hood) room; and the hood captures a fraction, (η_e) of the source where η_e is a function

of time; then the average concentration in the room at any time T is:

$$C(T) = \frac{Q_s}{V} \int_0^T (1 - \eta_e) dt \tag{3}$$

At steady state $\eta_e = 1.0$ and the concentration is given by equation (2). Thus, η_e which is the capture efficiency, must approach 1.0 in any real steady state situation. It is the integral of capture efficiency with respect to time which determines the volume of contaminant held up in the room at any particular moment. Exposure is related to this "hold up" which is a function of the room mixing pattern, but more importantly in LEV applications, the mixing that develops in the vicinity of the worker, source, and hood.

If the worker's breathing zone concentration is proportional to the the average room concentration at time T i.e. $C_{bz} \propto C(T)$ then breathing zone concentration at time T should be directly proportional to the contaminant flow rate (Q_s) and inversely proportional to the time averaged capture efficiency. This was examined experimentally with the mannequin and several local exhaust hoods.

Methods and Materials

A department store mannequin 41 inches in height was modified such that a continuous air sample could be withdrawn through the mouth. A 0.25 inch diameter diffusing stone was placed in the hands of the mannequin through which 10% sulfur hexafluoride tracer gas was metered at a flow of 0.78 lpm (0.027 cfm). The mannequin was positioned in front of flanged circular hoods in either one of two positions. In position 1 the source is on the centerline but the mannequin stands to the side such that a line connecting the source and mannequin is at right angles to the hood centerline. In position 2 the source is on the hood centerline as is the mannekin itself. This represents the standard configuration where the source is located between the hood and the worker. Figure 1 presents a plan view of the orientations.

Flanged circular hoods of 4, 9, and 12 inches in diameter were operated at flows of 100, 300, and 535 cfm. The mannequin-source configurations described above were positioned such that the source was located at 6, 9, or 15 inches from the hood face. An infrared spectrophotometer was used to measure sulfur hexafluoride concentration in the mannequin breathing zone over a period of 20 minutes. A data logger sampling at 1 Hz, stored half-minute averages for the 20 minute logging time.

Simultaneously a second spectrophotometer monitored sulfur hexafuoride concentration in the duct downstream of the hood at a well-mixed location. Capture efficiency was determined by forming the ratio of the measured concentration to the 100% capture reference concentration which was determined by placing the source inside the hood and measuring the downstream level of sulfur hexafluoride. This method has been described previously in the literature.[1] The raw file thus consists of paired measurements of capture efficiency and breathing zone concentration every half minute for 20 minutes.

The initial experimental design included four factors: (1) hood flow (Q), (2) hood diameter (D), (3) source-to-hood centerline distance (Z), and (4) mannequin position, 1 or 2, (POS). This results in 54 paired values of capture efficiency and breathing-zone concentration.

Results and Analysis

In order to use the data to evaluate the model it would be necessary to compare the instantaneous breathing zone concentration at time T to the time averaged capture efficiency up to that point. An approximation was made by taking the last 4 minute time weighted average of breathing zone concentration and comparing it to the 20-minute time weighted average capture effieciency. The raw data are presented graphically in Figure 2.

The SYSTAT statistical package was used to calculate a Pearson correlation coefficienct, (ρ), between breathing zone concentration and capture efficiency ($\rho_\eta = -0.73$) and also between breathing zone concentration and capture velocity ($\rho_v = -0.22$) as predicted

from the ACGIH Ventilation Manual Formula $V=Q/(10X^2+A)$.

Discussion and Conclusions

As described in Manuscript III, despite control efforts, some leakage of sulfur hexafluoride was experienced from the positive pressure side of the fan. This leakage was directly proportional to the concentration in the duct; at high capture efficiency and low flow maximal leakage would be expected. The effect of this leakage is to obscure the ability of the study to determine the functional relationship between capture efficiency and breathing zone concentration. The leakage would result in higher breathing zone concentrations at the higher efficiencies than would truly exist. Thus we suspect a stronger relationship between efficiency and concentration exists than we have been able to show here. In the case of low flow and low efficiencies, i.e. the highest breathing zone concentrations shown in Figure 2, the maximal estimated leakage (see Manuscript III) accounts for less than 10% of the measured values.

It appears that the time integral of capture efficiency is inversely proportional to the instantaneous breathing zone concentration. The use of capture efficiency as a design parameter appears superior to the capture velocity concept in that a stronger relationship exists with the parameter of interest i.e. the exposure. The difficulty in predicting capture efficiency for actual operations makes its use in modelling questionable; one may as well simulate the concentration directly. However, its true potential for application lies in monitoring and measurement since duct concentrations are easily obtained. Further research is needed to confirm the functional relationship for more realistic laboratory simulations and field studies. It is important that the time integral of the efficiency be used and that the start-up of the operation be included since efficiencies tended to approach 100% rather quickly.

References

1. Flynn, M.R. and Ellenbecker, M.J. The Capture Efficiency of Flanged Circular Local Exhaust Hoods. *Ann. Occup. Hug.* 30:4 497-513, (1986).

Figure 1

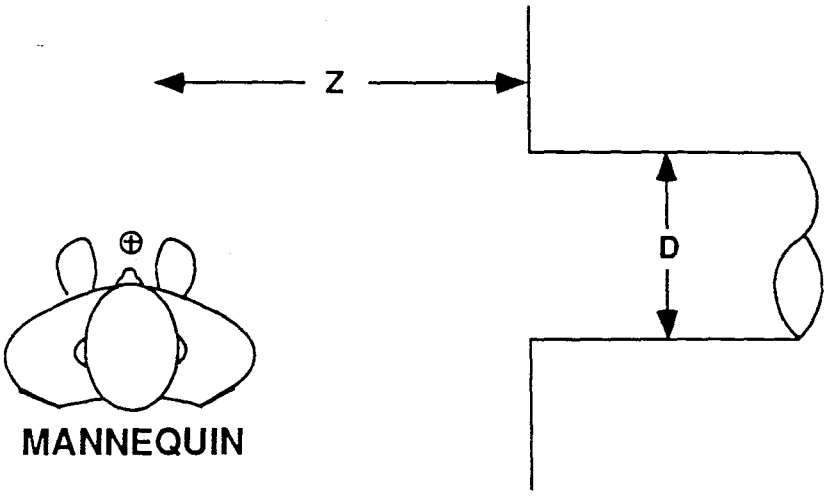

POS = 1

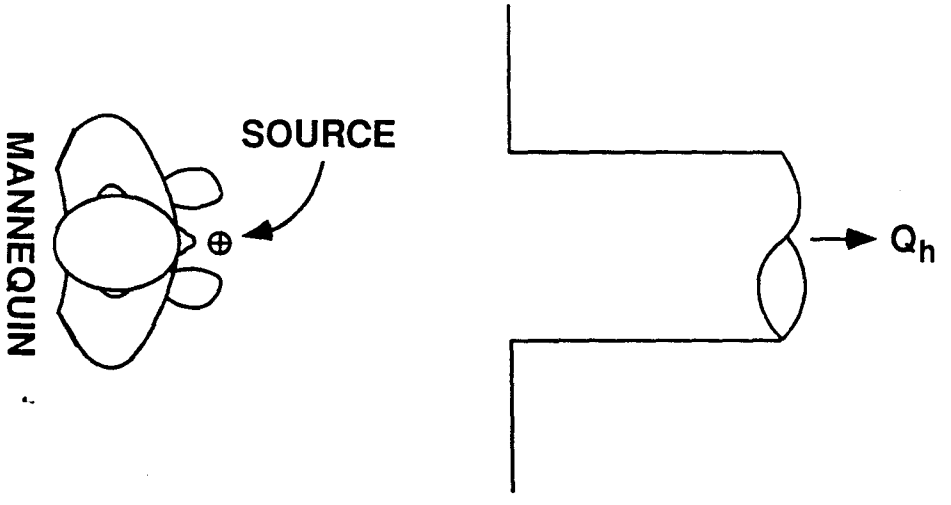

POS = 2

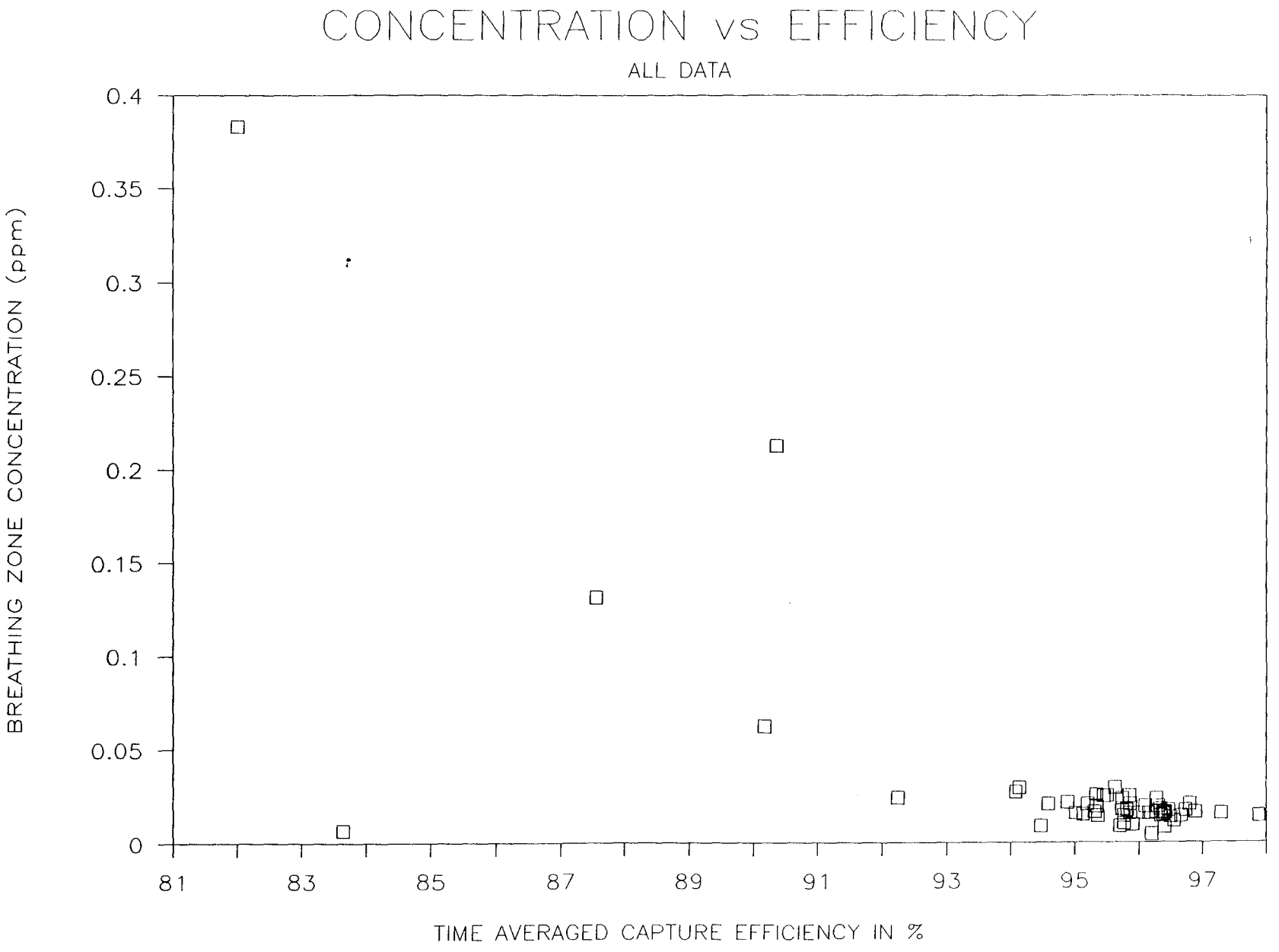
CONCENTRATION vs EFFICIENCY
ALL DATA
BREATHING ZONE CONCENTRATION (ppm)
0.4
0.35
0.3
0.25
0.2
0.15
0.1
0.05
0
81
83
85
87
89
91
93
95
97
TIME AVERAGED CAPTURE EFFICIENCY IN %

Figure 2

APPENDIX B

The Discrete Vortex Method Algorithm

```
C
C
C   THIS IS THE DVM ALGORITHM
C   Copyright Michael R. Flynn and Casey T. Miller
C   Sept. 9, 1989.
C
$DEBUG
      IMPLICIT REAL*8(A-H,O-Z)
      REAL*8 NBLT
      CHARACTER*80 TITLE
      DIMENSION
XE(3000,2),YE(3000,2),SE(3000,2),H(21,21),LIND(3000),

1XC(20),YC(20),UPGP(20),VPGP(20),VXBLBGP(20),VYBLBGP(20),
     2VT(20),ARC(20),XRHS(21),XTS(50),YTS(50),X(50),Y(50),
     3XSTRGP(20),THETA(50),THEM(50),BVEC(21),
     4XX(17,40),YY(17,40),VELX(17,40),VELY(17,40)
      COMMON /SIZE/ MAXEQN /BLK/ XE,YE,SE,LIND,SEFAC,
     1XC,YC,UPGP,VPGP,VXBLBGP,VYBLBGP,VT,SHTL,VCX,VCY,NBLT,

2ARC,XRHS,XTS,YTS,X,Y,XSTRGP,A,B,BR,NEL,UMIN,UMAX,XSEED,VISC
,DELT
      OPEN (5,FILE='DVMIN')
      OPEN (6,FILE='DVMOUT1')
      OPEN (7,FILE='DVMOUT2')
      READ (5,1111) TITLE
 1111 FORMAT (A80)
      READ (5,*)
N,A,B,VCX,VCY,DELT,NTS,VISC,NBLFAC,XSEED,SEFAC
      UMIN=0.D00
      UMAX=1.D00
      MAXEQN=21
      RENO=(2.D00*A*DSQRT(VCX**2+VCY**2))/VISC
      NBLT=NBLFAC*(2.D00*A/DSQRT(RENO))
      NEL=0
      SHTL=0.242211206
      L=N+1
      PI=3.141592654
      BR=SHTL/PI
C
C   CLEARING COEEFICIENT MATRIX
C
      DO 10 I=1,MAXEQN
      DO 20 J=1,MAXEQN
      H(I,J)=0.0
   20 CONTINUE
      XRHS(I)=0.0
      BVEC(I)=0.0
```

```
   10 CONTINUE
      ARC(1)=0.D00
      ARC(2)=0.08718345
      ARC(3)=0.17387013
      ARC(4)=0.25956996
      ARC(5)=0.34380631
      ARC(6)=0.42612308
      ARC(7)=0.50609207
      ARC(8)=0.58332103
      ARC(9)=0.65746255
      ARC(10)=0.72822416
      ARC(11)=0.79538015
      ARC(12)=0.85878561
      ARC(13)=0.91839329
      ARC(14)=0.97427354
      ARC(15)=1.02663689
      ARC(16)=1.07585669
      ARC(17)=1.12248590
      ARC(18)=1.16725747
      ARC(19)=1.21105603
C
C
C     DISCRETIZATION OF THE ELLIPSE
C     AND INITIALIZATION OF CONTROL POINTS
C
       THETA(1)=0.0
       THETA(2)=0.445066813
       THETA(3)=0.787378588
       THETA(4)=1.07110193
       THETA(5)=1.326744145
       THETA(6)=PI/2.D00
      DO 30 I=7,L
      IF(I.LE.11) THEN
       THETA(I)=PI-THETA(12-I)
      ELSEIF(I.LE.16) THEN
       THETA(I)=PI+THETA(I-10)
      ELSEIF(I.LE.20) THEN
       THETA(I)=2.D00*PI-THETA(22-I)
      ELSE
       THETA(I)=THETA(1)
      ENDIF
   30 CONTINUE
      THEM(1)=0.235896083
      THEM(2)=0.626432353
      THEM(3)=0.934183991
      THEM(4)=1.201210117
      THEM(5)=1.449424211
      DO 40 I=6,20
      IF(I.LE.10) THEN
       THEM(I)=PI-THEM(11-I)
      ELSEIF(I.LE.15) THEN
       THEM(I)=PI+THEM(I-10)
      ELSE
       THEM(I)=2.D00*PI-THEM(21-I)
```

```
      ENDIF
   40 CONTINUE
      DO 50 I=1,L
      X(I)=(A/1.1)*DCOS(THETA(I))
      Y(I)=(B/1.1)*DSIN(THETA(I))
   50 CONTINUE
      DO 60 I=1,N
      XC(I)=A*DCOS(THEM(I))
      YC(I)=B*DSIN(THEM(I))
      YTS(I)=(Y(I)+Y(I+1))/2.D00
      XTS(I)=(X(I)+X(I+1))/2.D00
      IF(I.EQ.1) THEN
       XSTRGP(I)=0.121105603
      ELSE
       XSTRGP(I)=XSTRGP(I-1)+SHTL
      ENDIF
   60 CONTINUE
      DO 70 I=1,N
      ST=-(B**2*XC(I))/(A**2*YC(I))
      BETA=DSQRT(1.D00/(1.D00+ST**2))
      IF(YC(I).GT.0.0) THEN
       BETA=BETA
       ALPHA=-BETA*ST
      ELSE
       BETA=(-BETA)
       ALPHA=-BETA*ST
      ENDIF
      DO 80 J=1,N
      CALL INTGRT(XC(I),YC(I),XFCT,YFCT,XINT,YINT,J)
      H(I,J)=(XFCT*ALPHA*XINT)+(YFCT*BETA*YINT)
   80 CONTINUE
   70 CONTINUE
      CALL FACTOR(N,H)
C
C      AT THIS POINT WE FORM THE B VECTOR BY DOTTING THE
C      OUTWARD UNIT NORMAL WITH THE VELOCITY DUE TO
CROSSDRAFT
C      AND BLOBS, THIS GETS DONE EVERY TIME STEP.
C
C
C
C       SOLVING GLOBAL EQS FOR NODAL UNKNOWNS
      DO 5555 K=1,NTS
      IF(K.NE.1) THEN
        DO 101 J=1,N
        CALL BLOBS(XC(J),YC(J),VXBLBGP(J),VYBLBGP(J))
  101   CONTINUE
      ELSE
        DO 108 J=1,N
        VXBLBGP(J)=0.D00
        VYBLBGP(J)=0.D00
        UPGP(J)=0.D00
        VPGP(J)=0.D00
  108   CONTINUE
```

```
      ENDIF
      DO 21 I=1,N
      D=DSQRT(XC(I)**2+16.D00*YC(I)**2)
      BVEC(I)=-(VCX+VXBLBGP(I))*(XC(I)/D)-
     1(VCY+VYBLBGP(I))*(4.D00*YC(I)/D)
   21 CONTINUE
      CALL SOLVE(N,H,BVEC,XRHS)
      DO 102 I=1,N
      CALL POTVEL(XC(I),YC(I),UPGP(I),VPGP(I))
  102 CONTINUE
      CALL TANGVEL
      CALL SHEETS
C
C   CALCULATE OUTPUT
C
      IF(K.EQ.NTS) THEN
      DO 222 I=1,17
      DO 333 J=1,40
        XX(I,J)=0.25*I-2.25
        YY(I,J)=0.25*J-1.5
        CALL POTVEL(XX(I,J),YY(I,J),UPXXYY,VPXXYY)
        CALL BLOBS(XX(I,J),YY(I,J),UBXXYY,VBXXYY)
        VELX(I,J)=UPXXYY+UBXXYY
        VELY(I,J)=VPXXYY+VBXXYY
        WRITE(6,*) XX(I,J),YY(I,J),VELX(I,J),VELY(I,J)
  333 CONTINUE
  222 CONTINUE
      WRITE(7,*) NEL
      NPLSCT=0
      NMNSCT=0
      NXPLCT=0
      NXMNCT=0
      DO 444 I=1,NEL
        WRITE(7,*) XE(I,2),YE(I,2),SE(I,2),LIND(I)
        IF(SE(I,2).GT.0.D00) THEN
         NPLSCT=NPLSCT+1
        ELSE
         NMNSCT=NMNSCT+1
        ENDIF
        IF(XE(I,2).GT.0.D00) THEN
         NXPLCT=NXPLCT+1
        ELSE
         NXMNCT=NXMNCT+1
        ENDIF
  444 CONTINUE
      WRITE(7,*) NPLSCT,NMNSCT,NXPLCT,NXMNCT
      ENDIF
      CALL DIFF
      CALL META
      CALL CONVECT
      CALL META
      CALL DIFF
      CALL META
 5555 CONTINUE
```

```
      STOP
      END
C
C
CCCCCCCCCCCCCCCCCCCCCCCCCCCCCCCCCCCCCCCCCCCCCCCCCCCCCCCCCCCC
CCCCCCCCCCC
C
C
C     SUBROUTINE FOR FACTORING THE A MATRIX USING THE LOWER-
UPPER     C
C     DECOMPOSITION METHOD WHICH ALLOWS FOR MULTIPLE
SOLUTIONS OF     C
C     THE FINITE ELEMENT MATRICES FROM JUST ONE FACTORING
GIVEN       C
C     CONSTANT AQUIFER PROPERTIES AND A CONSTANT TIME STEP
C
C
C
CCCCCCCCCCCCCCCCCCCCCCCCCCCCCCCCCCCCCCCCCCCCCCCCCCCCCCCCCCCC
CCCCCCCCCCC

      SUBROUTINE FACTOR(NEQNS,A)
      IMPLICIT REAL*8(A-H, O-Z)
      DIMENSION A(MAXEQN,MAXEQN)
      COMMON /SIZE/ MAXEQN

C.....FACTOR THE [A] MATRIX---STORING OPERATION PERFORMED IN
THE
C.....LOWER DIAGONAL PORTION OF THE MATIRX

      M = NEQNS-1
      DO 100 I = 1,M
         DO 100 J = I+1,NEQNS
            A(J,I) = -A(J,I)/A(I,I)
            DO 100 K = I+1,NEQNS
               A(J,K) = A(J,K)+A(J,I)*A(I,K)
  100 CONTINUE
      RETURN
      END
C
CCCCCCCCCCCCCCCCCCCCCCCCCCCCCCCCCCCCCCCCCCCCCCCCCCCCCCCCCCCC
CCCCCCCCCCC
C
C
C     SUBROUTINE FOR SOLVING THE SYSTEM OF EQUATIONS GIVEN A
FACTORED C
C     A MATRIX USING THE LOWER-UPPER DECOMPOSITON METHOD FOR
C
C     SOLUTION
C
C
C
CCCCCCCCCCCCCCCCCCCCCCCCCCCCCCCCCCCCCCCCCCCCCCCCCCCCCCCCCCCC
CCCCCCCCCCC
```

```
      SUBROUTINE SOLVE(NEQNS,A,B,X)
      IMPLICIT REAL*8(A-H, O-Z)
      DIMENSION A(MAXEQN,MAXEQN), B(MAXEQN), X(MAXEQN)
      COMMON /SIZE/ MAXEQN

C.....UPDATE {b} VECTOR

      M = NEQNS-1
      DO 100 I = 1,M
         DO 100 J = I+1,NEQNS
            B(J) = B(J)+A(J,I)*B(I)
  100 CONTINUE

C.....PERFORM BACK SUBSTITUTION TO SOLVE FOR {x} VECTOR

      X(NEQNS) = B(NEQNS)/A(NEQNS,NEQNS)
      DO 110 J = M,1,-1
         DO 120 K = J+1,NEQNS
            B(J) = B(J)-X(K)*A(J,K)
  120    CONTINUE
         X(J) = B(J)/A(J,J)
  110    CONTINUE
      RETURN
      END

C
C
C
C   SUBROUTINE #3A "TANGVEL"
C
C   THIS SUBROUTINE IS DESIGNED TO PROVIDE THE TANGENTIAL
VELOCITIES
C   AT THE GENERATION POINTS OF AN ELLIPTIC CYLINDER. THE
TANGENTIAL
C   VELOCITY AT THE GENERATION POINTS IS CALCULATED AS THE
SUM OF THE
C   POTENTIAL AND BLOB COMPONENTS, AND THEN ADJUSTED FOR THE
SHEETS.
C   THE COQRDINATE TRANSFORMS ARE CRITICAL. THE PROGRAM
RECIEVES THE
C   POTENTIAL AND BLOB X,Y VELOCITY COMPONENTS
(UPGP,VPGP,VXBLBGP,
C   VYBLBGP) AT THE GENERATION POINTS; THESE ARRAYS ARE
CALCULATED
C   IN SUBROUTINES #1A AND #2 AND ARE RECALCULATED EVERY
TIME STEP.
C   THESE COMPONENTS ARE SUMMED AND DOTTED WITH THE UNIT
TANGENTIAL
C   VECTOR TO GIVE THE TANGENTIAL FREESTREAM
VELOCITY(TGFSV). THIS
C   VELOCITY IS ADJUSTED VIA CHORINS ALGORITHM TO PRODUCE
THE TANGENTIAL
C   VELOCITY AT THE GEN. PT. VT(I).
```

```
C
C   THE ARRAY ARC(20) GIVES THE ARCLENGTHS ALONG THE ELLIPSE
FOR
C   SPECIFIED VALUES (AT 5 DEGREE INCREMENTS) OF THE ANGLE
PHI
C   THE ARRAY XSTRGP(20) CONTAINS THE ARCLENGTHS FOR THE 20
GENERATION
C   POINTS.
C
C
      SUBROUTINE TANGVEL
      IMPLICIT REAL *8(A-H,O-Z)
      REAL*8 NBLT
      DIMENSION
XE(3000,2),YE(3000,2),SE(3000,2),H(21,21),LIND(3000),

1XC(20),YC(20),UPGP(20),VPGP(20),VXBLBGP(20),VYBLBGP(20),
     2VT(20),ARC(20),XRHS(21),XTS(50),YTS(50),X(50),Y(50),
     3XSTRGP(20),THETA(50),THEM(50),BVEC(21),
     4XX(17,40),YY(17,40),VELX(17,40),VELY(17,40)
      COMMON /SIZE/ MAXEQN /BLK/ XE,YE,SE,LIND,SEFAC,
     1XC,YC,UPGP,VPGP,VXBLBGP,VYBLBGP,VT,SHTL,VCX,VCY,NBLT,

2ARC,XRHS,XTS,YTS,X,Y,XSTRGP,A,B,BR,NEL,UMIN,UMAX,XSEED,VISC
,DELT
      SSUM=0.D00
      PI=3.141592654
      ANG=0.087266462
      DO 100 I=1,20
      UTDEN=DSQRT(XC(I)**2+16.D00*YC(I)**2)
      VX=UPGP(I)+VXBLBGP(I)
      VY=VPGP(I)+VYBLBGP(I)
      TGFSV=-(4.D00*YC(I)/UTDEN)*VX+((XC(I)/UTDEN)*VY)
      SSUM=0.0
      DO 200 J=1,NEL
      IF (LIND(J).LE.1) THEN
C   THE FOLLOWING CODE IS DESIGNED TO CALCULATE THE X*
COORDINATE FOR
C   THE SHEET AND ADD THE SHEET VELOCITY COMPONENTS
        F=DSQRT(A**2-B**2)
        GAM1E=DSQRT(YE(J,2)**2+(XE(J,2)+F)**2)
        GAM2E=DSQRT(YE(J,2)**2+(XE(J,2)-F)**2)
        ENE=(GAM1E-GAM2E)/DSQRT(3.D00)
        GAM2=(2.D00*F)/DSQRT(3.D00)-(DSQRT(3.D00)/2.D00)*ENE
        GAM1=DSQRT(3.D00)*ENE+GAM2
        IF(XE(J,2).EQ.0.D00) THEN
          XR=0.0
          IF(YE(J,2).GT.0.D00) THEN
           YR=B
          ELSE
           YR=-B
```

```
        ENDIF
      ELSEIF(YE(J,2).EQ.0.D00) THEN
        YR=0.0
        IF(XE(J,2).GT.0.D00) THEN
         XR=A
        ELSE
         XR=-A
        ENDIF
      ELSE
        XR=(GAM1**2-GAM2**2)/(4.D00*F)
        IF(YE(J,2).GT.0.0) THEN
         YR=DSQRT(GAM2**2-(XR-F)**2)
        ELSE
         YR=-DSQRT(GAM2**2-(XR-F)**2)
        ENDIF
      ENDIF
C      PREX=DABS(XR)
      PHI=DACOS(XR)
      PHISTR=DABS(PHI-1.570796327)
      IBTLM=INT(PHISTR/ANG)+1
      ARC1=ARC(IBTLM)
      ARC2=ARC(IBTLM+1)
      IF(IBTLM.EQ.1) THEN
      ANGG=0.D00
      ELSE
      ANGG=(IBTLM-1)*ANG
      ENDIF
      ARCINC=(PHISTR-ANGG)/ANG
      TARC=ARC1+ARCINC*(ARC2-ARC1)
      IF(PHI.GE.1.570796327) THEN
      ARCL=1.21105603+TARC
      ELSE
      ARCL=1.21105603-TARC
      ENDIF
      IF(YR.GE.0.D00) THEN
       XSTR=ARCL
      ELSE
       XSTR=4.84422412-ARCL
      ENDIF
      PRED=DABS(XSTRGP(I)-XSTR)
      IF (PRED.LE.(SHTL)) THEN
        D=1.D00-(PRED/(SHTL))
      ELSE
        D=0.D00
      ENDIF
      SSUM=SSUM+D*SE(J,2)
      ELSE
      GOTO 200
      ENDIF
  200 CONTINUE
      VT(I)=TGFSV-SSUM
  100 CONTINUE
      RETURN
      END
```

```
C
C
C
C
C
C
C
C   THIS SUBROUTINE IS DESIGNED TO PROVIDE THE SHEET
STRENGTHS FOR
C   THE NEWLY GENERATED SHEETS
C
C
C
C
      SUBROUTINE SHEETS
      IMPLICIT REAL *8(A-H,O-Z)
      REAL*8 NBLT
      DIMENSION
XE(3000,2),YE(3000,2),SE(3000,2),H(21,21),LIND(3000),

1XC(20),YC(20),UPGP(20),VPGP(20),VXBLBGP(20),VYBLBGP(20),
     2VT(20),ARC(20),XRHS(21),XTS(50),YTS(50),X(50),Y(50),
     3XSTRGP(20),THETA(50),THEM(50),BVEC(21),
     4XX(17,40),YY(17,40),VELX(17,40),VELY(17,40)
      COMMON /SIZE/ MAXEQN /BLK/ XE,YE,SE,LIND,SEFAC,
     1XC,YC,UPGP,VPGP,VXBLBGP,VYBLBGP,VT,SHTL,VCX,VCY,NBLT,

2ARC,XRHS,XTS,YTS,X,Y,XSTRGP,A,B,BR,NEL,UMIN,UMAX,XSEED,VISC
,DELT
      SEMAX=SEFAC*VCY
      ISSHTS=0
      DO 100 I=1,20
      VTII=2.D00*VT(I)
      NOSHE=ABS(INT(VTII/SEMAX))+1
      DO 200 J=1,NOSHE
      SE(NEL+ISSHTS+J,2)=2.D00*VT(I)/NOSHE
      XE(NEL+ISSHTS+J,2)=XC(I)
      YE(NEL+ISSHTS+J,2)=YC(I)
      LIND(NEL+ISSHTS+J)=0
  200 CONTINUE
      ISSHTS=ISSHTS+NOSHE
```

```
  100 CONTINUE
      DO 300 J=1,NEL
      IF(LIND(J).EQ.0) LIND(J)=1
  300 CONTINUE
      NEL=NEL+ISSHTS
      RETURN
      END
C
C
C
C
C
C
C   THIS SUBROUTINE IS DESIGNED TO PROVIDE THE DIFFUSIVE
DISPLACEMENT
C   IF THE ELEMENT IS A SHEET ONLY A DISPLACEMENT NORMAL TO
THE CYLINDER
C   SURFACE IS USED. IF THE ELEMENT IS A BLOB BOTH X AND Y
DISPALCEMENTS
C   ARE USED.
C
C
C
C
C
      SUBROUTINE DIFF
      IMPLICIT REAL *8(A-H,O-Z)
      REAL*8 MU
      REAL*8 NBLT
      DIMENSION
XE(3000,2),YE(3000,2),SE(3000,2),H(21,21),LIND(3000),

1XC(20),YC(20),UPGP(20),VPGP(20),VXBLBGP(20),VYBLBGP(20),
     2VT(20),ARC(20),XRHS(21),XTS(50),YTS(50),X(50),Y(50),
     3XSTRGP(20),THETA(50),THEM(50),BVEC(21),
     4XX(17,40),YY(17,40),VELX(17,40),VELY(17,40)
      COMMON /SIZE/ MAXEQN /BLK/ XE,YE,SE,LIND,SEFAC,
     1XC,YC,UPGP,VPGP,VXBLBGP,VYBLBGP,VT,SHTL,VCX,VCY,NBLT,

2ARC,XRHS,XTS,YTS,X,Y,XSTRGP,A,B,BR,NEL,UMIN,UMAX,XSEED,VISC
,DELT
      MU=0.D00
      REN=2.D00*A*DSQRT(VCX**2+VCY**2)/VISC
c      SIGBLB=DSQRT(DELT/REN)
      SIG=DSQRT(DELT*VISC)
      DO 100 I = 1,NEL
         XE(I,1)=XE(I,2)
         YE(I,1)=YE(I,2)
         IF(LIND(I).LE.1) THEN
           CALL NORM(MU,SIG,XN)
           PI=3.141592654
           ANG=0.087266462
C   THE FOLLOWING CODE IS DESIGNED TO CALCULATE THE X*
COORDINATE FOR
```

```
            F=DSQRT(A**2-B**2)
            GAM1E=DSQRT(YE(I,2)**2+(XE(I,2)+F)**2)
            GAM2E=DSQRT(YE(I,2)**2+(XE(I,2)-F)**2)
            ENE=(GAM1E-GAM2E)/(DSQRT(3.D00))
            GAM2=(2*F)/DSQRT(3)-(DSQRT(3)/2.D00)*ENE
            GAM1=DSQRT(3.D00)*ENE+GAM2
            IF(XE(I,2).EQ.0.D00) THEN
            XR=0.D00
                 IF(YE(I,2).GT.0.D00) THEN
                 YR=B
                 ELSE
                 YR=-B
                 ENDIF
             ELSEIF(YE(I,2).EQ.0.D00) THEN
             YR=0.D00
                 IF(XE(I,2).GT.0.D00) THEN
                 XR=A
                 ELSE
                 XR=-A
                 ENDIF
             ELSE
                XR=(GAM1**2-GAM2**2)/(4.D00*F)
                 IF(YE(I,2).GT.0.D00) THEN
                 YR=DSQRT(GAM2**2-(XR-F)**2)
                 ELSE
                 YR=-DSQRT(GAM2**2-(XR-F)**2)
                 ENDIF
             ENDIF
            YSTR=DSQRT((XE(I,2)-XR)**2+(YE(I,2)-YR)**2)
            D=DSQRT(XR**2+16.D00*YR**2)
            XINC=XN*XR/D
            YINC=XN*4.D00*YR/D
            XE(I,2)=XE(I,1)+XINC
            YE(I,2)=YE(I,1)+YINC
          ELSE
           CALL NORM(MU,SIG,XN)
           XE(I,2)=XE(I,1)+XN
           CALL NORM(MU,SIG,XN)
           YE(I,2)=YE(I,1)+XN
          ENDIF
  100 CONTINUE
      RETURN
      END

      SUBROUTINE NORM(MU,SIGMA,XN)
      IMPLICIT REAL*8(A-H,O-Z)
      REAL*8 MU
      REAL*8 NBLT
      DIMENSION
XE(3000,2),YE(3000,2),SE(3000,2),H(21,21),LIND(3000),
```

```
1XC(20),YC(20),UPGP(20),VPGP(20),VXBLBGP(20),VYBLBGP(20),
     2VT(20),ARC(20),XRHS(21),XTS(50),YTS(50),X(50),Y(50),
     3XSTRGP(20),THETA(50),THEM(50),BVEC(21),
     4XX(17,40),YY(17,40),VELX(17,40),VELY(17,40)
      COMMON /SIZE/ MAXEQN /BLK/ XE,YE,SE,LIND,SEFAC,
     1XC,YC,UPGP,VPGP,VXBLBGP,VYBLBGP,VT,SHTL,VCX,VCY,NBLT,

2ARC,XRHS,XTS,YTS,X,Y,XSTRGP,A,B,BR,NEL,UMIN,UMAX,XSEED,VISC
,DELT
  100 U1 = (DMOD (24298.D00*XSEED + 99991.D00, 199017.D00))
      XSEED  = U1
      U1 = U1*(UMAX - UMIN)/199017.D00 + UMIN
      U2 = (DMOD (24298.D00*XSEED + 99991.D00, 199017.D00))
      XSEED  = U2
      U2 = U2*(UMAX - UMIN)/199017.D00 + UMIN
      IF(U1 .EQ. 0.D00) GO TO 100
      XN = DSQRT (-2.D00 * DLOG (U1))*DCOS
(2.D00*3.14159D00*U2)
     1     *SIGMA + MU
      RETURN
      END
C
C
C
C
C
C
C
C
C
C
C   THIS SUBROUTINE IS DESIGNED TO PROVIDE THE METAMORPHOSIS
BETWEEN
C   SHEETS AND BLOBS. THE STRENGTH OF A VORTEX IS EQUAL TO
THE STRENGTH
C   OF A SHEET TIMES THE SHEET LENGTH (SLOPPY NOMENCLATURE
HERE).
C   THE KEY TO METAMORPHOSIS IS IDENTIFYING WHETHER THE
ELEMENT HAS MOVED
C   FROM, INTO, OUTOF, OR ACROSS THE NUMERICAL BOUNDARY
LAYER. THEREFOR
C   FOR EACH ELEMENT IT IS NECESSARY TO DETERMINE AN
INDICATOR VARIABLE
C   NBLIND FOR ITS CURRENT POSITION, TELLING WHERE IT IS
C   WITH REGARD TO THE NBL, THE SAME INFORMATION FOR ITS
C   PREVIOUS POSITION IS GIVEN BY THE LIND(I) ARRAY.
C
C
C
```

```
C
      SUBROUTINE META
      IMPLICIT REAL *8(A-H,O-Z)
      REAL*8 NBLT
      DIMENSION
XE(3000,2),YE(3000,2),SE(3000,2),H(21,21),LIND(3000),

1XC(20),YC(20),UPGP(20),VPGP(20),VXBLBGP(20),VYBLBGP(20),
     2VT(20),ARC(20),XRHS(21),XTS(50),YTS(50),X(50),Y(50),
     3XSTRGP(20),THETA(50),THEM(50),BVEC(21),
     4XX(17,40),YY(17,40),VELX(17,40),VELY(17,40)
      COMMON /SIZE/ MAXEQN /BLK/ XE,YE,SE,LIND,SEFAC,
     1XC,YC,UPGP,VPGP,VXBLBGP,VYBLBGP,VT,SHTL,VCX,VCY,NBLT,

2ARC,XRHS,XTS,YTS,X,Y,XSTRGP,A,B,BR,NEL,UMIN,UMAX,XSEED,VISC
,DELT
C
C   THE FIRST TASK IS TO CALCULATE THE VALUE
C   OF THE NBLIND.
      DO 100 I=1,NEL
      DOX=A+NBLT
      DOY=B+NBLT
      DIX=A-NBLT
      DIY=B-NBLT
      EO=(YE(I,2)/DOY)**2+(XE(I,2)/DOX)**2
      EI=(YE(I,2)/DIY)**2+(XE(I,2)/DIX)**2
      ES=(YE(I,2)/B)**2+(XE(I,2)/A)**2
      IF(EO.GE.1.D00) THEN
        NBLIND=1
      ELSEIF(ES.GT.1.D00.AND.EO.LT.1.D00) THEN
        NBLIND=2
      ELSEIF(ES.EQ.1.D00) THEN
        NBLIND=3
      ELSEIF(ES.LT.1.D00.AND.EI.GT.1.D00) THEN
        NBLIND=4
      ELSE
        NBLIND=5
      ENDIF
C
C   AT THIS POINT IT IS NECESSARY TO MAKE THE METAMORPHOSIS
C   DECISIONS FIRST THE REMOVAL OF 1) NEW SHEETS WHICH
DIFFUSE
C   INTO THE CYLINDER (AT A LATER TIME IT MAY BE NECESSARY
C   TO CHANGE THIS SECTION TO BE OPERATIVE ONLY AFTER THE
DIFFUSIVE
C   DISPLACEMENT) AND 2) REMOVAL OF BLOBS PASSING THROUGH
THE
C   IMAGE LAYER
```

```
C
      IF(((LIND(I).EQ.0).AND.(NBLIND.GE.4)).OR.
     1((LIND(I).EQ.2).AND.(NBLIND.EQ.5))) THEN
           DO 200 J=I,NEL-1
           SE(J,1)=SE(J+1,1)
           SE(J,2)=SE(J+1,2)
           XE(J,1)=XE(J+1,1)
           XE(J,2)=XE(J+1,2)
           YE(J,1)=YE(J+1,1)
           YE(J,2)=YE(J+1,2)
           LIND(J)=LIND(J+1)
  200     CONTINUE
         SE(NEL,1)=0.0
         SE(NEL,2)=0.0
         XE(NEL,1)=0.0
         XE(NEL,2)=0.0
         YE(NEL,1)=0.0
         YE(NEL,2)=0.0
         LIND(NEL)=0
         NEL=NEL-1
C
C   THE NEXT STEP IS TO CONSIDER A SHEET(OLD OR NEW) WHICH
MOVES FROM
C   WITHIN THE NBL TO THE EXTERNAL FLOW, A SHEET TO BLOB
CONVERSION
C
      ELSEIF((LIND(I).LE.1).AND.(NBLIND.EQ.1)) THEN
        SE(I,1)=SE(I,2)
        SE(I,2)=SE(I,2)*SHTL
        LIND(I)=2
C   NOW AN OLD SHEET WHICH GOES FROM THE NBL TO THE IMAGE
NBL, A
C   SHEET REFLECTION
C
      ELSEIF((LIND(I).EQ.1).AND.(NBLIND.EQ.4)) THEN
        CALL REFLECT(I,XNEW,YNEW)
        XE(I,1)=XE(I,2)
        YE(I,1)=YE(I,2)
        XE(I,2)=XNEW
        YE(I,2)=YNEW
C   NOW AN OLD SHEET WITHIN THE NBL WHICH PASSES THROUGH THE
IMAGE
C   NBL, A SHEET TO BLOB CONVERSION AND REFLECTION AS BLOB
C
      ELSEIF((LIND(I).EQ.1).AND.(NBLIND.EQ.5)) THEN
        SE(I,1)=SE(I,2)
        SE(I,2)=SE(I,2)*SHTL
        LIND(I)=2
        CALL REFLECT(I,XNEW,YNEW)
        XE(I,1)=XE(I,2)
        YE(I,1)=YE(I,2)
        XE(I,2)=XNEW
        YE(I,2)=YNEW
C   A BLOB THAT ENTERS THE NBL, A BLOB TO SHEET CONVERSION
```

```
C
      ELSEIF((LIND(I).EQ.2).AND.(NBLIND.EQ.2)) THEN
        SE(I,1)=SE(I,2)
        SE(I,2)=SE(I,2)/SHTL
        LIND(I)=1
C   A BLOB THAT ENTERS THE IMAGE NBL, A REFLECTION AS A
SHEET INTO
C   THE NBL
C
      ELSEIF((LIND(I).EQ.2).AND.(NBLIND.EQ.4)) THEN
        SE(I,1)=SE(I,2)
        SE(I,2)=SE(I,2)/SHTL
        LIND(I)=1
        CALL REFLECT(I,XNEW,YNEW)
        XE(I,1)=XE(I,2)
        YE(I,1)=YE(I,2)
        XE(I,2)=XNEW
        YE(I,2)=YNEW
      ENDIF
  100 CONTINUE
      RETURN
      END
C
C
C
C
C
C   THIS SUBROUTINE IS DESIGNED TO PROVIDE THE CONVECTION
C   OF EACH OF THE ELEMENTS. IT EMPLOYS A FIRST ORDER
ACCURATE
C   INTEGRATION SCHEME INSTEAD OF TIEMROTH'S EQ 2.40 TO SAVE
C   COMPUTATIONAL COST. THE SUBROUTINE HAS TWO PARTS: 1)
BLOBS
C   ARE CONVECTED BY CONSIDERING OTHER BLOBS AND POTENTIAL
FLOW
C   COMPONENNTS BUT NOT SHEETS, 2) SHEETS ARE CONVECTED BY
OTHER
C   SHEETS, BLOBS, AND POTENTIAL FLOW. NOTE NEWLY CREATED
SHEETS
C   MUST NOT ADD TO THEIR OWN CONVECTION.
C
C
C
C
      SUBROUTINE CONVECT
      IMPLICIT REAL *8(A-H,O-Z)
      REAL*8 NBLT
      DIMENSION
XE(3000,2),YE(3000,2),SE(3000,2),H(21,21),LIND(3000),
```

```
1XC(20),YC(20),UPGP(20),VPGP(20),VXBLBGP(20),VYBLBGP(20),
     2VT(20),ARC(20),XRHS(21),XTS(50),YTS(50),X(50),Y(50),
     3XSTRGP(20),THETA(50),THEM(50),BVEC(21),
     4XX(17,40),YY(17,40),VELX(17,40),VELY(17,40)
      COMMON /SIZE/ MAXEQN /BLK/ XE,YE,SE,LIND,SEFAC,
     1XC,YC,UPGP,VPGP,VXBLBGP,VYBLBGP,VT,SHTL,VCX,VCY,NBLT,

2ARC,XRHS,XTS,YTS,X,Y,XSTRGP,A,B,BR,NEL,UMIN,UMAX,XSEED,VISC
,DELT
      ANG=0.087266462
      DO 100 I=1,NEL
      CALL BLOBS(XE(I,2),YE(I,2),VXBLB,VYBLB)
C
C   MAY NEED TO MODIFY BLOBS TO ACCOUNT FOR COINCIDENCE OF
C   COORDINTAES - NO
C
      CALL POTVEL(XE(I,2),YE(I,2),VXPOT,VYPOT)
       IF (LIND(I).EQ.2) THEN
        VXB=VXPOT+VXBLB
        VYB=VYPOT+VYBLB
        XE(I,1)=XE(I,2)+(VXB*DELT)
        YE(I,1)=YE(I,2)+(VYB*DELT)
       ELSE
C
C   THIS IS THE DIFFICULT PORTION OF THE CODE, THE GLOBAL-
NBL
C   COORDINATE CONVERSIONS ARE CRITICAL TO ASSURE PROPER
C   CONVECTION OF THE SHEETS
C
C   NEXT CALCULATE Xr Yr ON THE CYLINDER FOR THE SHEET OF
INTEREST
C   USING THESE COORDINATES GET THE BLOB AND POTENTIAL
COMPONENTS AT
C   Xr,Yr AND DOT WITH UNIT TANGENTIAL. THIS WILL BE
FREESTREAM TANGENTIAL
C   VELOCITY.
      CALL NBLCOOR(XE(I,2), YE(I,2), XRI, YRI, XSTRI, YSTRI)
      D=DSQRT(XRI**2+16.D00*YRI**2)
C
C   NOW CALCULATE THE POTENTIAL AND BLOB COMPONENTS AT THE
LOCATION
C   Xr,Yr AND GET TGFSV TANGENTIAL FREE STREAM VELOCITY
C
      CALL BLOBS(XRI,YRI,VXBLB,VYBLB)
      CALL POTVEL(XRI,YRI,VXPOT,VYPOT)
      VX=VXPOT+VXBLB
      VY=VYPOT+VYBLB
      TGFSV=-(4.D00*YRI/D)*VX+(XRI/D)*VY
C
C   NOW TO GET VELOCITIES OF ITH SHEET USE XSTRI YSTRI
C   COORDINATES
```

```
C
      SUMX=0.D00
      SUMYPLS=0.D00
      SUMYMNS=0.D00
      IF(XSTRI.LE.3.63316809) THEN
      XSTRII=XSTRI+1.21105603
      ELSE
      XSTRII=XSTRI-3.63316809
      ENDIF
      DO 200 J=1,NEL
      IF(LIND(J).LE.1) THEN
C
C CALL SUBROUTINE TO GET XSTR, AND YSTR OF JTH ELEMENT
C XSTRJ, YSTRJ
C
      CALL NBLCOOR(XE(J,2), YE(J,2), XRJ, YRJ, XSTRJ, YSTRJ)
      IF(XSTRJ.LE.3.63316809) THEN
      XSTRJJ=XSTRJ+1.21105603
      ELSE
      XSTRJJ=XSTRJ-3.63316809
      ENDIF
      PRED1=DABS(XSTRII-XSTRJJ)
      PRED2=1-(DABS(XSTRII-XSTRJJ+SHTL/2.D00))/SHTL
      PRED3=1-(DABS(XSTRII-XSTRJJ-SHTL/2.D00))/SHTL
      IF((PRED1.LT.SHTL).AND.(YSTRJ.GT.YSTRI)) THEN
        DJ=1.D00-(PRED1/SHTL)
      ELSE
        DJ=0.0
      ENDIF
      IF((PRED2.LE.1.0).AND.(PRED2.GE.0.0)) THEN
        DJPLS=PRED2
      ELSE
        DJPLS=0.0
      ENDIF
      IF((PRED3.LT.1.0).AND.(PRED3.GE.0.0)) THEN
        DJMNS=PRED3
      ELSE
        DJMNS=0.D00
      ENDIF
      YSTRMIN=DMIN1(YSTRI,YSTRJ)
      PLSINC=SE(J,2)*DJPLS*YSTRMIN
      MNSINC=SE(J,2)*DJMNS*YSTRMIN
      SUMYPLS=SUMYPLS+PLSINC
      SUMYMNS=SUMYMNS+MNSINC
      SUMXINC=SE(J,2)*DJ
      SUMX=SUMX+SUMXINC
      ELSE
       CONTINUE
      ENDIF
  200 CONTINUE
      IF (LIND(I).EQ.0) THEN
        UI=TGFSV-SUMX
      ELSE
        UI=TGFSV-5.D-1*SE(I,2)-SUMX
```

```
      ENDIF
C
C  I WILL NEED NOW TO CALCULATE TANGENTIAL FREESTREAM
VELOCITIES
C  AT THE ENDPOINTS OF EACH SHEET ELEMENT, IN ORDER
C  TO COMPLETE THE Y-VELOCITY COMPONENTS IN THE  NBL
C  NEED THESE TO GET I1,I2 ETC. IN ORDER TO DO THIS IT IS
C  NECESSARY TO GET THE ENDPOINT XSTR VALUE AND GO
C  BACKWARDS TO XR AND YR OF THE ENDPOINTS.
C
      PREX1=XSTRI+SHTL/2.D00
      PREX2=XSTRI-SHTL/2.D00
      IF(PREX1.GT.4.84422412) THEN
        PREX1=PREX1-4.84422412
      ELSEIF(PREX1.LT.0.D00) THEN
        PREX1=4.84422412+PREX1
      ENDIF
      IF(PREX2.GT.4.84422412) THEN
        PREX2=PREX2-4.84422412
      ELSEIF(PREX2.LT.0.D00) THEN
        PREX2=4.84422412+PREX2
      ENDIF
      IF(PREX1.GT.2.42211206) THEN
        ARCL1=4.84422412-PREX1
      ELSE
        ARCL1=PREX1
      ENDIF
      IF(PREX2.GT.2.42211206) THEN
        ARCL2=4.84422412-PREX2
      ELSE
        ARCL2=PREX2
      ENDIF
      IF(ARCL1.GT.1.21105603) THEN
        TARC1=ARCL1-1.21105603
      ELSE
        TARC1=DABS(1.21105603-ARCL1)
      ENDIF
      IF(ARCL2.GT.1.21150603) THEN
        TARC2=ARCL2-1.21105603
      ELSE
        TARC2=DABS(1.21105603-ARCL2)
      ENDIF
      DO 299 K=2,19
       IF(ARC(K).GT.TARC1) THEN
        PHINC1=((TARC1-ARC(K-1))/(ARC(K)-ARC(K-1)))*ANG
        PHISTR1=(0.087266462*(K-1))+PHINC1
        GOTO 421
       ENDIF
  299 CONTINUE
  421 CONTINUE
      DO 300 K=2,19
       IF(ARC(K).GT.TARC2) THEN
        PHINC2=((TARC2-ARC(K-1))/(ARC(K)-ARC(K-1)))*ANG
        PHISTR2=(0.087266462*(K-1))+PHINC2
```

```
        GOTO 422
       ENDIF
  300 CONTINUE
  422 CONTINUE
      IF(ARCL1.GT.1.21105603) THEN
        PHI1=PHISTR1+1.570796327
      ELSE
        PHI1=1.570796327-PHISTR1
      ENDIF
      IF(ARCL2.GT.1.21105603) THEN
        PHI2=PHISTR2+1.570796327
      ELSE
        PHI2=PHISTR2-1.570796327
      ENDIF
C
C   NOW DETERMINE XR1,YR1 AND XR2, YR2
C
      IF(PREX1.LE.2.42211206) THEN
        XR1=A*DCOS(PHI1)
        YR1=B*DSIN(PHI1)

ELSEIF((PREX1.GT.2.42211206).AND.(PREX1.LT.3.63316809)) THEN
        XR1=A*DCOS(PHI1)
        YR1=-B*DSIN(PHI1)
      ELSE
        XR1=A*DCOS(PHI1)
        YR1=-B*DSIN(PHI1)
      ENDIF
      IF(PREX2.LE.2.42211206) THEN
        XR2=A*DCOS(PHI2)
        YR2=B*DSIN(PHI2)

ELSEIF((PREX2.GT.2.42211206).AND.(PREX2.LT.3.63316809)) THEN
        XR2=A*DCOS(PHI2)
        YR2=-B*DSIN(PHI2)
      ELSE
        XR2=A*DCOS(PHI2)
        YR2=-B*DSIN(PHI2)
      ENDIF
C
C   NOW CALCULATE THE FREESTREAM TANGENTIAL VELOCITY AT EACH
C   LOCATION
C
      CALL BLOBS(XR1,YR1,VXBLB1,VYBLB1)
      CALL BLOBS(XR2,YR2,VXBLB2,VYBLB2)
      CALL POTVEL(XR1,YR1,VXPOT1,VYPOT1)
      CALL POTVEL(XR2,YR2,VXPOT2,VYPOT2)
      VX1=VXPOT1+VXBLB1
      VY1=VYPOT1+VYBLB1
      VX2=VXPOT2+VXBLB2
      VY2=VYPOT2+VYBLB2
      D1=DSQRT(XR1**2+16.D00*YR1**2)
      D2=DSQRT(XR2**2+16.D00*YR2**2)
      TG1=-(4.D00*YR1/D1)*VX1+(XR1/D1)*VY1
```

```
      TG2=-(4.D00*YR2/D2)*VX2+(XR2/D2)*VY2
C
C
C   NOW GET Y VELOCITIES FOR SHEETS
C
C
      SHTI1=TG1*YSTRI-SUMYPLS
      SHTI2=TG2*YSTRI-SUMYMNS
      VI=-(SHTI1-SHTI2)/SHTL
      UXI=UI*(-4.D00*YRI/D)+VI*(XRI/D)
      VYI=UI*(XRI/D)+VI*(4.D00*YRI/D)
      XE(I,1)=XE(I,2)+(UXI*DELT)
      YE(I,1)=YE(I,2)+(VYI*DELT)
      ENDIF
  100 CONTINUE
      DO 511 I=1,NEL
      XTMP=XE(I,2)
      YTMP=YE(I,2)
      XE(I,2)=XE(I,1)
      YE(I,2)=YE(I,1)
      XE(I,1)=XTMP
      YE(I,1)=YTMP
  511 CONTINUE
      RETURN
      END
C
C
C
C   THIS SUBROUTINE IS DESIGNED TO
C
C
C
C
C
      SUBROUTINE POTVEL(SUBX, SUBY, POTVX, POTVY)
      IMPLICIT REAL *8(A-H,O-Z)
      REAL*8 NBLT
      DIMENSION
XE(3000,2),YE(3000,2),SE(3000,2),H(21,21),LIND(3000),

1XC(20),YC(20),UPGP(20),VPGP(20),VXBLBGP(20),VYBLBGP(20),
     2VT(20),ARC(20),XRHS(21),XTS(50),YTS(50),X(50),Y(50),
     3XSTRGP(20),THETA(50),THEM(50),BVEC(21),
     4XX(17,40),YY(17,40),VELX(17,40),VELY(17,40)
      COMMON /SIZE/ MAXEQN /BLK/ XE,YE,SE,LIND,SEFAC,
     1XC,YC,UPGP,VPGP,VXBLBGP,VYBLBGP,VT,SHTL,VCX,VCY,NBLT,

2ARC,XRHS,XTS,YTS,X,Y,XSTRGP,A,B,BR,NEL,UMIN,UMAX,XSEED,VISC
,DELT
C
C     POTENTIAL FLOW VELOCITIES
C
      XVELSM=0.0
      YVELSM=0.0
```

```
      DO 300 JW=1,20
      CALL INTGRT(SUBX,SUBY,XFCT,YFCT,XINT,YINT,JW)
      XVELINC=XRHS(JW)*XINT*XFCT
      YVELINC=XRHS(JW)*YINT*YFCT
      XVELSM=XVELSM+XVELINC
      YVELSM=YVELSM+YVELINC
  300 CONTINUE
      POTVX=XVELSM+VCX
      POTVY=YVELSM+VCY
      RETURN
      END

      SUBROUTINE INTGRT(SUBX,SUBY,XFCT,YFCT,XINT,YINT,J)
      IMPLICIT REAL *8(A-H,O-Z)
      REAL*8 NBLT
      DIMENSION
XE(3000,2),YE(3000,2),SE(3000,2),H(21,21),LIND(3000),

1XC(20),YC(20),UPGP(20),VPGP(20),VXBLBGP(20),VYBLBGP(20),
     2VT(20),ARC(20),XRHS(21),XTS(50),YTS(50),X(50),Y(50),
     3XSTRGP(20),THETA(50),THEM(50),BVEC(21),
     4XX(17,40),YY(17,40),VELX(17,40),VELY(17,40)
      COMMON /SIZE/ MAXEQN /BLK/ XE,YE,SE,LIND,SEFAC,
     1XC,YC,UPGP,VPGP,VXBLBGP,VYBLBGP,VT,SHTL,VCX,VCY,NBLT,

2ARC,XRHS,XTS,YTS,X,Y,XSTRGP,A,B,BR,NEL,UMIN,UMAX,XSEED,VISC
,DELT
      S=(Y(J+1)-Y(J))/(X(J+1)-X(J))
      E=(SUBY+S*X(J)-Y(J))
      F=(SUBX+Y(J)/S-X(J))
      ALPHX=SUBX
      ALPHY=SUBY
      CX=1+S**2
      CY=1+(1/S**2)
      BX=-2*(SUBX+E*S)
      BY=-2*(SUBY+F/S)
      AX=(E**2)+(SUBX**2)
      AY=(F**2)+(SUBY**2)
      DELX=4*AX*CX-(BX**2)
      DELY=4*AY*CY-(BY**2)
      RXLWR=AX+BX*X(J)+CX*X(J)**2
      RXUPR=AX+BX*X(J+1)+CX*X(J+1)**2
      RYLWR=AY+BY*Y(J)+CY*Y(J)**2
      RYUPR=AY+BY*Y(J+1)+CY*Y(J+1)**2
      PUPRX=(BX+2*CX*X(J+1))
      PLWRX=(BX+2*CX*X(J))
      PUPRY=(BY+2*CY*Y(J+1))
      PLWRY=(BY+2*CY*Y(J))
C
C      PRINT *,X(J),Y(J),X(J+1),Y(J+1),CX,DELX,DELY
```

```
C
      IF(DELX.LT.-1.E-35) THEN
       T1X=DSQRT(-DELX)
       IF((SUBX-X(J+1)).EQ.0.0) THEN
        XINT1UP=0.0
       ELSE
        XINT1UP=(1/T1X)*DLOG((-T1X+PUPRX)/(PUPRX+T1X))
       ENDIF
       IF((SUBX-X(J)).EQ.0.0) THEN
        XINT1LR=0.0
       ELSE
        XINT1LR=(1/T1X)*DLOG((-T1X+PLWRX)/(PLWRX+T1X))
       ENDIF
      ELSEIF(DELX.GT.1.E-35) THEN
       IF((SUBX-X(J+1)).EQ.0.0) THEN
        XINT1UP=0.0
       ELSE
        XINT1UP=(2/DSQRT(DELX))*(DATAN(PUPRX/(DSQRT(DELX))))
       ENDIF
       IF((SUBX-X(J)).EQ.0.0) THEN
        XINT1LR=0.0
       ELSE
        XINT1LR=(2/DSQRT(DELX))*(DATAN(PLWRX/(DSQRT(DELX))))
       ENDIF
      ELSE
       IF((SUBX-X(J+1)).EQ.0.0) THEN
        XINT1UP=0.0
       ELSE
        XINT1UP=(-2/(PUPRX))
       ENDIF
       IF((SUBX-X(J)).EQ.0.0) THEN
        XINT1LR=0.0
       ELSE
        XINT1LR=(-2/(PLWRX))
       ENDIF
      ENDIF
      XINT1=ALPHX*(XINT1UP-XINT1LR)
      PXINT2=(1/(2*CX))*(DLOG(RXUPR)-DLOG(RXLWR))
      XINT2=PXINT2-(BX/(2*CX))*(XINT1UP-XINT1LR)
      XINT=XINT1-XINT2
      IF(DELY.LT.-1.E-35) THEN
       T1Y=DSQRT(-DELY)
       IF((SUBY-Y(J+1)).EQ.0.0) THEN
        YINT1UP=0.0
       ELSE
        YINT1UP=(1/T1Y)*DLOG((-T1Y+PUPRY)/(PUPRY+T1Y))
       ENDIF
       IF((SUBY-Y(J)).EQ.0.0) THEN
        YINT1LR=0.0
       ELSE
        YINT1LR=(1/T1Y)*DLOG((-T1Y+PLWRY)/(PLWRY+T1Y))
       ENDIF
      ELSEIF(DELY.GT.1.E-35) THEN
       IF((SUBY-Y(J+1)).EQ.0.0) THEN
```

```
          YINT1UP=0.0
         ELSE
          YINT1UP=(2/DSQRT(DELY))*(DATAN(PUPRY/(DSQRT(DELY))))
         ENDIF
         IF((SUBY-Y(J)).EQ.0.0) THEN
          YINT1LR=0.0
         ELSE
          YINT1LR=(2/DSQRT(DELY))*(DATAN(PLWRY/(DSQRT(DELY))))
         ENDIF
        ELSE
         IF((SUBY-Y(J+1)).EQ.0.0) THEN
          YINT1UP=0.0
         ELSE
          YINT1UP=(-2/(PUPRY))
         ENDIF
         IF((SUBY-Y(J)).EQ.0.0) THEN
          YINT1LR=0.0
         ELSE
          YINT1LR=(-2/(PLWRY))
         ENDIF
        ENDIF
        YINT1=ALPHY*(YINT1UP-YINT1LR)
        PYINT2=(1/(2*CY))*(DLOG(RYUPR)-DLOG(RYLWR))
        YINT2=PYINT2-(BY/(2*CY))*(YINT1UP-YINT1LR)
        YINT=YINT1-YINT2
        IF(YTS(J).GT.0.0) THEN
         XFCT=-DSQRT(1+S**2)
        ELSE
         XFCT=DSQRT(1+S**2)
        ENDIF
        IF(XTS(J).GT.0.0) THEN
         YFCT=DSQRT(1+1/S**2)
        ELSE
         YFCT=-DSQRT(1+1/S**2)
        ENDIF
        RETURN
        END
C
C
C
C
C
C     THIS SUBROUTINE CALCULATES THE VELOCITY COMPONENTS AT A
C     LOCATION (SUBX,SUBY) DUE TO VORTEX BLOBS IN THE FLOW
C     SUBX, SUBY - THE X AND Y COORDINATES OF THE POINT AT
C     WHICH THE VELOCITY DUE TO THE BLOBS IS DESIRED
C     VXBLB, VYBLB - THE VELOCITY COMPONENTS AT SUBX,SUBY
C     DUE TO THE BLOBS
C     NEL = THE # OF ELEMENTS = NTS*20
C     XE,YE,SE ARE ARRAYS DEFINING THE LOCATION AND STRENGTH
OF
C     THE BLOBS
C     LIND =0 OR 1 IF THE ELEMENT IS A SHEET AND 2 IF A BLOB
C     BR IS THE BLOB CUT OFF RADIUS
```

```
C
      SUBROUTINE BLOBS(SUBX, SUBY, VXBLB, VYBLB)
      IMPLICIT REAL *8(A-H,O-Z)
      REAL*8 NBLT
      DIMENSION
XE(3000,2),YE(3000,2),SE(3000,2),H(21,21),LIND(3000),

1XC(20),YC(20),UPGP(20),VPGP(20),VXBLBGP(20),VYBLBGP(20),
     2VT(20),ARC(20),XRHS(21),XTS(50),YTS(50),X(50),Y(50),
     3XSTRGP(20),THETA(50),THEM(50),BVEC(21),
     4XX(17,40),YY(17,40),VELX(17,40),VELY(17,40)
      COMMON /SIZE/ MAXEQN /BLK/ XE,YE,SE,LIND,SEFAC,
     1XC,YC,UPGP,VPGP,VXBLBGP,VYBLBGP,VT,SHTL,VCX,VCY,NBLT,

2ARC,XRHS,XTS,YTS,X,Y,XSTRGP,A,B,BR,NEL,UMIN,UMAX,XSEED,VISC
,DELT
      SUMX1=0.D00
      SUMX2=0.D00
      SUMY1=0.D00
      SUMY2=0.D00
      PI=3.141592654
      DO 100 I=1,NEL
      IF(LIND(I).LE.1) THEN
       GOTO 100
      ELSE
       R=DSQRT((XE(I,2)-SUBX)**2+(YE(I,2)-SUBY)**2)
        IF(R.GT.BR) THEN
         SUMX1=SUMX1+((SUBY-YE(I,2))/R**2)*SE(I,2)
         SUMY1=SUMY1+((SUBX-XE(I,2))/R**2)*SE(I,2)
        ELSEIF((R.GT.1.D-8).AND.(R.LE.BR)) THEN
         SUMX2=SUMX2+((SUBY-YE(I,2))/(BR*R))*SE(I,2)
         SUMY2=SUMY2+((SUBX-XE(I,2))/(BR*R))*SE(I,2)
        ELSE
         SUMX2=SUMX2+0.D00
         SUMY2=SUMY2+0.D00
        ENDIF
      ENDIF
  100 CONTINUE
      VXBLB=-(1.D00/(2.D00*PI))*(SUMX1+SUMX2)
      VYBLB=(1.D00/(2.D00*PI))*(SUMY1+SUMY2)
      RETURN
      END
C
C
C
C
C
C
C
```

```
C
C
C    THIS SUBROUTINE IS DESIGNED TO MAKE THE CONVERSION FROM
C    GLOBAL X-Y COORDINATES TO LOCAL NUMERICAL BOUNDARY LAYER
C    COORDINATES XSTR, YSTR AND THE INTERMEDIATE POINTS XR,YR
C    ON THE CYLINDER
C
C
C
C
      SUBROUTINE NBLCOOR(SUBX, SUBY, XR, YR, XSTR, YSTR)
      IMPLICIT REAL *8(A-H,O-Z)
      REAL*8 NBLT
      DIMENSION
XE(3000,2),YE(3000,2),SE(3000,2),H(21,21),LIND(3000),

1XC(20),YC(20),UPGP(20),VPGP(20),VXBLBGP(20),VYBLBGP(20),
     2VT(20),ARC(20),XRHS(21),XTS(50),YTS(50),X(50),Y(50),
     3XSTRGP(20),THETA(50),THEM(50),BVEC(21),
     4XX(17,40),YY(17,40),VELX(17,40),VELY(17,40)
      COMMON /SIZE/ MAXEQN /BLK/ XE,YE,SE,LIND,SEFAC,
     1XC,YC,UPGP,VPGP,VXBLBGP,VYBLBGP,VT,SHTL,VCX,VCY,NBLT,

2ARC,XRHS,XTS,YTS,X,Y,XSTRGP,A,B,BR,NEL,UMIN,UMAX,XSEED,VISC
,DELT
      PI=3.141592654
      ANG=0.087266462
      F=DSQRT(A**2-B**2)
      GAM1E=DSQRT(SUBY**2+(SUBX+F)**2)
      GAM2E=DSQRT(SUBY**2+(SUBX-F)**2)
      ENE=(GAM1E-GAM2E)/DSQRT(3.D00)
      GAM2=(2.D00*F)/DSQRT(3.D00)-(DSQRT(3.D00)/2.D00)*ENE
      GAM1=DSQRT(3.D00)*ENE+GAM2
      IF(SUBX.EQ.0.D00) THEN
        XR=0.D00
        IF(SUBY.GT.0.D00) THEN
         YR=B
        ELSE
         YR=-B
        ENDIF
      ELSEIF(SUBY.EQ.0.D00) THEN
        YR=0.D00
        IF(SUBX.GT.0.D00) THEN
         XR=A
        ELSE
         XR=-A
        ENDIF
      ELSE
        XR=(GAM1**2-GAM2**2)/(4.D00*F)
        IF(SUBY.GT.0.D00) THEN
         YR=DSQRT(GAM2**2-(XR-F)**2)
        ELSE
         YR=-DSQRT(GAM2**2-(XR-F)**2)
        ENDIF
```

```
      ENDIF
      PHI=DACOS(XR)
      PHISTR=DABS(PHI-1.570796327)
      IBTLM=INT(PHISTR/ANG)+1
      ARC1=ARC(IBTLM)
      ARC2=ARC(IBTLM+1)
      IF(IBTLM.EQ.1) THEN
      ANGG=0.D00
      ELSE
      ANGG=(IBTLM-1)*ANG
      ENDIF
      ARCINC=(PHISTR-ANGG)/ANG
      TARC=ARC1+ARCINC*(ARC2-ARC1)
      IF(PHI.GE.1.570796327) THEN
      ARCL=1.21105603+TARC
      ELSE
      ARCL=1.21105603-TARC
      ENDIF
      IF(YR.GE.0.D00) THEN
       XSTR=ARCL
      ELSE
       XSTR=4.84422412-ARCL
      ENDIF
      YSTR=DSQRT((SUBX-XR)**2+(SUBY-YR)**2)
      RETURN
      END
C
C
C
C
C
C
C
C
C
C   THIS SUBROUTINE IS DESIGNED TO PROVIDE THE NEW POSITION
OF
C   AN ELEMENT BASED ON A REFLECTION. THE SUBROUTINE TAKES
THE
C   PRESENT AND PREVIOUS LOCATION OF THE ELEMENT, CALCULATES
THE
C   INTERSECTION POINT ON THE ELLIPSE (X,Y) AND THEN
PROCEEDS TO
C   REFLECT THE LOCATION TO THE NEW POSITION (XNEW,YNEW).
THE
C   SUBROUTINE IS CALLED ONLY UNDER CERTAIN CONDITIONS WHICH
C   ARE SPECIFIED IN THE META SUBROUTINE.
C
C   THIS SUBROUTINE WAS UPDATED TO BE GENERAL ENOUGH FOR ANY
C   ELLIPSE ON 9-7-89. ADDITIONAL CORRECTIONS WERE ALSO MADE
C
C
```

```
C
C
      SUBROUTINE REFLECT(K,XNEW,YNEW)
      IMPLICIT REAL *8(A-H,O-Z)
      REAL*8 NBLT
      DIMENSION
XE(3000,2),YE(3000,2),SE(3000,2),H(21,21),LIND(3000),

1XC(20),YC(20),UPGP(20),VPGP(20),VXBLBGP(20),VYBLBGP(20),
     2VT(20),ARC(20),XRHS(21),XTS(50),YTS(50),X(50),Y(50),
     3XSTRGP(20),THETA(50),THEM(50),BVEC(21),
     4XX(17,40),YY(17,40),VELX(17,40),VELY(17,40)
      COMMON /SIZE/ MAXEQN /BLK/ XE,YE,SE,LIND,SEFAC,
     1XC,YC,UPGP,VPGP,VXBLBGP,VYBLBGP,VT,SHTL,VCX,VCY,NBLT,

2ARC,XRHS,XTS,YTS,X,Y,XSTRGP,A,B,BR,NEL,UMIN,UMAX,XSEED,VISC
,DELT
      EPSL=1.D-6
      IF(DABS(XE(K,1)-XE(K,2)).LE.EPSL) THEN
        XO=(XE(K,1)+XE(K,2))/2.D00
        IF(YE(K,1).GE.0.0.AND.YE(K,2).GE.0.0) THEN
         YO=(B/A)*DSQRT(A**2-XO**2)
        ELSEIF(YE(K,1).LE.0.0.AND.YE(K,2).LE.0.0) THEN
         YO=-DSQRT(A**2-XO**2)*(B/A)
        ELSEIF(YE(K,1).LT.0.0) THEN
         YO=-DSQRT(A**2-XO**2)*(B/A)
        ELSE
         YO=DSQRT(A**2-XO**2)*(B/A)
        ENDIF
      ELSE
      S1=(YE(K,1)-YE(K,2))/(XE(K,1)-XE(K,2))
      AREF=(A**2*S1**2+B**2)
      BREF=(B**2)*(2.D00*S1*XE(K,1)-2.D00*YE(K,1))
      CREF=(B**2)*(-
2.D00*S1*XE(K,1)*YE(K,1)+S1**2.D00*XE(K,1)**2-
     1S1**2*A**2+YE(K,1)**2)
      TTT=BREF**2-4.D00*AREF*CREF
      IF(TTT.GT.0.D00) THEN
      PREY1=(-BREF+DSQRT(TTT))/(2.D00*AREF)
      PREY2=(-BREF-DSQRT(TTT))/(2.D00*AREF)
      ELSE
      PREY1=-BREF/(2.D00*AREF)
      PREY2=PREY1
      ENDIF
      IF((PREY1.LE.YE(K,1)).AND.(PREY1.GT.YE(K,2))) THEN
       YO=PREY1
      ELSEIF((PREY1.LE.YE(K,2)).AND.(PREY1.GT.YE(K,1))) THEN
       YO=PREY1
      ELSE
       YO=PREY2
      ENDIF
      XO=XE(K,1)-(1.D00/S1)*(YE(K,1)-YO)
      ENDIF
```

```
C
C   AT THIS POINT THE X,Y CORDINATES ON THE ELLIPSE ARE
SPECIFIED
C   NOW WE MUST SOLVE FOR THE REFLECTED POSITION
C
      A1=XE(K,1)-XO
      A2=YE(K,1)-YO
      AMAG=DSQRT(A1**2+A2**2)
      B1=(XE(K,2)-XO)
      B2=(YE(K,2)-YO)
      BMAG=DSQRT(B1**2+B2**2)
      D=DSQRT(B**4*XO**2+A**4*YO**2)
      CSALPH=(((A1*XO*B**2/D)+A2*A**2*YO/D)/AMAG)
      IF(CSALPH.GE.1.D00) THEN
       CSALPH=1.D00
      ELSEIF(CSALPH.LE.0.D00) THEN
       CSALPH=0.D00
      ELSE
       CSALPH=CSALPH
      ENDIF
      ALPHA=DACOS(CSALPH)
      BETA=3.141592654-2.D00*ALPHA
      CMAG2=(2.D00*BMAG**2)*(1.D00-DCOS(BETA))
      COEF1=2.D00*B1
      COEF2=2.D00*B2
      COEF3=(XO**2-XE(K,2)**2+YO**2-YE(K,2)**2)
      COEF4=BMAG**2-CMAG2
      COEF5=COEF4-COEF3
      COEF6=(B**2*XO/D)
      COEF7=(A**2*YO/D)
      COEF8=BMAG*DCOS(ALPHA)+COEF6*XO+COEF7*YO
      YNEW=(COEF8-(COEF6*COEF5/COEF1))/(COEF7-
(COEF6*COEF2/COEF1))
      XNEW=(COEF5-COEF2*YNEW)/COEF1
      RETURN
      END
```

APPENDIX C

Three-Dimensional Concentrations in

the Near-Wake of Mannequins

Appendix C. Three Dimensional Concentration Fields in the Near-Wake of Anthropomorphic Mannequins in Uniform Freestreams and Assessment of Vortex Shedding as a Mass Transfer Mechanism

This Appendix presents a summary of results indicating: 1) That the 3-D concentration field downstream of workers in uniform freestreams is unlikely to be very well-mixed if the source is in the near-wake; and 2) Vortex shedding is experimentally observed over certain regions of the body but not in others.

SUMMARY OF THE WORK FOR CONCENTRATION MEASUREMENTS

A set of concentration measurements was performed to obtain the spatial distribution of concentration with the fixed source placed in the recirculation zone. Sulfur Hexafluoride(SF_6) was used as a tracer gas. The gas was metered from a compressed gas cylinder of 10% SF_6 through a one-quarter inch diameter ceramic sphere with the flow rate of 0.005 CFM. The SF_6 source was positioned at 28" from the floor of the wind tunnel and 6" from the chest of a mannequin(41" tall and 8" wide), as depicted in figure 1. As shown in figure 2 and figure 3, a network of sampling points was set to have 4"x4"x4" uniform grid. Each horizontal plane of the network consists of 28 receptor points. The SF_6 concentration at each sampling point was detected through the sampling probe by a Mobile Infrared Analyzer(MIRAN) with the sampling flow rate of about 1 lpm. The concentration, as measured by the MIRAN, was logged and integrated over a 5 minute period by a Metrosonic dl 714 Data Logger after a 15 minute waiting time. A free-stream velocity of 200 fpm was used throughout this experiment.

Eight iso-contour maps were generated by using the results of this experiment, as shown in figures 4-11. The heights of planes(24", 28" and 36") are approximately the positions near the navel, the heart and the mouth of the mannequin, respectively. The result of these experiment shows the strong spatial gradient of SF_6 concentration in the recirculation zone and thus implies that it is inappropriate to build a conceptual model based on the complete mixing assumption.

The average concentration for all 128 points measured was 6.07 ppm; the average concentration predicted using the conceptual model in Manuscript I, equation (6) is 6.634 ppm.

Summary of Vortex Sheding Work.

I. Vortex shedding frequency measurement

In order to assess the possibility of vortex shedding behind a mannequin, velocity measurements using a TSI hot film anemometer with high frequency analog-digital data acquisition system were made and analyzed by Fast Fourier Transform and normalized periodogram estimates.

The essence of the Fourier transform(FT) of a waveform is to decompose or separate the waveform into a sum of sinusoids of different frequencies[3]. If these sinusoids sum to the original waveform, then the Fourier transform of the waveform has been determined.

The Fourier transform(FT) identifies or distinguishes the different frequency sinusoids(and their respective amplitudes) which combine to form an arbitrary waveform.

Results of vortex shedding frequency measurements

1) Circular and elliptical cylinder

Before measuring the frequency of vortices shed behind the mannequin, some measurements for a circular and an elliptical cylinder were conducted to check the experimental procedures and equipments. A 47.5" long circular and a 60" long elliptical cylinder, both 8" in diameter, were used as the test objects. Each object was mounted normally on the floor of the test section, 12" downstream of the inlet of the wind tunnel, 26" away from both side walls of the tunnel. An elliptical cylinder was actually spanned from the top to the bottom of the tunnel, that means two-dimensional cylinder.

According to literature review[7-10], the position of hot-wire sensor relative to the object(especially, a circular cylinder) is varying, for example, 1-6 diameters from the rear of the cylinder and 0.5-2 diameters from the wake centerline. In this experiment, the sensor was placed at a position, three diameters from the rear of the cylinder and one diameter from the wake centerline. The height of the sensor was 24" from the floor of the tunnel.

The sampling rate of the hot-film anemometer was determined so that approximately 80 samples can be sampled during a single vortex shedding event. The sampling rates and the total sampling time are shown in table 2.

Table 2. Sampling rate of the hot-film anemometer

air velocity (fpm)	sampling rate (samples/sec.)	sampling time (sec.)	number of samples
50	20	204.8	4096
150	60	68.3	4096
250	100	41.0	4096

Each experiment was repeated three times. The sampled data were later analyzed to estimate power spectra, using FFT.FOR.

As depicted in figure 12, the velocity signals behind each object were compared with the free stream velocity signals at the free stream velocity of 150 fpm. The saw type signals with the relatively high amplitude and the about same period can be easily observed from the signals behind each object. The power spectra of the fluctuating velocity indicate a prominent prevailing frequency; it is suggested that vortices with a prominent frequency are shed behind each cylinder. As shown in table 3, every measurement gives the consistent estimate of vortex shedding frequency.

Table 3. Vortex shedding frequency and Strouhal number for circular and elliptical cylinder

velocity (fpm)		circular cylinder		elliptical cylinder	
		frequency	S_t	frequency	S_t
50	1	0.2588	0.2070	0.2441	0.1953
	2	0.2295	0.1836	0.2441	0.1953
	3	0.2441	0.1953	0.2441	0.1953
	avg.	0.2441	0.1953	0.2441	0.1953
150	1	0.7764	0.2070	0.8203	0.2187
	2	0.7764	0.2070	0.7764	0.2070
	3	0.7764	0.2070	0.7324	0.1953
	avg.	0.7764	0.2070	0.7764	0.2070
250	1	1.2207	0.1953	1.2939	0.2070
	2	1.1475	0.1836	1.2939	0.2070
	3	1.2207	0.1953	1.2207	0.1953
	avg.	1.1963	0.1914	1.2695	0.2031
avg.			0.1979		0.2018

2) Mannequin

An anthropometric mannequin(41" tall and 8" wide at chest) was used as a test object. The hot-film sensor was placed at eight different positions, presented in table 4.

Table 4. Positions of the hot-film sensor for mannequin

unit:inches

Z	W	X	Y	reference
4	5.5	16.5	5.5	nose
8	3.0	9.0	3.0	neck
12	12.0	36.0	12.0	chest
16	14.0	42.0	14.0	elbows
20	7.5	22.5	7.5	waist
24	8.0	24.0	8.0	hip
28	7.0	21.0	7.0	thigh
32	7.5	22.5	7.5	shin

Z:vertical distance from the top of the mannequin
W:width of the mannequin normal to the freestream at the height of Z
X:downstream distance from the mannequin
Y:lateral distance from the center of the mannequin

The sensor was placed at a position, three widths at a given vertical level from the rear of the mannequin and one width from the wake centerline. Other experimental procedures and conditions are exactly the same as those in the case of circular and elliptical cylinder.

At the level of nose, neck, and chest one can not observe the periodic signals even though some intermittent peaks can be observed. From the level of elbows to that of waist, the tendency of the periodicity and the prominent peak is getting stronger (still weaker than those for the circular or elliptical cylinder). As going downward, that tendency is gradually decreased. The very similar phenomena were observed in other free stream velocities.

Table 5. The result of the frequency analysis

unit : Hz

free stream velocity		50 fpm	150 fpm	250 fpm
nose	1	0.054	0.029	0.122
	2	0.039	0.381	0.195
	3	0.024	0.381	0.195
	avg.	0.039	0.264	0.171
neck	1	0.010	0.117	0.195
	2	0.010	0.073	0.195
	3	0.024	0.952	0.195
	avg.	0.015	0.382	0.195
chest	1	0.024	0.908 *	0.049
	2	0.010	0.029	1.440 *
	3	0.273 *	0.073	1.733 *
	avg.	0.102	0.337	1.074
elbows	1	0.244 *	0.073	0.122
	2	0.288	0.645 *	1.221 *
	3	0.024	0.732 *	1.294 *
	avg.	0.185	0.483	0.879
waist	1	0.288 *	0.732 *	1.074 *
	2	0.244 *	0.688 *	1.074 *
	3	0.244 *	0.688 *	1.147 *
	avg.	0.259	0.703	1.098
hip	1	0.215 *	0.776 *	1.147 *
	2	0.229 *	0.732 *	1.074 *
	3	0.259 *	0.864 *	1.440 *
	avg.	0.234	0.791	1.220
thigh	1	0.009	0.073	1.294 *
	2	0.024	0.029	1.220 *
	3	0.024	0.029	1.294 *
	avg.	0.019	0.044	1.269
shin	1	0.024	0.073	0.122
	2	0.024	0.073	2.099 *
	3	0.039	0.029	0.049
	avg.	0.029	0.058	0.757

* : The frequency marked by * has the power spectrum of a

relatively prominent peak in the frequency range of interest.

3) Discussion

Flow around a two-dimensional cylinder in the free-stream has attracted enormous amount of research[11]. However, in most practical applications, there is at least one free end(chimney stacks, gas and oil reservoirs, mannequin, etc.).

When a circular cylinder has a finite length, the height-to-diameter ratio, H/D becomes an influencing parameter. Kawamura et al.[12] performed some flow visualization and measurements of Strouhal number around a finite circular cylinder with H/D=1-8 at Reynolds number of 3.2×10^4. Their result suggested that for Z/D<2, where Z is a vertical downward distance from the free end of a cylinder, a prominent spectrum peak can not be detected in the frequency analysis. They concluded that the free end region were dominated by the blow-down flow and the trailing vortex. The Strouhal number remained approximately constant at Z/D<4, but the value of S_t is smaller than that for the two-dimensional cylinder(S_t=0.2) and decreases with a decreasing H/D. In addition, for H/D<6 difficulties were encountered in detecting a dominant frequency in the frequency analysis. This is apparently due to the fact that the entire near wake flow region has been covered by a free-end region. Okamato and Yagita[13] reported the very similar result.

According to Sakamoto and Arie[14], whose result is somehow different from Kawamura et al.'s, as H/D is reduced, the type of vortex shedding behind a circular cylinder was found to change from the Karman-type vortex to the arch-type vortex at H/D of 2.5. Moreover, regardless of H/D, it was not possible to detect the prominent prevailing frequency for Z/D<1.5.

Farivar[15] proposed that a circular cylinder could be divided into three distinct parts with respect to the frequency of the vortex shedding associated with each part: a top region characterized by low frequency vortex shedding(or a stationary vortex system[16]), a middle region characterized by high frequency(still lower than that for a two-dimensional wake flow), and a lower region characterized by a Strouhal number equal to that for a two-dimensional wake flow.

The H/D of the mannequin is approximately 5, based on the height of 41" and the diameter of 8"(the width of the mannequin at the chest level, not including the arms). The H/D of 5 is in the range which the vortex shedding does not exist, according to Kawamura et al.. However, it was appeared that the frequency of the vortex shedding can be detected in the region from the waist to the hip of the mannequin. This difference may be resulted from the use of the different objects.

From the experimental results and the literature review, a mannequin could be divided into three regions with respect to the vortex shedding: the free-end region(from the top to the neck) characterized by a downwash effect, the intermediate region(from the chest to the elbows) characterized by the combination of the downwash effect and the vortex shedding, and the vortex shedding region(from the waist to the knee) characterized by the vortex shedding.

REFERENCES

1.
2. ACGIH, INDUSTRIAL VENTILATION, 20th ed.,1988
3. Brigham, E.O., THE FAST FOURIER TRANSFORM, Prentice -Hall,1974.
4. Bloomfield, P., FOURIER ANALYSIS OF TIME SERIES: AN INTRODUCTION, John Wiley & Sons, 1976.
5. Press, W.H. et. al., Numerical Recipes: The Art of Scientific Computing, Cambridge Univ. Press.
6. Ramirez, R.W., The FFT: Fundamentals and Concepts, Prentice-Hall, 1985.
7. Ayoub, A. & Karamcheti, K., "An experiment on the flow past a finite circular cylinder at high subcritical and supercritical Reynolds number," Journal of Fluid Mechanics, Vol. 118, 1-27, 1982.
8. Roshko, A., "On the Development of Turbulent Wakes from Vortex Streets," NACA Rep. 1191, 1954
9. West, G.S. & Apelt, C.J., "The effects of tunnel blockage and aspect ratio on the mean flow past a circular cylinder with Reynolds numbers between 10^4 and 10^5," Journal of Fluid Mechanics, Vol. 114, 361-377, 1982.
10. Bearman, P.W., "On vortex shedding from a circular cylinder in the critical Reynolds number regime," Journal of Fluid Mechanics, Vol. 28, 577-585,1969.
11. Zdravkovich, M.H., "Conceptual overview of laminar and turbulent flows past smooth and rough circular cylinders," Proc. Intl Colloq. on Bluff Body Aerodynamics and Its Applications, Journal of Wind Engineering(Japan Assoc Wind Engng), Tokyo, No. 37, 93-102, 1988.
12. Kawamura, T.,et al., "Flow around a Finite Circular Cylinder on a Flat Plate," Bulletin of JSME, Vol. 27, No. 232, 2142-2151, 1984.
13. Okamato, T. & Yagita, M., "The Experimental Investigation on the Flow Past a Circular Cylinder of Finite Length Placed Normal to the Plane Surface in a Uniform Stream," Bulletin of JSME, Vol. 16, No. 95, 805-814, 1973.
14. Sakamoto, H. & Arie, M., "Vortex shedding from a rectangular prism and a circular cylinder placed vertically in a turbulent boundary layer," Journal of Fluid Mechanics, Vol. 126, 147-165, 1983.
15. Farivar, D., "Turbulent Uniform Flow around Cylinders of Finite Length," AIAA J., Vol. 19, No. 3, 275-281, 1981.
16. Etzold, F. & Fielder, H., "The Near-Wake Structure of a Cantilevered Cylinder in a Cross-Flow," Z. Flugwiss, Vol. 24, 77-81, 1976.

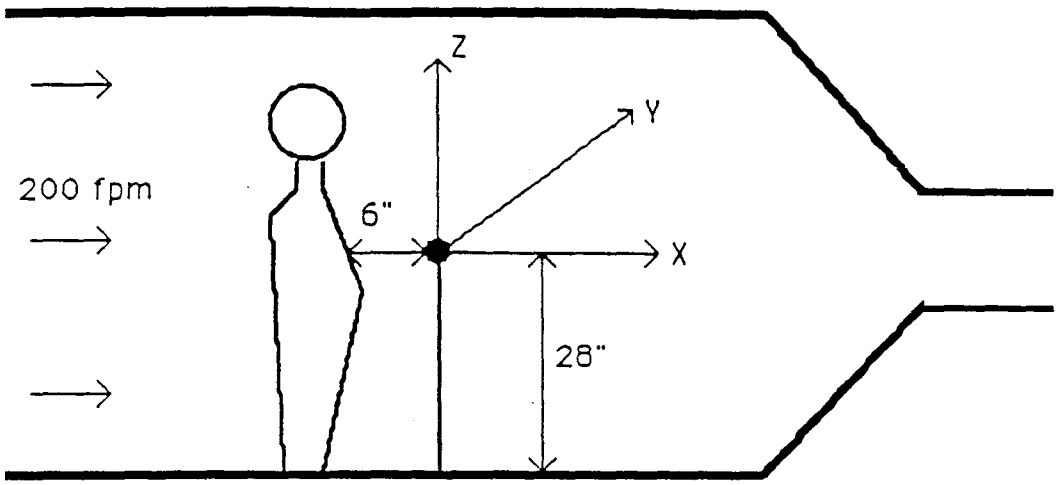

Fig.**1**. SIDEVIEW OF MANNEQUIN AND SOURCE POSITION

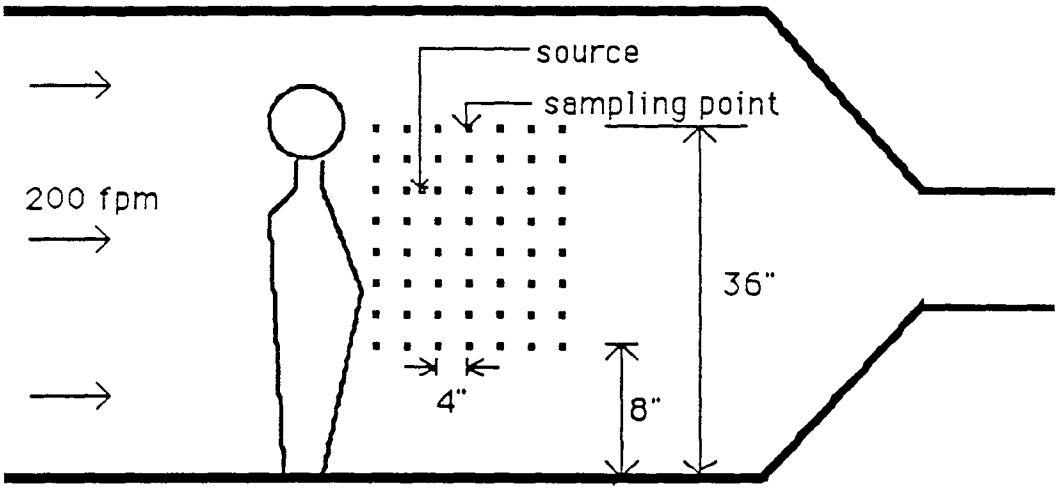

Fig.**2** SIDEVIEW OF SAMPLING NETWORK

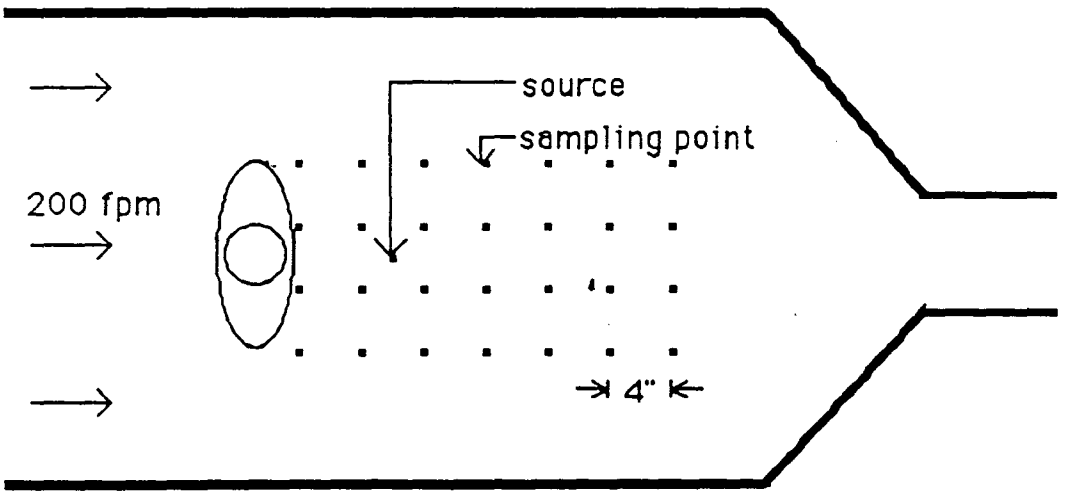

Fig.**3** PLANVIEW OF SAMPLING NETWORK

Fig. 4

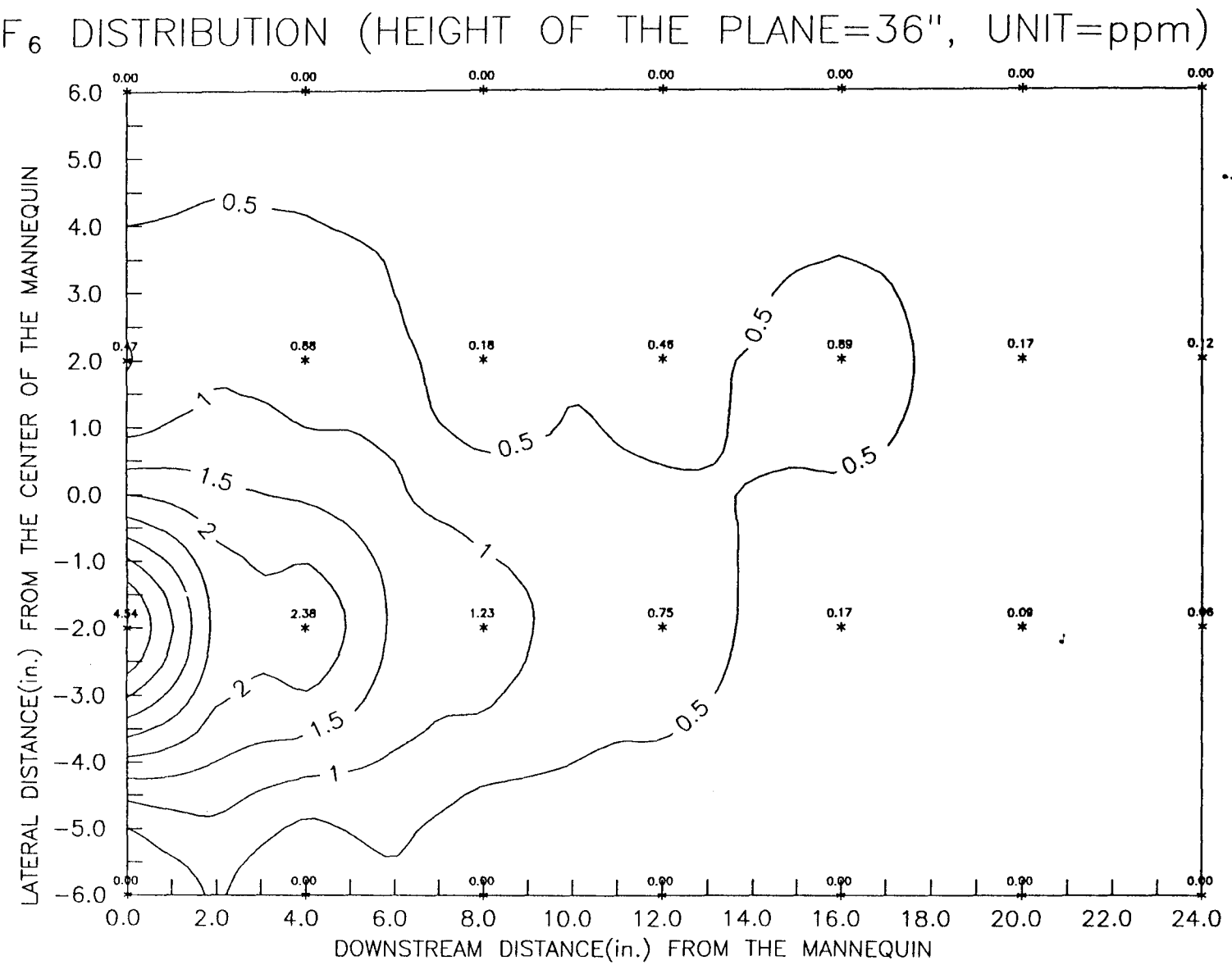
SF6 DISTRIBUTION (HEIGHT OF THE PLANE=36", UNIT=ppm)
LATERAL DISTANCE(in.) FROM THE CENTER OF THE MANNEQUIN
DOWNSTREAM DISTANCE(in.) FROM THE MANNEQUIN
6.0
5.0
4.0
3.0
2.0
1.0
0.0
-1.0
-2.0
-3.0
-4.0
-5.0
-6.0
0.0
2.0
4.0
6.0
8.0
10.0
12.0
14.0
16.0
18.0
20.0
22.0
24.0
0.5
1
1.5
2
0.88
0.18
0.46
0.89
0.17
2.38
1.23
0.75
0.17
0.09
4.54

Fig. 5

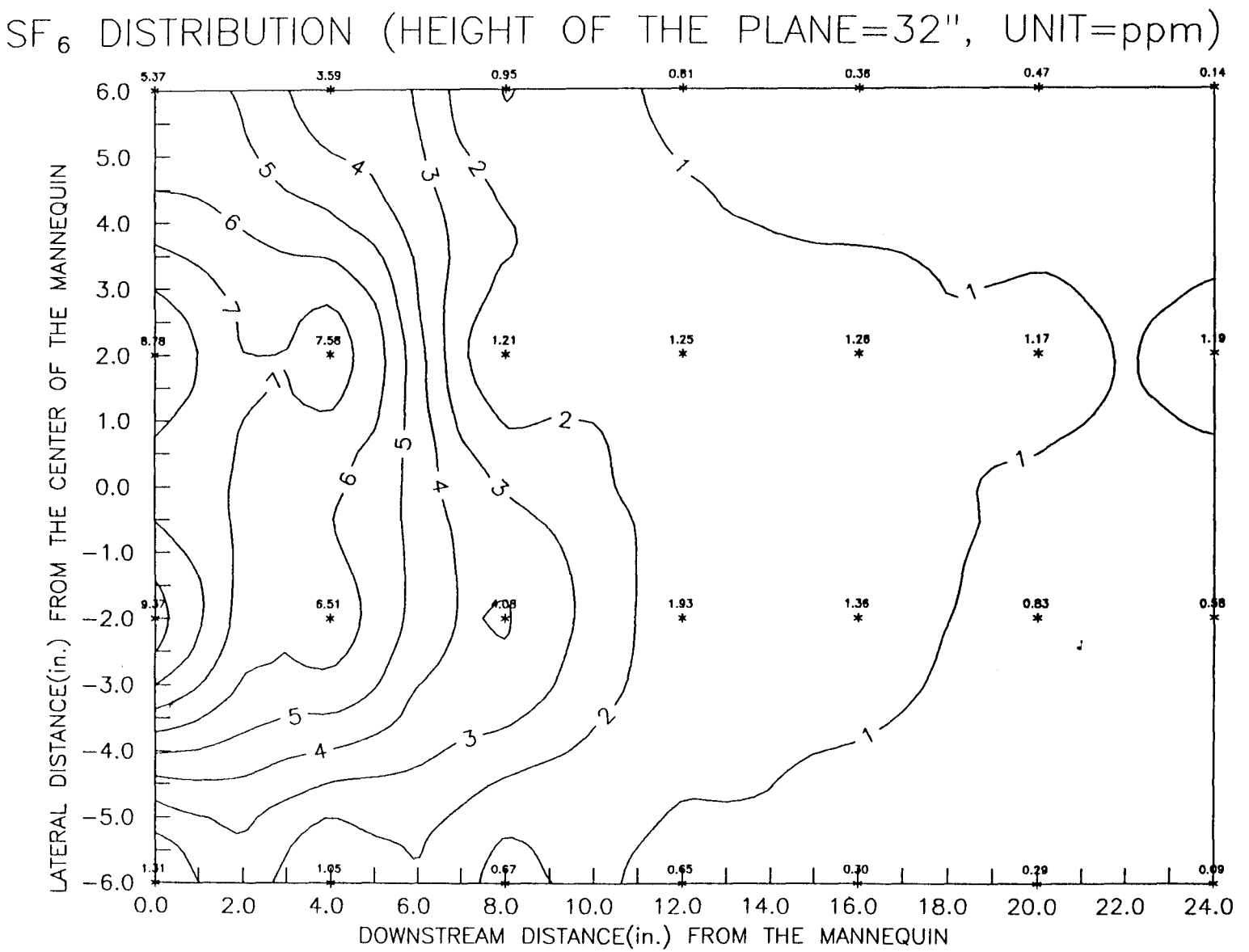
SF6 DISTRIBUTION (HEIGHT OF THE PLANE=32", UNIT=ppm)
LATERAL DISTANCE(in.) FROM THE CENTER OF THE MANNEQUIN
DOWNSTREAM DISTANCE(in.) FROM THE MANNEQUIN
6.0
5.0
4.0
3.0
2.0
1.0
0.0
-1.0
-2.0
-3.0
-4.0
-5.0
-6.0
0.0
2.0
4.0
6.0
8.0
10.0
12.0
14.0
16.0
18.0
20.0
22.0
24.0
5.37
3.59
0.95
0.81
0.38
0.47
0.14
8.78
7.58
1.21
1.25
1.26
1.17
1.19
9.37
6.51
4.08
1.93
1.36
0.83
0.58
1.31
1.05
0.67
0.65
0.30
0.29
0.09

Fig. 6

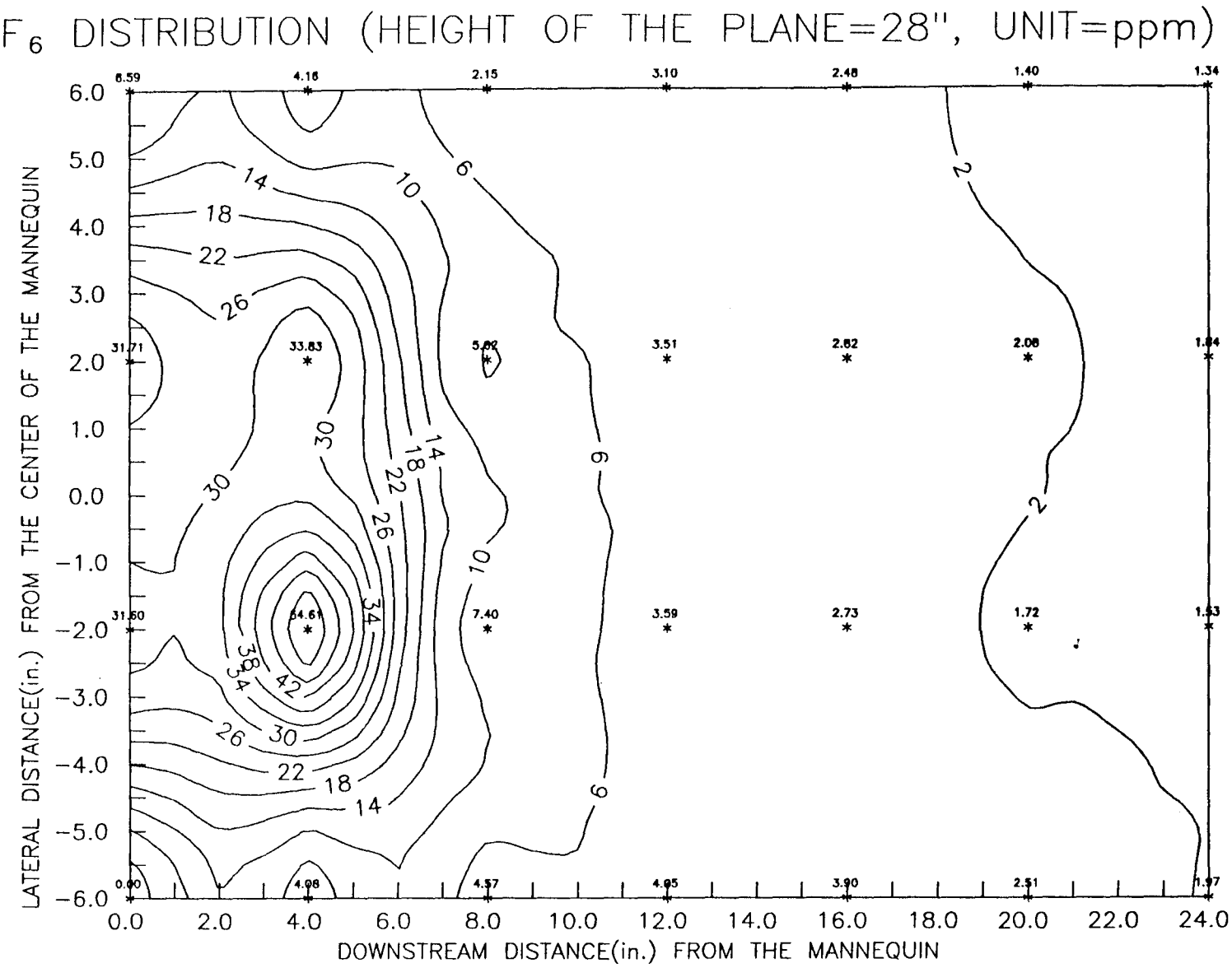
SF6 DISTRIBUTION (HEIGHT OF THE PLANE=28", UNIT=ppm)
LATERAL DISTANCE(in.) FROM THE CENTER OF THE MANNEQUIN
DOWNSTREAM DISTANCE(in.) FROM THE MANNEQUIN
6.0
5.0
4.0
3.0
2.0
1.0
0.0
-1.0
-2.0
-3.0
-4.0
-5.0
-6.0
0.0
2.0
4.0
6.0
8.0
10.0
12.0
14.0
16.0
18.0
20.0
22.0
24.0
6.59
4.16
2.15
3.10
2.48
1.40
1.34
31.71
33.83
5.82
3.51
2.82
2.08
1.84
31.60
54.61
7.40
3.59
2.73
1.72
1.53
0.00
4.08
4.57
4.05
3.90
2.51
1.97
2
6
10
14
18
22
26
30
34
38
42

Fig. 7

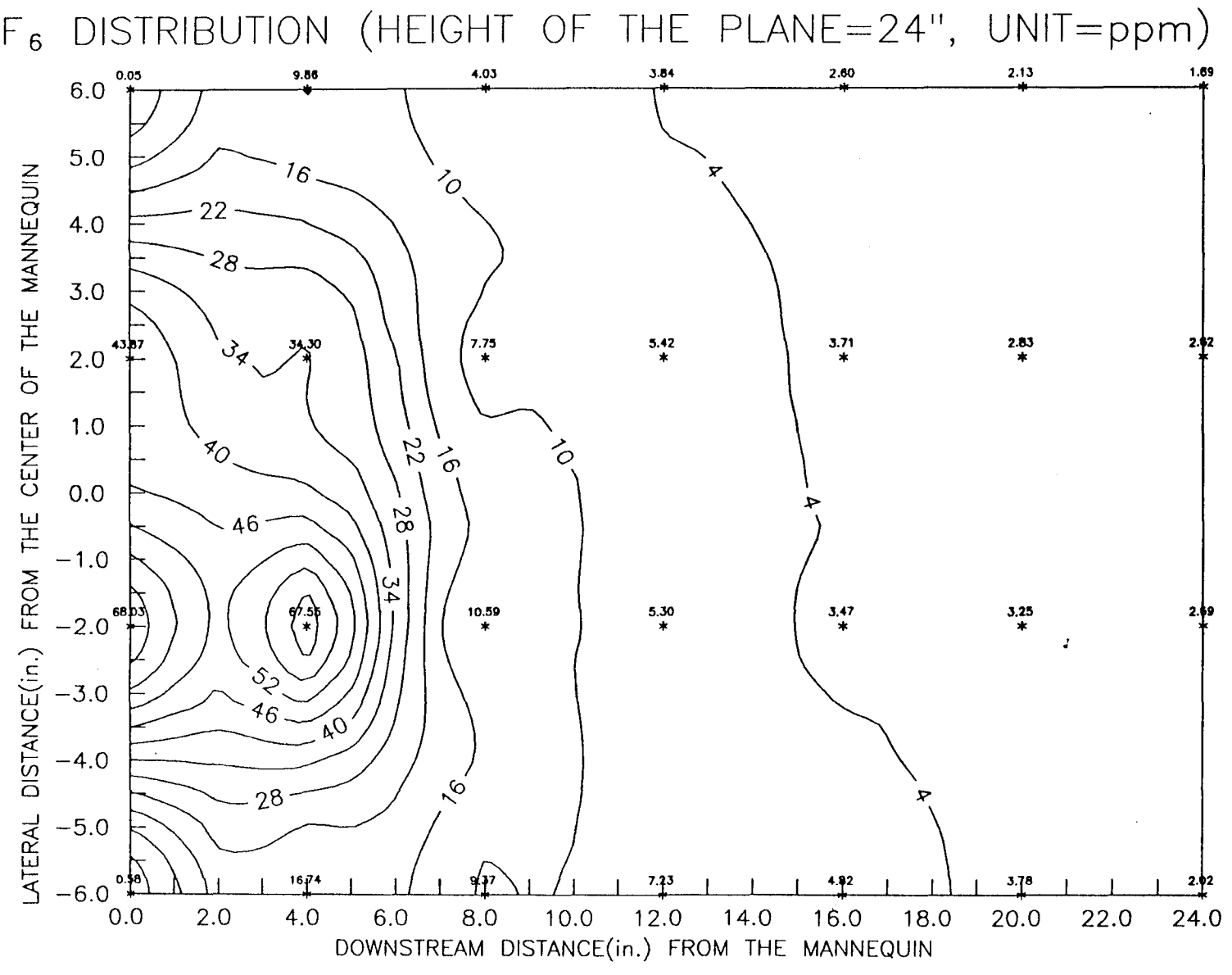
SF6 DISTRIBUTION (HEIGHT OF THE PLANE=24", UNIT=ppm)
LATERAL DISTANCE(in.) FROM THE CENTER OF THE MANNEQUIN
DOWNSTREAM DISTANCE(in.) FROM THE MANNEQUIN
6.0
5.0
4.0
3.0
2.0
1.0
0.0
-1.0
-2.0
-3.0
-4.0
-5.0
-6.0
0.0
2.0
4.0
6.0
8.0
10.0
12.0
14.0
16.0
18.0
20.0
22.0
24.0
0.05
9.86
4.03
3.84
2.60
2.13
1.69
43.87
34.30
7.75
5.42
3.71
2.83
2.92
68.03
67.56
10.59
5.30
3.47
3.25
2.69
0.58
16.74
9.37
7.23
4.92
3.78
2.92
4
10
16
22
28
34
40
46
52

Fig. 8

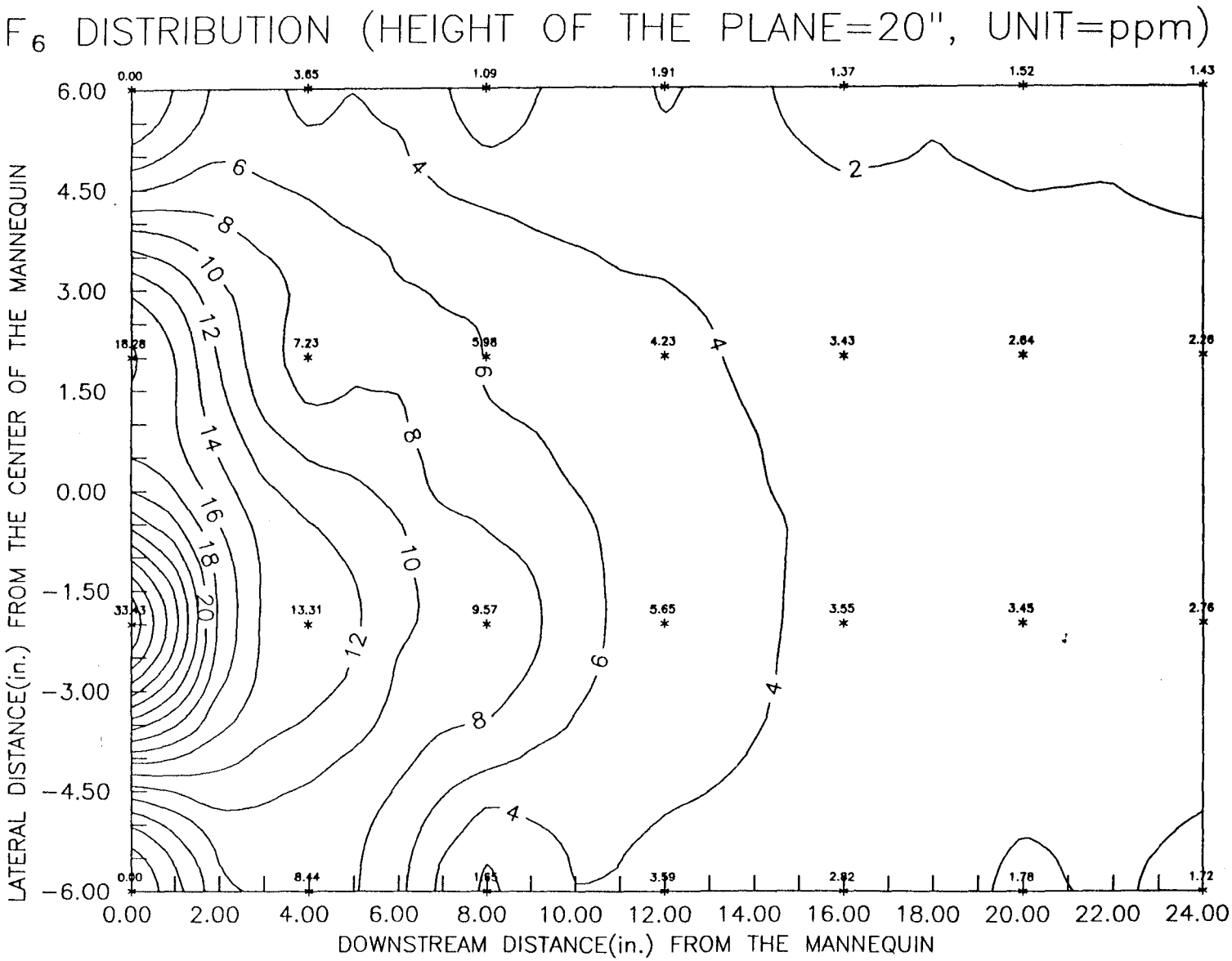
SF6 DISTRIBUTION (HEIGHT OF THE PLANE=20", UNIT=ppm)
LATERAL DISTANCE(in.) FROM THE CENTER OF THE MANNEQUIN
6.00
4.50
3.00
1.50
0.00
-1.50
-3.00
-4.50
-6.00
0.00
2.00
4.00
6.00
8.00
10.00
12.00
14.00
16.00
18.00
20.00
22.00
24.00
DOWNSTREAM DISTANCE(in.) FROM THE MANNEQUIN
0.00
3.65
1.09
1.91
1.37
1.52
1.43
7.23
5.98
4.23
3.43
2.64
13.31
9.57
5.65
3.55
3.45
8.44
3.59
2.82
1.78
2
4
6
8
10
12
14
16
18
20

Fig. 9

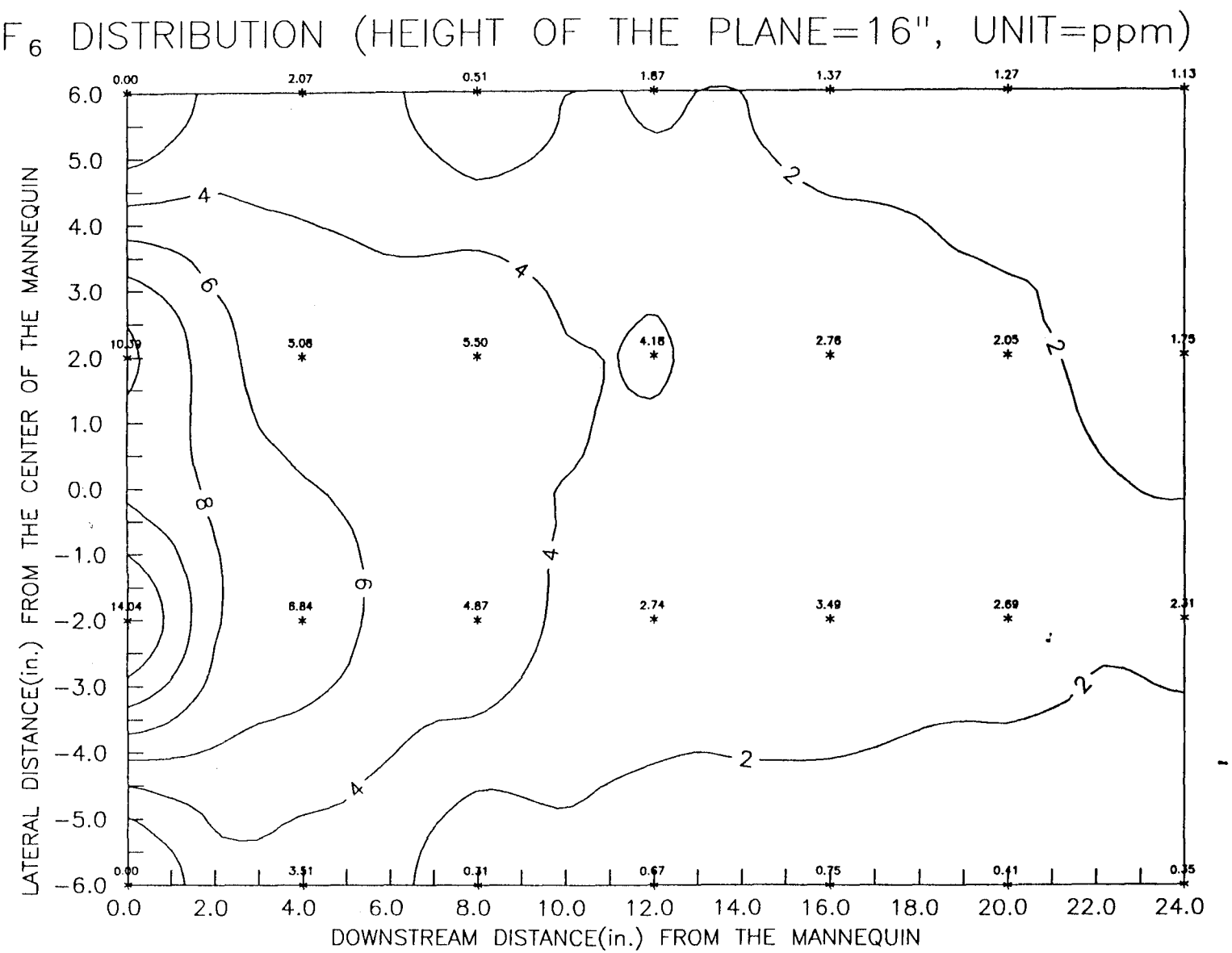
SF6 DISTRIBUTION (HEIGHT OF THE PLANE=16", UNIT=ppm)
LATERAL DISTANCE(in.) FROM THE CENTER OF THE MANNEQUIN
DOWNSTREAM DISTANCE(in.) FROM THE MANNEQUIN
6.0
5.0
4.0
3.0
2.0
1.0
0.0
-1.0
-2.0
-3.0
-4.0
-5.0
-6.0
0.0
2.0
4.0
6.0
8.0
10.0
12.0
14.0
16.0
18.0
20.0
22.0
24.0
0.00
2.07
0.51
1.87
1.37
1.27
1.13
10.39
5.08
5.50
4.16
2.76
2.05
1.75
14.04
6.84
4.87
2.74
3.49
2.69
2.31
0.00
3.51
0.31
0.67
0.75
0.41
0.35
2
4
6
8
9

Fig. 10

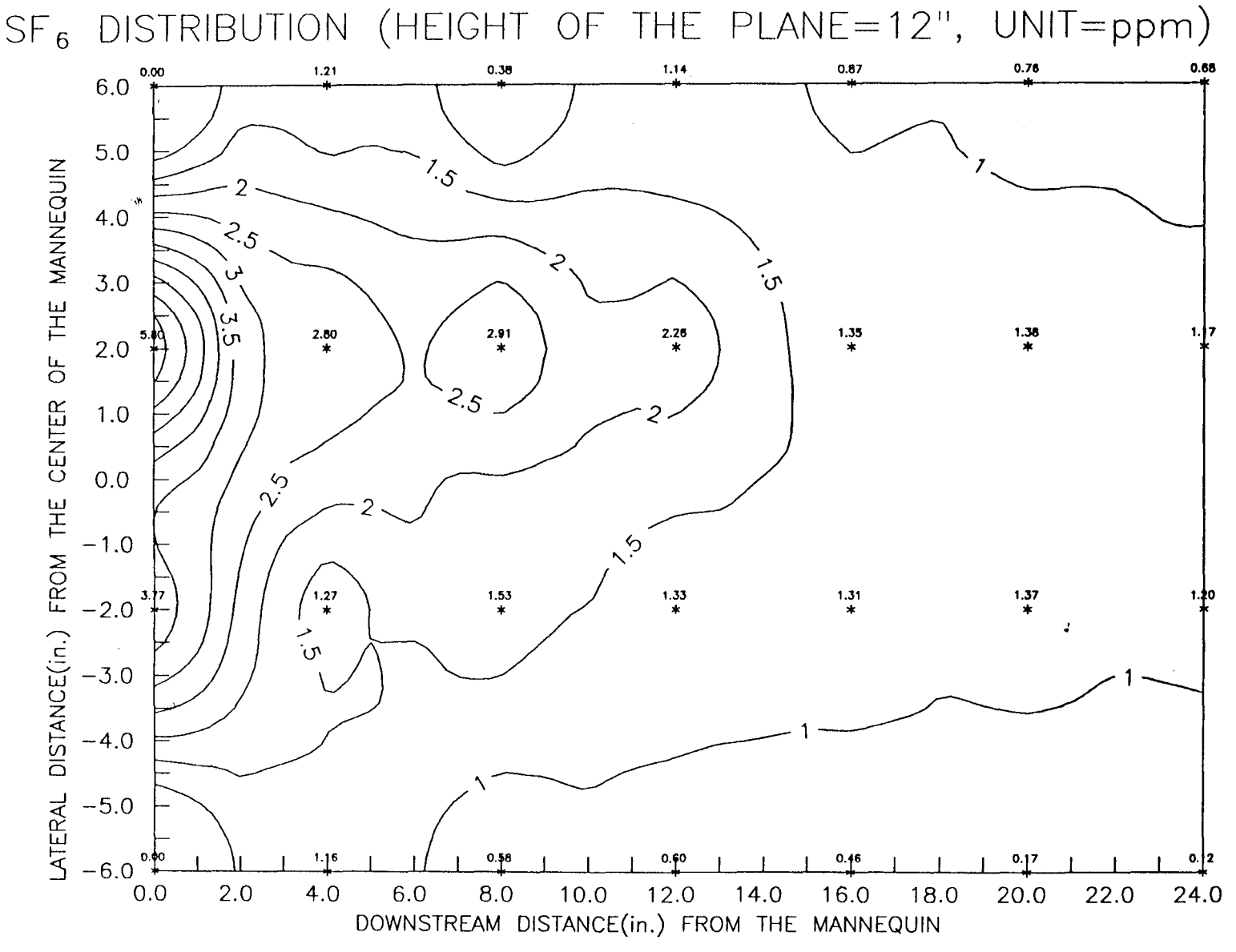
SF6 DISTRIBUTION (HEIGHT OF THE PLANE=12", UNIT=ppm)
LATERAL DISTANCE(in.) FROM THE CENTER OF THE MANNEQUIN
DOWNSTREAM DISTANCE(in.) FROM THE MANNEQUIN
6.0
5.0
4.0
3.0
2.0
1.0
0.0
-1.0
-2.0
-3.0
-4.0
-5.0
-6.0
0.0
2.0
4.0
6.0
8.0
10.0
12.0
14.0
16.0
18.0
20.0
22.0
24.0
0.00
1.21
0.38
1.14
0.87
0.76
0.68
2.80
2.91
2.26
1.35
1.38
1.27
1.53
1.33
1.31
1.37
1.20
1.16
0.58
0.60
0.46
0.17
1
1.5
2
2.5
3
3.5

Fig. 11

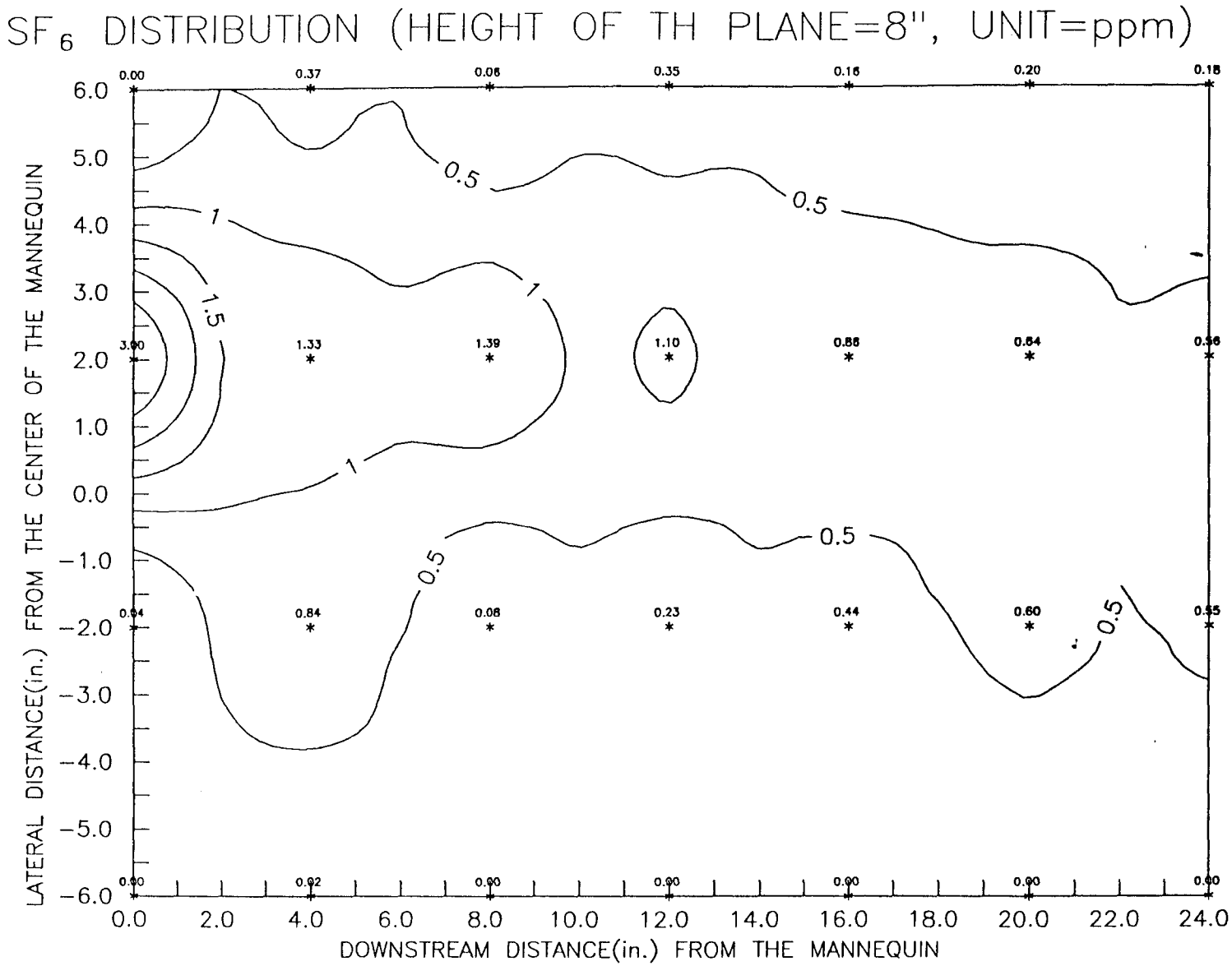
SF6 DISTRIBUTION (HEIGHT OF TH PLANE=8", UNIT=ppm)
LATERAL DISTANCE(in.) FROM THE CENTER OF THE MANNEQUIN
DOWNSTREAM DISTANCE(in.) FROM THE MANNEQUIN
6.0
5.0
4.0
3.0
2.0
1.0
0.0
-1.0
-2.0
-3.0
-4.0
-5.0
-6.0
0.0
2.0
4.0
6.0
8.0
10.0
12.0
14.0
16.0
18.0
20.0
22.0
24.0
0.5
1
1.5
0.00
0.37
0.06
0.35
0.16
0.20
0.18
1.33
1.39
1.10
0.84
0.08
0.23
0.44
0.60
0.55
0.84
0.02
0.00

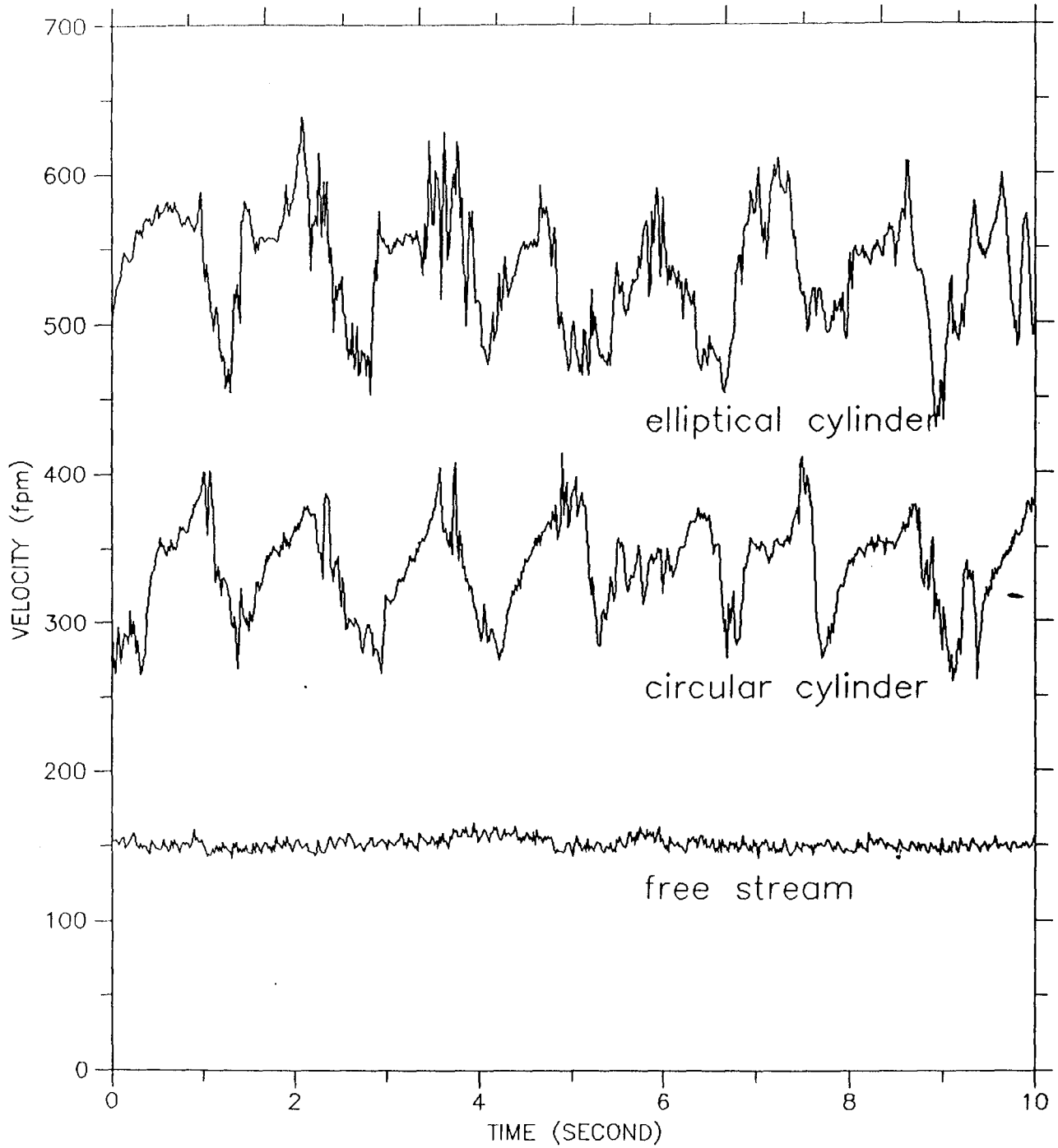

Fig. 12

COMPARISON OF VELOCITY SIGNALS : CIRCULAR & ELLIPTICAL CYL.